
# Impact resistance of ship hull to berthing loads: quantifying critical fender impact.

E.A. Berendsen

TU Delft

PIANC A.D. 1885 AIPCN NAVIGARE NECESSE

Port of Rotterdam

# Impact resistance of ship hull to berthing loads: quantifying critical fender impact

by

E.A. Berendsen

to obtain the degree of Master of Science
at the Delft University of Technology
to be defended on Tuesday November 1, 2022 at 14:30 PM.


| | | |
|---|---|---|
| Student number: | 4474988 | |
| Thesis number: | MT.22/23/008.m | |
| Project duration: | February 14, 2022 – November 1, 2022 | |
| Thesis committee: | Dr. C. L. Walters, | TU Delft, daily supervisor |
| | Dr. Ir. L. Pahlavan, | TU Delft, committee member |
| | Dr. A. Grammatikopoulos, | TU Delft, committee member |
| | Dr. Ir. A. A. Roubos, | TU Delft & Port of Rotterdam Authority, supervisor |
| | Ir. E. J. Broos, | Port of Rotterdam Authority, supervisor |


Cover image: Ship at berth in the Port of Rotterdam retrieved from Mediabank Havenbedrijf Rotterdam.

An electronic version of this thesis is available at http://repository.tudelft.nl/.

TU Delft

# Abstract

Over the last two decades, the size and capacity of (container) vessels calling port at the Port of Rotterdam have increased considerably. To moor these huge and heavy ships safely at the quay, fenders are frequently installed. The present guidelines for the “Design of Fender Systems”, which were established in 2002, are due to be updated in 2023. Part of the update of these new guidelines for the design of fenders by working group 211 of the Permanent International Commission for Navigation congresses (PIANC) consists of the verification and validation of the hull pressure criterion, taking into account the recent growth of (container) vessels. Obtaining a generic criterion is challenging due to the enormous diversity in vessel sizes and structural layouts. In addition, fender dimensions and types may also have a significant influence on the fender-induced load. This leads to the following research question: “How can critical fender-induced loads acting on the parallel side hull be quantified, accounting for the diversity of vessels and fenders?”

In this research, parallel hull sections are used in numerical simulations to investigate the allowable load of fenders and to derive the influence of panel size and dimensions (tall or wide). Including detailed parallel hull sections for a representative group of vessels, makes it possible to look beyond simplified geometries, such as stiffened panels, and specific case studies. First, the structural response and corresponding governing failure modes were studied. In addition to existing failure modes described in fender-induced loads, tripping of stiffeners as a possible governing failure mode was included. A modification to available analytical formulations was made to describe the critical tripping pressure of stiffeners with a flange under patch loads more accurately. The proposed critical tripping pressure induced by a fender is underestimated by the analytical model in comparison to the numerical simulations of the parallel sections. When the rotational restraint of the web frame attached to the tripping stiffener is considered, a closer correlation between the analytical results and the numerical simulations of the parallel hull is foreseen. For the numerical simulations, a parametric approach was adopted, where different impact locations and contact areas were applied for several vessel types and sizes. The lowest steel grade of vessels currently applied in shipbuilding was implemented to obtain the lower limit of allowable fender-induced loads.

The key finding of this study is that allowable fender-induced loads are largely influenced by the vessel’s structural dimensions, such as web frame spacing, and the size of the fender panel with respect to the ship’s geometry. The constant hull pressure criterion currently used by PIANC can be maintained but should be limited to a total allowable reaction force, because, for large panels, it overestimates the capacity. Furthermore, it has been shown that for large ships, wide panels outperform tall panels because they activate web frame(s). Making panels much wider does not necessarily yield more capacity because the stress concentration remains in the web frames. For small vessels, the trend is less clear, as the web frame is activated at an earlier stage (less far apart) and the capacity does not increase exponentially with the width. In addition, high panels on small vessels sometimes lead to the activation of a deck and thus increase the allowable load. The overall conclusion of this research is that the PIANC criterion should be limited to a total reaction force. Furthermore, by correctly sizing fender panels, more efficient use of the vessel’s capacity can be ensured, as web frames provide more capacity. The findings of this research can be used to allow small and large vessels to safely berth onto existing facilities.

# Preface

This research project was proposed by Ir. E.J. Broos, chairman of PIANC MarCom WG211 ”Guidelines for the design of fender systems” and senior port engineer at Port of Rotterdam Authority, and Dr. Ir. A.A. Roubos, member of PIANC MarCom WG211, senior port engineer at Port of Rotterdam Authority and researcher maritime structures of the Civil Engineering and Geosciences Faculty of Delft University of Technology. This study is supervised by Dr. C.L. Walters, Associate Professor Ship and Offshore Structures at the Maritime and Transport Technology Department of Delft University of Technology. The research contributes to the new PIANC guidelines by WG211 on the design of fender systems to improve the hull capacities in the PIANC guidelines. This study is carried out as a master thesis project at the department of Ship and Offshore Structures at Delft University of Technology.

In general, I would like to express my gratitude to the department of Maritime and Transport Technology of Delft University of Technology, the Port of Rotterdam and PIANC for facilitating this study. I would like to thank my daily supervisor at Delft University of Technology, Carey Walters, for his input and guidance. I would also like to thank my supervisors at the Port of Rotterdam Authority, Erik Broos and Alfred Roubos for their support and guidance. To the Port Engineering Natte Infrastructuur team at the Port of Rotterdam Authority, thank you for making me feel so welcome! I have had a great time at the Port of Rotterdam Authority. To the members of PIANC Working group 211, thank you for taking the time to share your knowledge with me. I am grateful for having had the opportunity to learn from experts in the field, and I have fond memories of the working group meeting in Valencia. Furthermore, I would like to express my appreciation to TNO, and more specifically, Lex Vredeveldt and Marnix Rhijnsburger for kindly offering to be available for my questions regarding LS-DYNA.

I would like to thank my parents, my brothers, Stijn, Joost and Mees, and my cousin, Klara, for their never-ending support during my thesis and my studies at TU Delft. To my friends, and especially my friends from Maritieme Techniek, thank you for your support, the memories and all the long coffee breaks. And lastly, I would like to thank Koen for his loving support and for being there every step along the way.

As this thesis marks the end of my time as a student in Delft, I can only be grateful for the opportunities I have had during my years at Delft University of Technology. Being an engineering student can be challenging from time to time, but it has been a privilege to be able to expand my knowledge and discover my passion. I am proud to finish my degree in Marine Technology with this thesis and I look forward to the challenges ahead.

***E.A. (Emma) Berendsen***
*Delft, November 2022*

# Contents


**1 Introduction** **1**

**2 Background** **3**
2.1 Cylindrical fenders . . . 3
2.2 Tripping failure formulations . . . 4
2.3 Impact energy shared by fender and ship . . . 6
2.4 Sensitivity to impact location and area . . . 9
2.5 Conclusion . . . 9

**3 Methodology** **11**
3.1 Analytical model . . . 11
3.2 Numerical simulations . . . 11

**4 Analytical model** **13**
4.1 Adamchak's formulation . . . 13
4.2 Shahabian and Roberts' formulation . . . 15
4.3 Validation of pre-buckling stress fields . . . 17
4.4 Modified Shahabian and Roberts' formulation . . . 18
4.5 Parametric study . . . 21

**5 Numerical simulations** **23**
5.1 Dynamic and deformation modelling . . . 23
5.2 Components and assumptions . . . 24
5.2.1 Material model . . . 24
5.2.2 Boundary conditions and prescribed motion . . . 24
5.2.3 Contact . . . 25
5.2.4 Structural layout hulls . . . 25
5.3 Calibration and validation . . . 25
5.4 Coupled system force-displacement behaviour . . . 26
5.4.1 Fender force-displacement curves . . . 26
5.4.2 Ship force-displacement curves . . . 27
5.4.3 Coupled force-displacement curve . . . 27
5.5 Onset of plasticity . . . 30
5.5.1 Post-processing of the simulations . . . 31
5.6 Parametric sensitivity . . . 31
5.6.1 Panel location . . . 31
5.6.2 Panel dimension . . . 31
5.6.3 Ship type . . . 32

**6 Results** **35**
6.1 Analytical model . . . 35
6.2 Numerical simulations . . . 36
6.2.1 Impact location . . . 36
6.2.2 Rated fender reaction force . . . 36
6.2.3 Large container vessel . . . 37
6.2.4 Small tanker vessel . . . 38
6.2.5 Single shell bulk carrier . . . 40
6.2.6 Container vessel 1 . . . 41
6.2.7 Container vessel 2 . . . 43
6.2.8 Container vessel 3 . . . 44
6.2.9 Bulk carrier 1 . . . 46
6.2.10 Bulk carrier 2 . . . 47

6.3 Observed failure modes . . . 49
6.4 Comparison to prior results . . . 49
6.4.1 Systematic cylindrical fender study by Vredeveldt and Rhijnsburger . . . 49
6.4.2 Plate- and stiffener-induced failure formulations by IJzerman . . . 49

**7 Discussion and recommendations 55**
7.1 Interpretation of the results . . . 55
7.2 Relevance . . . 55
7.3 Limitations . . . 56
7.4 Recommendations for future research . . . 56
7.5 Recommendations for PIANC WG211 . . . 57

**8 Conclusion 59**

**A Ship properties and structural layout 63**
A.1 Tanker 1 . . . 64
A.2 Container vessel 4 . . . 65
A.3 Bulk carrier 3 . . . 66
A.4 Container vessel 1 . . . 67
A.5 Container vessel 2 . . . 68
A.6 Container vessel 3 . . . 69
A.7 Bulk carrier 1 . . . 70
A.8 Bulk carrier 2 . . . 71

**B Trend lines allowable equivalent hull pressure fender 73**

**C Trend lines allowable total fender force 77**

**D Comparison analytical result Vredeveldt and Rhijnsburger (2019) 81**

# List of Figures


2.1 Schematic stiffener tripping behaviour [5]. . . . 4
2.2 Cross-section of steel stiffened panel with three HP-stiffeners. . . . 5
2.3 Design principles with respect to the share of strain energy dissipation between systems [20]. . . . 6
2.4 Energy absorption behaviour of different fender types [8]. . . . 7
2.5 Load-displacement curve for a steel stiffener panel in a study to ship-ice floe impact [22]. 8
2.6 Schematic representation of a shared-energy load-deformation curve for ship and installation (fender) [20]. . . . 8

4.1 Comparison of the analytical pre-buckling stress field proposed by Adamchak [1] and Shahabian and Roberts [25]. . . . 16
4.2 Stiffener web with load to validate analytical pre-buckling stress fields. . . . 17
4.3 FEA stiffener web $\sigma_x$ pre-buckling stress field [Pa]. . . . 17
4.4 FEA stiffener web $\sigma_y$ pre-buckling stress field [Pa]. . . . 17
4.5 FEA stiffener web $\tau_{xy}$ pre-buckling stress field [Pa]. . . . 18
4.6 Comparison of the analytical pre-buckling stress field of Shahabian and Roberts [25] and the modified formulation for a flanged stiffener. . . . 19
4.7 Stiffener web and flange combination with load to validate analytical pre-buckling stress fields. . . . 20
4.8 Stiffener web with plate and flange with load to validate analytical pre-buckling stress fields. . . . 20
4.9 Pre-buckling stress fields for two configurations of a stiffener web in LS-DYNA. . . . 20
4.10 Schematic representation of panel dimensions in relation to a stiffened panel in ship hull where Adamchak [1] or Shahabian and Roberts [25] is representative. . . . 21
4.11 Layout of a single shell structure parallel ship hull [32]. . . . 22
4.12 Layout of a cell structure parallel ship hull [32]. . . . 22

5.1 Cone fender equipped with panel that is constrained by chains [19]. . . . 24
5.2 Force-displacement curves for the fenders included in the research [27]. . . . 27
5.3 Force-displacement curves for the vessels included in this research. . . . 28
5.4 Coupled force-displacement curve of small tanker vessel and SPC cone fender 1200 G2.9. 29
5.5 Visualizing the onset of plasticity in LS-DYNA software with example hull large container vessel and 6m x 2m panel. . . . 30
5.6 Local details of the onset of plasticity in stiffened panel in LS-DYNA software in large container vessel (C4) and 6m × 2m fender panel. The local detail shows L-profile stiffeners ($275mm \times 12mm$ + $125mm \times 12mm$) with stiffener spacing $b = 850mm$ and HIP ($900mm \times 2000mm$) web frames with $3160mm$ spacing. . . . 31
5.7 Fender panel located on the middle of a stiffened panel, the shell plate is transparent to indicate the structural components behind the plate. . . . 32
5.8 Fender panel located asymmetrically on stiffened panel, the shell plate is transparent to indicate the structural components behind the plate. . . . 32
5.9 Fender panel located on a web frame, the shell plate is transparent to indicate the structural components behind the plate. . . . 32
5.10 Overview of the panel dimensions in relation to 19,000 TEU container parallel hull section (12.6m wide). . . . 34

6.1 Allowable equivalent hull pressure on a large container vessel. . . . 37
6.2 Allowable total reaction force on the parallel hull of a large container vessel. . . . 38
6.3 Allowable equivalent hull pressure on a small tanker vessel. . . . 38

6.4 Allowable total reaction force on the parallel hull of a small tanker vessel. . . . . 39
6.5 Allowable equivalent hull pressure on a large bulk carrier. . . . . 40
6.6 Allowable total reaction force on the parallel hull of a large bulk carrier. . . . . 41
6.7 Allowable equivalent hull pressure on a container feeder. . . . . 41
6.8 Allowable total reaction force on the parallel hull of a container feeder. . . . . 42
6.9 Allowable equivalent hull pressure on a container coaster. . . . . 43
6.10 Allowable total reaction force on the parallel hull of a container coaster. . . . . 44
6.11 Allowable equivalent hull pressure on a Post-Panamax container vessel. . . . . 44
6.12 Allowable total reaction force on the parallel hull of a Post-Panamax container vessel. . 45
6.13 Allowable equivalent hull pressure on a Handysize bulk carrier. . . . . 46
6.14 Allowable total reaction force on the parallel hull of a Handysize bulk carrier. . . . . 47
6.15 Allowable equivalent hull pressure on a Capesize bulk carrier. . . . . 47
6.16 Allowable total reaction force on the parallel hull of a Capesize bulk carrier. . . . . 48
6.17 Comparison of the safe equivalent hull pressure for a small tanker according to prior research by IJzerman [12], the numerical simulations and PIANC. . . . . 50
6.18 Comparison of the safe reaction force for a small tanker according to prior research by IJzerman [12], the numerical simulations and PIANC. . . . . 50
6.19 Comparison of the safe equivalent hull pressure for a large bulk carrier according to prior research by IJzerman [12], the numerical simulations and PIANC. . . . . 51
6.20 Comparison of the safe reaction force for a large bulk carrier according to prior research by IJzerman [12], the numerical simulations and PIANC. . . . . 51
6.21 Comparison of the safe equivalent reaction force for a large container carrier according to prior research by IJzerman [12], the numerical simulations and PIANC. . . . . 52
6.22 Comparison of the safe reaction force for a large container carrier according to prior research by IJzerman [12], the numerical simulations and PIANC. . . . . 52

A.1 Structural layout of tanker coaster, where the inner hull is transparent for visual purposes. 64
A.2 Structural layout of ULCV, where the inner hull is transparent for visual purposes. . . . . 65
A.3 Structural layout of Panamax bulk carrier. . . . . 66
A.4 Structural layout of container feeder, where the inner hull is transparent for visual purposes. 67
A.5 Structural layout of container coaster, where the inner hull is transparent for visual purposes. . . . . 68
A.6 Structural layout of Post-Panamax container vessel, where the inner hull is transparent for visual purposes. . . . . 69
A.7 Structural layout of Handysize bulk carrier, where the inner hull is transparent for visual purposes. . . . . 70
A.8 Structural layout of Capesize bulk carrier. . . . . 71

# List of Tables


3.1 Vessels and corresponding properties [32]. . . . . 12

4.1 Comparison of the pre-buckling stress field without a flange. . . . . 18
4.2 Comparison of the pre-buckling stress field with patch load with and without a flange. . 20

5.1 Numerical simulations to determine influence of fender panel dimensions. . . . . 32

6.1 Analytically determined critical distributed load to induce tripping in investigated stiffened panels. . . . . 35
6.2 Sheikh et al. influential parameters to tripping failure for investigated stiffened panels [26]. 35
6.3 Maximum hull capacities to determine the influence of the impact locations with different structural components on a container vessel. . . . . 36
6.4 Maximal fender reaction force from analytical dynamics. . . . . 36
6.5 Maximum hull pressure for a large container vessel to determine the influence of the direction of the dimensions of the fender panel. . . . . 37
6.6 Comparison of hull capacities according to numerical single stiffener cylindrical fender impact study [32] and LS-DYNA simulations. . . . . 49

7.1 Recommendation for the update of the PIANC hull pressure criterion for WG211. . . . . 57

A.1 Vessel types covered in study for update of the PIANC hull pressure criterion for WG211. 63
A.2 Vessel properties of tanker coaster (T1). . . . . 64
A.3 Vessel properties of ULVC (C4). . . . . 65
A.4 Vessel properties of Panamax bulk carrier (B3). . . . . 66
A.5 Vessel properties of container feeder (C1) . . . . . 67
A.6 Vessel properties of container coaster (C2) . . . . . 68
A.7 Vessel properties of Post-Panamax container vessel (C3) . . . . . 69
A.8 Vessel properties of Handysize bulk carrier (B1) . . . . . 70
A.9 Vessel properties of Capesize bulk carrier (B2) . . . . . 71

D.1 Comparison of hull capacities according to analytical single stiffener impact study [32] and LS-DYNA simulations. . . . . 81

# Nomenclature

*The next list describes symbols that are used within the body of the document*

**Abbreviations**

DWT Deadweight tonnage

FEA Finite Element Analysis

FEM Finite Element Model

MAT 024 Elasto-plastic material category in LS-DYNA

NORSOK N-004 Design of Steel Structures of the Norwegian Standards Institute

OSV Offshore supply vessel

PIANC Permanent International Association of Navigation Congresses

TEU Twenty-foot equivalent unit

ULCV Ultra large container vessel

ULS Ultimate Limit State

VLBC Very large bulk carrier

WG Working group

**Greek Symbols**

$\beta$ Assumed displacement of the stiffener web

$\beta_1$ Plate transverse flexural slenderness ratio

$\beta_4$ Stiffener torsional slenderness to plate transverse flexural slenderness ratio

$\ddot{\Delta}$ Acceleration

$\Delta$ Displacement

$\dot{\Delta}$ Velocity

$\Gamma$ Longitudinal warping constant

$\mu_d$ Dynamic friction coefficient

$\mu_s$ Static friction coefficient

$\nu$ Poisson's ratio

$\Phi$ Yield function

$\sigma_y$ Yield strength of the material

$\sigma_{x,AC}$ X stress field component proposed by Adamchak [1]

$\sigma_{y,AC}$ Y stress field component proposed by Adamchak [1]

$\tau_{xy,AC}$ Shear stress field component proposed by Adamchak [1]

$\varepsilon$ Strain

$\varepsilon_p$ Effective plastic strain

$\xi$ Empirical variable in IJzerman [12]

$\bar{\sigma}$ Effective stress

**Roman Symbols**

$A$ Area of contact

$a$ Web frame spacing, also stiffener length

$A_f$ Stiffener flange area

$b$ Stiffener spacing

$b_e$ Effective plate width [13]

$C$ Rotational restrain of the attached plate

$c$ Patch dimensions

$C_c$ Berthing configuration coefficient

$C_e$ Eccentricity coefficient

$C_m$ Added mass coefficient

$C_s$ Softness coefficient

$d_c$ Depth of the stiffener to the mid-thickness of the flange

$d_w$ Stiffener web height

$E$ Young's modulus

$E_d$ Design kinetic energy

$E_s$ Strain energy

$f_f$ Stiffener flange width

$G$ Shear modulus

$h$ Height of the neutral axis above the mid plate

$h_f$ Height of fender panel

$h_{stiffener}$ Total height of the stiffener

$I$ Moment of inertia of stiffener

$J$ Saint Venant's constant

$K$ Buckling coefficient

$k_{coupled}$ Coupled stiffness of system

$m$ Mode number

$M_d$ Mass of the berthing ship incl. added mass

$P$ Total fender load

$p$ (Hull) pressure

| | |
|---|---|
| $Q$ | Shear force |
| $q$ | Distributed fender load or patch load |
| $r$ | Radius of gyration |
| $R_f$ | Reaction force in the fender |
| $R_s$ | Reaction force in the ship |
| $R_{d,allow}$ | Allowable loading of vessel stiffeners retrieved by IJzerman [12] |
| $t$ | Thickness of the shell plate |
| $t_w$ | Thickness of the web |
| $V$ | Internal strain energy |
| $V_b$ | Initial berthing velocity perpendicular to the berth |
| $W$ | Work |
| $w_i$ | Deformation of ship, fender or installation |
| $w_f$ | Width of the fender panel |
| $z$ | Height of stiffener centroid above toe |
| $\bar{H}_m$ | Quadratic functions for tripping under lateral pressure |
| $\bar{s}$ | Height of stiffener shear center above toe |

# 1 Introduction

In August 2022, the Ever Alot called port at the Port of Rotterdam. At that moment, with a capacity of 24,004 TEU, it is the largest container vessel in the world. A couple of years earlier, in 2017, the OOCL Hong Kong was the largest, with a capacity of 21,413 TEU. The trend of the increasing capacity and size of (container)vessels comes with an increase in the mass of these vessels [30]. To bring these huge and heavy ships to a safe stop at the quay, fenders are frequently installed. The current guidelines for fender design were established in 2002 by the Permanent International Commission for Navigation Congresses (PIANC) and are due to be updated by Working group 211 in 2023 [18, 19]. Part of the update of these guidelines is verifying and validating the hull pressure criterion, taking into account the growth of vessels over the last two decades.

To ensure the safe berthing of small and large ships onto existing berthing facilities, it is necessary to know the critical berthing load after which permanent deformation can occur, the Ultimate Limit State (ULS). Contact damage has been studied extensively with respect to vessels impacted by ice, in order to quantify the hull's structure capacities [2, 14, 21]. However, these situations are regarded as accidental, where permanent, i.e. plastic, deformation is accepted. As vessels berth in ports every day, this cannot be considered to be accidental and, therefore, plastic deformation is not allowed. Determining resistance to fender-induced load requires quantification of these capacities in the elastic deformation region.

As both vessels and fenders come in many configurations, it is challenging to obtain a general criterion for the fender-induced load. Prior studies in the field of arctic engineering showed a significant influence of the vessel's structures and contact area on the plastic response in large deformation [14, 33, 34]. Therefore, the diversity of vessels and fenders have to be accounted for when quantifying the critical loads for the fender design guidelines. Prior studies on fender impact have focussed on specific cases, for example, cylindrical fenders in the Port of Rotterdam [4, 32]. Furthermore, IJzerman came up with a general semi-analytical formulation for plate- and stiffener-induced failure in stiffened panels impacted by soft and rigid fenders [12]. However, in addition to these failure modes, experiments on stiffened panels, which show similarities to fender impact, have suggested tripping as a possible governing failure mode [17, 29]. The structural response of the ship's hull to fender-induced loads activating several components, taking into account the diversity of the vessel and the fender, has not yet been described. Therefore, the main objective of this study is to gain insight into the governing structural response when the ship's hull is impacted by a fender. Moreover, the critical fender-induced load has to be quantified, while accounting for a representative range of vessels and fenders.

This leads to the following research question:

*"How can critical fender-induced loads acting on the parallel side hull be quantified, accounting for the diversity of vessel and fender?"*

The following sub-questions are introduced to answer the main research question:

1. What is the governing failure mode in loading of the ship's side hull by fenders equipped with panels?

2. How can the critical failure load for the governing failure mode be analytically formulated?
3. To what extent are the critical fender-induced loads influenced by the impact location and the dimensions of the fender panel?
4. What is the influence of the vessel's dimensions and type on the critical fender-induced loads?
5. Which structural components can be identified as the weakest link(s) in contact between fenders and vessels?
6. What is the optimal fender panel dimension, considering critical failure mechanism and vessel diversity?

To answer the research questions, numerical simulations are used to determine the structural response of the parallel hull during fender impact. First, the failure modes that occur in the contact between the ship and the fender are analysed. Moreover, the additional governing failure mode of tripping is described analytically. Next, extensive numerical simulations are executed for different vessels and fenders to quantify the allowable fender load. In the numerical models, representative values of the berthing loads and material properties are implemented to obtain a lower limit for the critical fender-induced loads. Furthermore, a group of eight representative vessels is included in these simulations to validate or update the PIANC hull pressure criterion. Additionally, a group of representative fenders is included in these simulations. The research is limited to the parallel berthing condition, where the parallel side hull of the vessel is considered. Furthermore, the focus lies on the structural capacities of the ship itself and other berthing conditions are not extensively examined.

Before elaborating on the research question, Chapter 2, provides a discussion of the relevant literature. Secondly, the methodology of the research is presented in Chapter 3, followed by the analytical formulations of tripping failure under patch load in Chapter 4. Furthermore, Chapter 5 elaborates on the numerical simulations executed to determine the critical fender-induced loads. The results of the analytical formulations and the numerical simulations, including the parametric studies, are presented in Chapter 6. Subsequently, Chapter 7 will discuss the findings of the study and present recommendations for future research and the implementation of the results by PIANC WG211. Finally, Chapter 8 will answer the research question. Additionally, Appendix A contains the properties of the ship hulls included in the body of this research. The obtained trend lines in the research are summarized in Appendices B and C. In Appendix D, a comparison is made between analytical results from prior research and the outcomes of the numerical simulations.

# 2

# Background

Fenders are rubber elements mounted on berthing facilities in ports and offshore environments to protect both the berth and vessels. The fender design guidelines by the Permanent International Commission for Navigation Congresses (PIANC) are often used in practice to design these fender systems. The purpose of the PIANC guidelines for fender design is to facilitate the safe berthing of vessels and improve of fender design. Fenders are designed in the berth-ship interface to absorb the kinetic energy of the berthing vessel. This thesis focuses on the impact of fenders equipped with panels in contact with the parallel hull of a ship. The hull pressure criteria of the guidelines should provide a range within which safe berthing can be ensured. The kinetic energy method is used to translate the initial velocity of the berthing vessel into hull pressure on the ship [19]. In the coming sections, topics related to the ship-fender contact are discussed, to determine solutions for the quantification and identification of failure behaviour in the fender panel contact.

## 2.1. Cylindrical fenders

First, the previous research on ship-fender contact is studied. Several studies were executed to gain insight into the topic of berthing impacts [4, 9, 12, 28, 32]. One of the first studies on ship-fender contact was published in 1989 by Gudmunsen and Morris, who studied the capacities of the side shell structure of ships to withstand quayside loading by fenders. Although their study approach might be of use to answer the research question of this study, the increase of vessel size over the past three decades makes their results outdated. The study by Vredeveldt and Rhijsburger consists of a systematic investigation of the berthing loads by cylindrical fenders with berthing speeds corresponding to those of the Port of Rotterdam [4, 32]. The study showed that the berthing speeds in the Port of Rotterdam did not result in hull pressures that exceed the typical hull pressure values of the PIANC guidelines. For a cylindrical fender on a large container vessel, the onset of plasticity occurred at a compression force of 623 kN in the fender. The applied fender has a width of 2.2 m and the height of the contact area changes over time. The results can be applied to cylindrical fenders used in the Port of Rotterdam or in ports with similar berthing conditions, but more research is needed on fender panels to establish a general formulation for the fender impact. IJzerman added to the study of Vredeveldt and Rhijsbuger by studying cylindrical fenders and fenders equipped with panels [12]. Therefore, he studied fenders with soft and rigid interfaces to retrieve a formulation for plate- and stiffener-induced failure in fender loading. His research was focused on the impact on steel stiffened panels using different dimensions of fenders. The semi-analytical formulation he retrieved for the maximum allowable loading on the stiffened panel is shown below.

$$R_{d,allow} = \left\lfloor \frac{h_f}{b} \right\rfloor \cdot \min\left( \frac{1483w_f^6 - 3115w_f^5 + 2561w_f^4 - 985.8w_f^3 + 195.6w_f^2 - 13.5w_f + 15.21}{\xi}, \frac{32.4}{\xi} \right) \tag{2.1}$$

Where $w_f$ indicates the fender width. The empirical constant $\xi = \frac{s_{wf} \cdot d_c}{I \cdot \sigma_y}$ with $s_{wf}$ for the web frame spacing, $d_c$ for the height of the stiffener, $I$ is the interia moment of the stiffener and $\sigma_y$ the yield strength

of the material. Furthermore, $\left\lfloor \frac{h_f}{b} \right\rfloor$ means the floored value of the indicated fracture.

According to IJzerman's study, the current PIANC hull pressure criterion is too optimistic, as certain configurations with impact loads by fenders exceeded the capacity of the stiffened panel to carry those loads. The study was limited to stiffened panels without looking at fender impact engaging with different structural components. In 2022, Sisworo also found that berthing loads of fender panels on a double hull tanker (5600DWT) exceeded the structural capacities in one of his cases, while the load case was safe according to the PIANC guidelines [28].

The literature discussed above forms a basis for a revision of the typical hull pressure criterion of the PIANC design guidelines for fenders. The study of IJzerman already found a semi-analytical solution for plate- and stiffener-induced failure by fenders. Barber's article in the Naval Architect suggests that a third failure mode occurs in the contact between fenders and the ship hull [3]: tripping failure. In the next section, the analytical tripping failure formulations are discussed.

## 2.2. Tripping failure formulations

To describe the onset of tripping failure in the contact between the fender and the ship, analytical solutions for critical loads inducing tripping are explored in this section. Figure 2.1 gives a graphical representation of the tripping behaviour of stiffeners in stiffened panels.

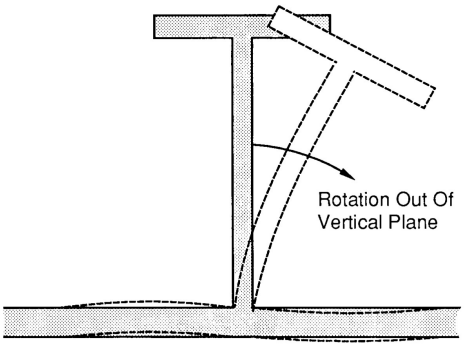


Figure 2.1: Schematic stiffener tripping behaviour [5].

One of the first to address and analytically formulate critical loading to tripping failure was Adamchak in 1979 [1]. In his research, he introduced formulations for lateral-torsional buckling of stiffeners around the point of attachment to a plate. Shortly before his study, some experiments had shown tripping to have the potential to be a primary ductile failure mode in grillages [29]. The load cases Adamchak found formulations for are uniaxial compression and uniform lateral pressure. These formulations take into account the resistance of the plating to rotation of the stiffener, non-linear material and web deformations. The lateral pressure load case shows agreement with the fender panel load case. Depending on the dimensions of the parallel hull and the panel, uniform lateral pressure is a sufficient representation of the contact between the fender and the ship.

Adamchak emphasizes the complexity of tripping under lateral pressure. In the case of uniaxial compression, the stress in the stiffener can be determined relatively easy. The pre-buckling stress field is vital for the formulation of critical loading in stiffeners. The stress field proposed by Adamchak is presented in the equations below.

$$\sigma_{x,AC} = \frac{1}{2}\left(\frac{q}{l}\right)\left(z - h + \frac{1}{2}t\right)\left(x^2 - ax\right) \tag{2.2}$$

$$\begin{aligned}\sigma_{z,AC} = \left(\frac{q}{t_w}\right) - \left(\frac{q}{l}\right)\Bigg[&\frac{A_f z}{t_w}\left(d_c - h + \frac{1}{2}t\right) \\ &+ z\left\{\frac{1}{2}d_w^2 - \frac{1}{6}z^2 + \left(h - \frac{1}{2}t\right)\left(\frac{1}{2}z_{w-d_w}\right)\right\}\Bigg]\end{aligned} \tag{2.3}$$

$$\tau_{xz,AC} = \frac{1}{2}\left(\frac{q}{I}\right)(a-2x)\left[\frac{A_f}{t_w}\left(d-h+\frac{1}{2}t\right) + \frac{1}{2}d_w^2 - \frac{1}{2}z^2 + \left(h-\frac{1}{2}t\right)(z-d_w)\right] \tag{2.4}$$

When the pre-buckling stress field for the load is obtained, the work done by the external load is calculated over the area of the stiffener web and the width of the flange. The flange is considered fairly thin and has a constant stress value over the thickness, thus as one dimensional. Figure 2.2 shows the properties of the stiffeners and the coordinate system considered for the stress field. According to the Rayleigh-Ritz approximation, the critical load can be derived based on the minimum potential energy principle. The principle follows from equating the virtual work of elastic materials. The work by the applied load is equated to the internal strain energy. The critical point occurs when the sum of the total potential energy is equal to zero, when this critical load value is exceeded plasticity occurs. According to the theory, any other solution, which satisfies the boundary condition leads to greater potential energy.

Adamchak discussed the possibility to incorporate several load cases at the same time. He argued that it is possible to consider these loads separately and determine the sum of the work done by the sum of the loads. Shahabian and Roberts based their solution on the proposition made by Adamchak to consider the loads separately [25]. Shahabian and Roberts proposed a pre-buckling stress field formulation for tripping failure of a (stiffener) web under a concentrated distributed load. This kind of load is known as patch load. The patch load is applicable when the fender panel does not cover the entire width of the stiffened panel.

The stress components of the pre-buckling stress field are divided into three parts, both sides of the patch load and the region below the patch load. In Chapter 4, the stress field of Shahabian and Roberts will be further discussed and related to a critical patch pressure following the procedure proposed by Adamchak. The shortcoming of the solution as proposed by Shahabian and Roberts lies in the fact that no force equilibrium was reached in the application to a web with a flange. The consequences of this shortcoming in Shahabian and Roberts and the possible application of both methods to describe critical fender load will be validated in the chapter on analytical formulations.

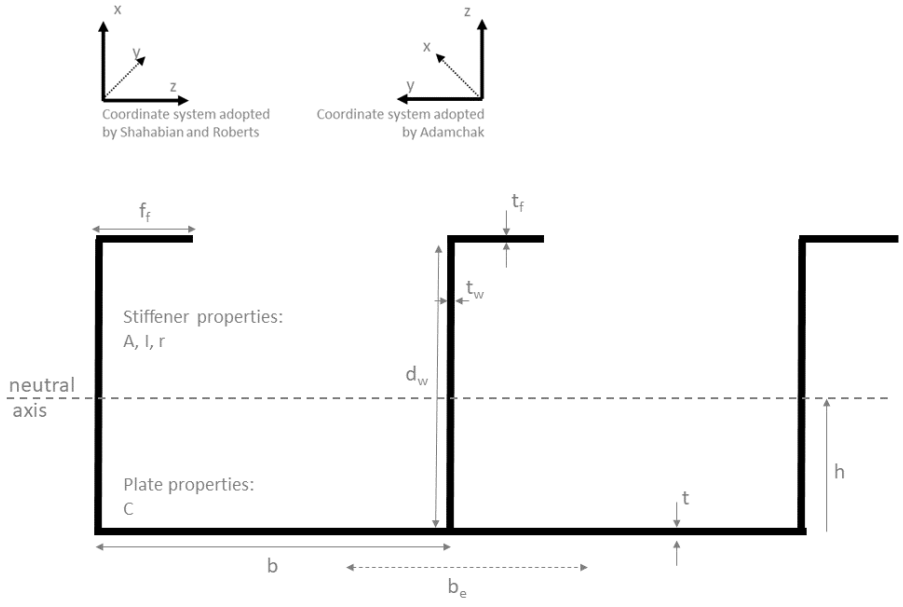


Figure 2.2: Cross-section of steel stiffened panel with three HP-stiffeners.

It has been suggested by Barber that tripping occurs in situations in practice, such as fender panel loading [3]. In 1996, Hughes and Ma found this elastic tripping behaviour while executing numerical

simulations for stiffeners under lateral and combined loading [11]. Similarly, Sheikh, Elwi and Grondin found the most influential parameters for tripping failure in stiffened panels. Their findings endorsed the weakness of bulk carriers to tripping failure by identifying $\beta_1$ and $\beta_4$ as the most influential parameters in tripping failure. Typically, bulk carriers do not have good plate transverse flexural slenderness ($\beta_1$) and stiffener torsional slenderness to plate transverse flexural slenderness ratio ($\beta_4$) properties [26]. Recently, Ma, Xiong and Wang studied several load combinations in an experimental study on lateral-torsion buckling [17]. They found that transverse components mainly dominate in cases of lateral-torsional buckling, or tripping, occurring in stiffeners. As transverse load components are dominant when parallel hulls are loaded by fender panels, it endorses the importance to derive a sufficient analytical formulation for this failure mechanism.

Several of these studies address the influence of initial imperfections or deformations of the stiffener on the occurrence of tripping failure [1, 17, 26]. In 1998, Danielson proposed an addition to the earlier discussed tripping formulation of Adamchak to include these initial deformations[7]. However, it lies out of the scope of this research.

## 2.3. Impact energy shared by fender and ship

In the previous section, the energy capacities of the ship before the tripping of the stiffeners occurs were discussed. This section takes a broader approach to impact energy on parallel hulls. The literature included provides a basis for the simulations that will be executed in the research. The impact energy shared by fender and ship is studied to determine a sufficient way to model the contact. Traditionally, contact damage is considered as a situation that can be mitigated [14, 34]. Especially in the elastic deformation region, the ship is normally assumed not to absorb energy.

The N-004 Design of Steel Structures of the Norwegian Standards Institute (NORSOK) is a very well-established rule for the design of vessels and other steel structures [20]. In their design rules, three principles with respect to the distribution of strain energy dissipation between systems are identified: ductile design, shared-energy design and strength design. These principles are illustrated in the figure below.

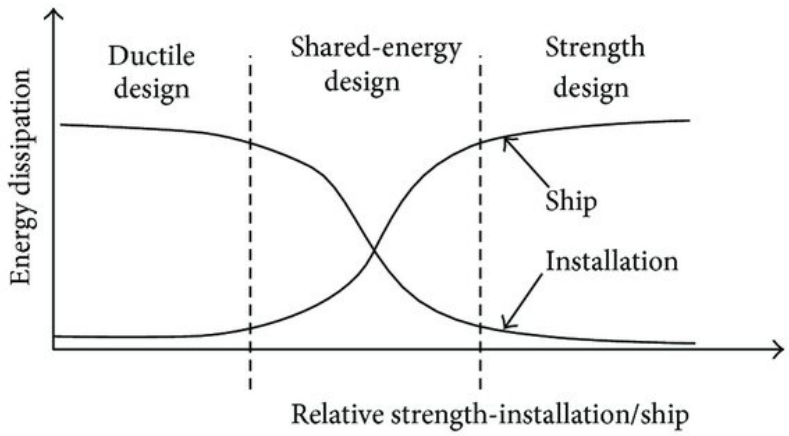


Figure 2.3: Design principles with respect to the share of strain energy dissipation between systems [20].

In strength design, the body impacting the ship is fairly strong, in the sense that it resists the contact by showing little deformation. To dissipate the impact energy, the ship, however, undergoes large deformation. In ductile design, the opposite is assumed, i.e. the body in contact dissipates almost all the energy by undergoing large plastic deformation. The shared-energy approach assumes that both bodies dissipate energy and that in the ship-fender contact the ship's compliance contributes to the dissipation of energy during berthing. The strength design approach is not useful for fender-ship contact. As a fender is designed to absorb the energy of a berthing vessel and does so by deformation of the rubber. However, the ductile approach assumes that no energy is dissipated by the ship. As a fender panel is relatively rigid, the ductile design concept might be too simple.

However, the ductile design approach has been applied in previous research and has been shown

to be an adequate assumption when the (buckling) fender is relatively flexible compared to the ship [14]. Nevertheless, for vessels with small kinetic energy, a buckling fender might perform as rigid, as a result of the low mass of the ship. Figure 2.4 shows the absorbing capacity of different fenders. To determine whether the shared-energy or ductile design concept of the ship's side structure is more realistic, fenders equipped with panels are studied in relation to the ship's compliance. In general, in the Ultimate Limit State (ULS), which focuses on the onset of plasticity, the resistance of the hull has to lie within the strength domain, as the structural response is essentially elastic with only very little plastic deformation [2].


Figure 2.4: Energy absorption behaviour of different fender types [8].

Li, Hu and Jiang studied the elastic and plastic response of a ship in contact with a jacked platform and conducted a sensitivity analysis of the contact points [14]. The analysis is discussed in the following section. Li, Hu and Jiang argued that the NORSOK rules underestimate the capacity of a ship to dissipate energy in elastic response. It underlines the importance of closely determining the contribution of a ship's compliance during impact. The elastic deformation in a collision, the subject of the Li et al. study, reduced the impact loads by local energy dissipation. They showed that the elastic energy absorption results in a 'buffering effect' during dynamic impact on a ship hull.

Quinton studied the load-displacement behaviour of ship parallel side hulls [22]. He looked at the behaviour of steel stiffened panels, to determine the energy dissipation of a ship's parallel side structure in the ice floe-ship impact. On a basic level, he simulates the ship's side hull as a stiffened steel panel. The force-displacement curve for a steel stiffened panel, representative of a ship's parallel side hull, is shown in Figure 2.5. The load-displacement curve of the stiffened panel contains a linear elastic region before the yield point. Quinton showed that is it possible to determine the elastic response of a specific ship side structure using the finite element analysis (FEA).

When applying the shared-energy concept of the NORSOK rule, a shared load-displacement curve for the fender-ship system is obtained. The dissipation of strain energy in the ship-fender shared load-deformation curve looks similar to Figure 2.3. The corresponding equation to determine the strain energy dissipated in the ship, $E_{s,s}$ and the fender, $E_{s,f}$ is given below.

$$E_S = E_{s,s} + E_{s,f} = \int_0^{W_{s,max}} R_s dw_s + \int_0^{W_{f,max}} R_f dw_f \tag{2.5}$$

Where $R_s$ is the reaction force in the ship, $R_f$ is the reaction force in the fender. The displacements for the ship and fender are $w_s$ and, $w_f$ respectively.

A formulation for the total energy that should be absorbed by ship and fender during berthing is given in the PIANC guidelines [19]. The equation for the kinetic design energy is given below.

$$E_d = (\frac{1}{2} M_d V_B^2) \cdot C_e \cdot C_m \cdot C_s \cdot C_c \tag{2.6}$$

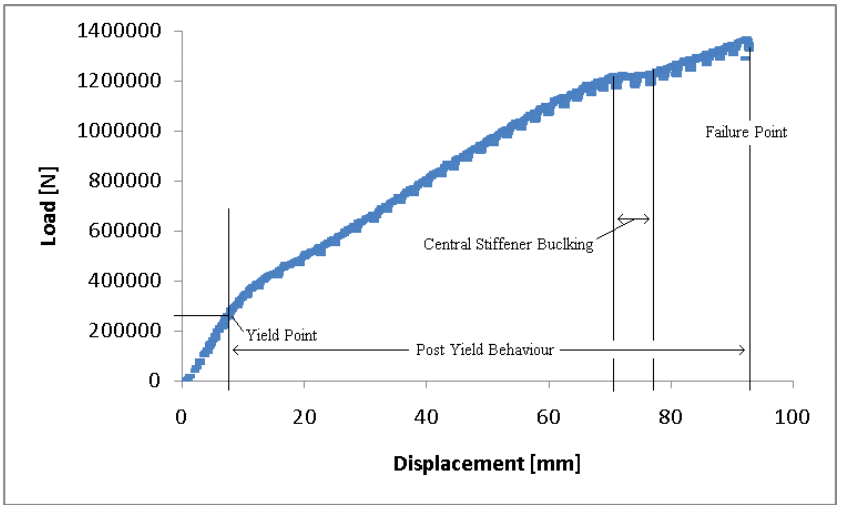


Figure 2.5: Load-displacement curve for a steel stiffener panel in a study to ship-ice floe impact [22].

Where $E_d$ is the design kinetic energy, $M_d$ is the mass and added mass of the berthing vessel and $V_B$ is the initial berthing velocity perpendicular to the berth. Furthermore, $C_e$ is the eccentricity factor that accounts for reduced energy absorption under an angle. Typical values are between 0.3 and 1.0, for parallel berthing, $C_e = 1.0$ is adopted. $C_m$ is the virtual mass factor accounting for the hydrodynamic added mass. It enlarges the mass of the ship by including the virtual mass, depending on the clearance under the keel. For $C_m$, a value between 1.5 and 1.8 can be adopted. $C_s$ is the softness factor to incorporate the proportion of the energy that is absorbed by the elastic deformation of a ship's side hull. As pointed out before, the softness factor will be validated in this research using the shared-energy design approach. $C_c$ includes the berthing configuration. A solid quay wall for parallel approach, under keel less than 15% of the vessel's draught, results in a value of $C_c = 0.9$ [10]. All other berthing configurations adopt $C_c = 1.0$.

Generally speaking, it is fair to assume that the relative strong object experiences less damage with a ductile approach [20]. However, Quinton [22] and Li et al. [14] endorsed the importance of mapping the share of the ship's compliance. Therefore, Chapter 5 elaborates on the generation of the load-displacement curves for the fender, ship and the combined system. The load curves for the ship and fender are obtained in simulations where the other body acts as rigid.

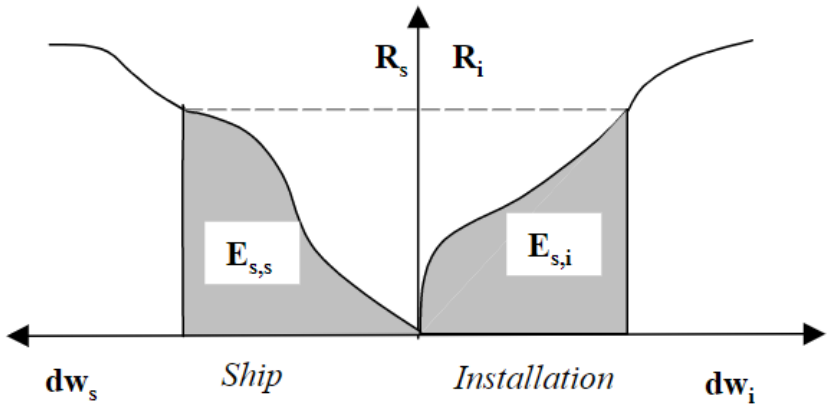


Figure 2.6: Schematic representation of a shared-energy load-deformation curve for ship and installation (fender) [20].

## 2.4. Sensitivity to impact location and area

To determine the parameter sensitivity, several studies on the influence of the location and the area on contact damage to ships are analysed [2, 14, 33]. The significance of the impact location and distribution for ultimate strength assessment of stiffened panels in impact problems was addressed at an early stage by Luo and Edlund [16]. They stressed the influence of load position, load distribution length and other geometrical parameters on the ultimate strength in patch load impact.

Wang, Yu and Basu studied the load-carrying capacity of LNG vessels to withstand ice loads [34]. They presented the pressure-deflection curve for accidental loads of five different locations on the bow and the parallel hull. The impact resistance to the ice floe was highest at a web frame or an intersection of a web frame and stringer (vertical frame). Wang, Tamura, Jiang and Zhou proposed a systematic study to assess the structural response of offshore supply vessels to impact [33]. They determined the design criteria that should be addressed for contact damage:

- Design berthing condition, including maximum kinetic energy;
- Areas of Offshore Supply Vessel (OSV) hull for design against contact damage;
- Design load and considered marine rubber fenders;
- Scantling criteria of structural members (side beam, web frames, deck beams);
- Design of structural arrangements and details such as brackets;
- Options for mitigating contact damage.

The allowable impact pressure for OSV's according to their study is 15 tonnes/m$^2$, which is roughly 150 kN/m$^2$. This type of vessel is not described in the PIANC guidelines and, therefore, this vessel type is not within the scope of this research. However, the design criteria proposed by Wang et al. are relevant to and applied in this study.

More examples of studies on patch loading were found in the field of Arctic engineering, where ice collides with vessels regularly [2, 21, 33]. The main difference between ice collision and fender contact is that in fender contact, plastic deformation is not acceptable. Price et al. proposed an algorithm for the shared-energy approach for ship-ice interaction. This algorithm is based on the ice collision energy and the internal response of the ice and the structure. Furthermore, Amdahl studied the pressure-area ($p - A$) relationship in ship-ice floe contact[2]. In the Ultimate Limit State (ULS) region, where small yielding and plastic deformations are accepted, the pressure-area relationship is different for local and global structural vessel geometry. Amdahl studied the local and global structural response to the crushing of ice and energy-absorbing capacities. Amdahl's study suggests that the current constant pressure-area relationship proposed by PIANC might not result in the safe application when large panel areas are concerned. As Amdahl focuses on plastic deformation, this hypothesis has to be tested in the current study to the onset of plasticity. Moreover, Wang et al. found the governing failure to occur in different structural components depending on the impact location of ice [33]. The study endorses the importance of the location of the impact, which can influence the dimensions of the fender panel. The pressure-area relationship and the impact location are discussed and applied in Chapter 5.

The structural diversity of vessels results in different failure behaviour as well as different failure thresholds. This also applies to the design conditions that are considered for the modelling of fender panel loading. The influence of these parameters as well as the determination of the critical loading condition of the vessel in fender panel loading is of crucial importance to be able to define a safe hull pressure range for vessels within the PIANC guidelines. As Amdahl showed, the pressure-area relationship is important in ice floe impact and Wang et al. showed that the plastic failure differed in case of ice impact, depending on the impact location [2, 33].

## 2.5. Conclusion

Topics related to fender-ship contact and impact of concentrated patches on the hull of ships have been found in the literature. Systematic numerical simulations for the impact of cylindrical fenders were executed by Vredeveldt and Rhijsburger [32]. IJzerman came up with a semi-analytical formulation for plate and stiffener failure of fender impact on stiffened panels in between web frames [12], however,

tripping failure in contact with fenders has not been described. Nevertheless, there are indications in practice that tripping occurs due to fender loading [3]. Sheikh et al. determined two parametric ratios that influence the occurrence of tripping in stiffened panel elements [26]. The formulations for critical tripping pressure by Adamchak and Shahabian and Roberts show to be applicable for the fender panel application [1, 25]. However, modifications have to be made to the pre-buckling stress fields. Moreover, Li et al. suggested that the shared energy approach can play a small but significant part in elastic impact problems as well [14]. Furthermore, a possible hypothesis that might be of use for this research is found in the study of Amdahl [2]. Amdahl researched the pressure-area ($p-A$) relationship in ship-ice floe contact. In the Ultimate Limit State (ULS) region, where small yielding and plastic deformations are accepted, the pressure-area relationship is different for the geometry of local and global structural elements of the vessel. He studied the pressure-area relation for the crushing of ice and energy absorbing capacities of the structure. The research by Amdahl underlines the importance of this relation, which could also be of importance to fender panel allowable pressure-area relationships. Wang et al. found the governing failure to occur in different structural components depending on the impact location of ice [33]. In this research, the following elements from the literature are further elaborated and applied to ship-fender contact. The numerical simulations of Vredeveldt and Rhijsburger are expanded by implementing fenders with larger areas. The formulation of IJzerman is extended with tripping failure by modifying the pre-buckling stress field of Shahabian and Roberts. The sensitivity of tripping is examined using the parametric ratios proposed by Sheikh. In the numerical simulations, the elastic energy absorbing proportion of the vessels is tested. Furthermore, the influence of the fender area and impact location are investigated.

# 3

# Methodology

The aim of this thesis is to assess the main research question by determining the governing failure modes due to fender loading and by quantifying the hull loading that results in critical failure modes both analytically and with numerical simulations. In this chapter, the key concepts of the literature are translated into the methodology of this thesis. The scope of the research is divided into two parts, analytical models and numerical simulations. The analytical part is limited to tripping failure under patch loading, as other indicated failure modes are covered in prior studies. The numerical simulations cover the parallel hull of three vessel types. The onset of plasticity, also known as the Ultimate Limit State (ULS), is the threshold that is studied. Other load cases, for example, fenders with bow and stern region or belting, are beyond the scope of this master thesis.

## 3.1. Analytical model

The objective of the analytical approach is to quantify the critical contact pressure for lateral-torsional buckling, i.e. tripping failure, of stiffeners. The advantage of analytical formulations is the possibility to swiftly obtain results for different dimensions and properties. Several approaches are available to obtain critical pressure on stiffeners. The formulations considered in this study are both based on the Rayleigh-Ritz approximation. The lowest energy state where the energy of the external load equals the internal strain energy of the tripping deformation is estimated as the lower limit of the external load to deformation. The first formulation is proposed by Adamchak and describes critical in-plane loads and uniform lateral pressure, or a combination of these loads [1]. The uniform lateral pressure is relevant to this research. Therefore, it is discussed and validated for the fender load case in Chapter 4. The internal stress field arising from lateral pressure is determined by integrating the work done over the web of the stiffener. The second approach is by Shahabian and Roberts, they modified the pre-buckling stress field of Adamchak to describe the critical lateral pressure concentrated on an area of the stiffener web [25]. The stress field of Shahabian and Roberts has limitations in the applicability to flanged stiffeners, as the stress field does not reach an equilibrium. For the other failure modes occurring in contact between the ship and the fender panel, the semi-analytical formulation by IJzerman is relied on. In the last part of this thesis, the outcomes of those formulations are held against the outcomes of the research by IJzerman. In order to investigate the influence of the dimensions of fender panels and hull geometries, a parametric study is carried out. The study of Sheikh et al. determined two parameters that are influential for tripping failure and are subjected to a parametric study of the selected hulls [26]. Furthermore, the obtained critical pressures of the analytical approach are subjected to a parametric range to study the influential parameters.

## 3.2. Numerical simulations

In order to quantify the allowable loading of fender panels on different parallel hulls, numerical simulations are executed. The models are constructed in LS-DYNA Finite Element Software (FEM) and are also used in the systematic impact simulations of cylindrical fenders by Vredeveldt and Rhijsburger [32]. An overview of the vessel types and sizes included in this study is given in Table 3.1. In Appendix A the parallel hull sections and properties of the vessels are shown. The study of cylindrical fenders showed

the safe application of the fenders in the Port of Rotterdam. The methodology applied is useful for this research, but is enhanced by doing an intensive study to search for a trend in critical loading. The NORSOK strength and shared-energy approach described in Section 2.3 is investigated using force-displacement curves for the fenders and vessel hulls obtained from the numerical simulations. The elastic buffering effect of structures as addressed by Li et al. is quantified [14]. The study by Amdahl on ship-ice floe contact suggested that the pressure-area relationship is not linear or constant when the impact geometry moves from local to global structural zones [2]. Moreover, Wang et al. showed that for ice impact, the governing failure mode varied in different impact locations [33]. Therefore, the numerical simulations are tested for the sensitivity to these parameters.

Table 3.1: Vessels and corresponding properties [32].

| **Ship** | **Vessel type** | **Capacity** | **Length o.a. [m]** | **Breadth mld. [m]** | **Depth [m]** | **Draught [m]** | **PIANC allowable hull pressure [kN/m$^2$]** |
|---|---|---|---|---|---|---|---|
| **T1** | Tanker (coaster) | 7000t DWT | 104.52 | 17.00 | 9.50 | 6.30 | 350 |
| **B1** | Bulk carrier (coaster) Handy-size | 39,000t DWT | 179.90 | 30.00 | 14.80 | 10.60 | 200 to 320 |
| **B3** | Bulk carrier Handy-max/Panamax | 58,800t DWT | 196.00 | 32.26 | 18.60 | 13.00 | 200 to 320 |
| **B2** | Bulk carrier Cape-size (VLBC) | 250,000t DWT | 330.07 | 57.00 | 25.10 | 18.00 | 200 to 320 |
| **C1** | Container vessel | 754 TEU | 146.25 | 19.70 | 11.45 | 8.25 | 400 |
| **C2** | Container feeder | 8200t DWT | 118.14 | 15.90 | 8.80 | 7.21 | 400 |
| **C3** | Container vessel Panamax/Post-Panamax | 9000 TEU | 299.92 | 48.20 | 24.80 | 14.50 | 300 |
| **C4** | Container vessel New Panamax (ULVC) | 19,000 TEU | 400.00 | 58.60 | 30.50 | 14.50 | 200 |

# 4

# Analytical model

This chapter discusses the analytical solutions for the ship-fender panel contact. The analytical model is limited to stiffened panels. Plate- and stiffener-induced failure modes for the ship's parallel side hull loaded by transverse patch loads are already formulated [12]. The tripping failure mode lacks an analytical solution for stiffeners with a flange with loads such as fenders. In order to describe the critical tripping loading of a fender panel on the parallel hull, two analytical formulations are explored. First, the model of Adamchak for uniform lateral pressure is discussed. Then, the Shahabian and Roberts approach is considered for patch loading on the web. After both solutions are introduced, Section 4.3 compares the pre-buckling stress field to a patch-loaded stiffener web in a Finite Element Model (FEM). Then, modifications to the solutions are suggested for patch loads of flanges stiffeners (and ship hulls) and compared to two FEM configurations are discussed. The modified formulation is applied to representative stiffened panels, and the parametric approach for the tripping model is discussed.

## 4.1. Adamchak's formulation

In this section, the derivation by Adamchak of the critical lateral pressure to induce tripping is introduced [1]. In section 4.2, the same principle is used to derive the critical pressure, but for a patch load.

The critical load is derived based on the Rayleigh-Ritz method. The method describes that an unknown solution can be estimated by minimizing the value for the parameters that are substituted into the energy balance. According to the theory, any other solution which satisfies the boundary condition leads to greater potential energy. The principle holds for elastic materials and uses virtual work in the material. The work by the applied load is equated to the internal strain energy. The formulations account for the rotational resistance of the plating to which the stiffener is attached and stiffener web deformations for in-plane loading. Furthermore, the formulations allow taking non-linear material and structural behaviour by a tangent modulus approach into account. However, as this research focuses on the elastic behaviour and the onset of plasticity in tripping, the latter is not considered. At the onset of tripping failure, the internal strain energy ($V$) is equal to the external work ($W$) for an assumed displacement function, which is shown in the following equation.

$$V = W \tag{4.1}$$

$W$ is work done by the internal stress field arising from the lateral loading or the axial stress integrated over the stiffener end. In the case of a combined loading condition, the stress field can be separated and computed according to the following formulations. After, the work of the axial compression and the lateral pressure add up to the total work by the combined loads.

The work by axial compression is formulated by integrating the axial stress over the end of the stiffener, the coordinate system corresponding to Equation 4.2 is shown in Figure 2.2.

$$W = \int\int \sigma_x \delta(y,z) dy dz \tag{4.2}$$

Work done by lateral pressure on the stiffener is calculated using the internal stress field.

$$W = \frac{1}{2}\int_0^a \int_0^{d_w(x)} \left[\sigma_x (v_x)^2 + \sigma_z (v_z)^2 - 2\tau_{xz} v_x v_z\right] t_w dz dx + \frac{1}{2}\int_0^a \left[\sigma_x \left(v_x^2 + w_x^2\right)\right]_{z=d_c} f_w t_f dx \tag{4.3}$$

The first part in Equation 4.3 describes the work of the stress field in the web of the stiffener. The latter captures the contribution of the stress field in the flange of the stiffener. In the above, the work done by axial load, Equation 4.2, and lateral load, Equation 4.3 are presented. For the ship-fender impact, the uniform lateral pressure formulation is relevant. Therefore, the axial load formulation is not considered after this, but axial stress arises naturally in the stress field of lateral pressure.

The corresponding equilibrium for in-plane axial stress and shear stress are as follows.

$$\frac{\partial \sigma_x}{\partial x} - \frac{\partial \tau_{xy}}{\partial y} = 0 \qquad \frac{\partial \sigma_y}{\partial y} - \frac{\partial \tau_{xy}}{\partial x} = 0 \tag{4.4}$$

The pre-buckling stress field is the starting point of this derivation. Where the stress field proposed by Adamchak is given below for a single stiffener with the relevant frame spacing and simply supported at the ends. The stress field representing uniform lateral pressure on a single stiffener with attached plating with simply supported boundaries is:

$$\sigma_x = \frac{1}{2}\left(\frac{q}{I}\right)\left(z - h + \frac{1}{2}t\right)\left(x^2 - ax\right) \tag{4.5}$$

$$\sigma_z = \left(\frac{q}{t_w}\right) - \left(\frac{q}{I}\right)\left[\frac{A_f z}{t_w}\left(d_c - h + \frac{1}{2}t\right) + z\left\{\frac{1}{2}d_w^2 - \frac{1}{6}z^2 + \left(h - \frac{1}{2}t\right)\left(\frac{1}{2}z_{w-d_w}\right)\right\}\right] \tag{4.6}$$

$$\tau_{xz} = \frac{1}{2}\left(\frac{q}{I}\right)(a - 2x)\left[\frac{A_f}{t_w}\left(d_c - h + \frac{1}{2}t\right) + \frac{1}{2}d_w^2 - \frac{1}{2}z^2 + \left(h - \frac{1}{2}t\right)(z - d_w)\right] \tag{4.7}$$

Where $q$ is the pressure, $I$ the moment of inertia of the stiffener, $h$ the height of the neutral axis, $a$ the web frame spacing, i.e. stiffener length, and $A_f$ the area of the stiffener flange, $t_w$ the thickness of the web plate and $d_c$ and $d_w$, respectively, the stiffener depth to the mid-thickness of the flange and the web height. A schematic overview of the dimensions is presented in Figure 2.2.

The internal strain energy for flat bars and stiffeners with a flange is determined with the following equation:

$$V_{\text{flanged stiffener}} = \frac{1}{2}\int_0^a \left[E\left(I_z \bar{s}^2 + \Gamma\right)\beta_{xx}^2 + GJ\beta_x^2 + C\beta^2\right] dx \tag{4.8}$$

To calculate the internal strain energy in the stiffener and the external work by the load an assumed displacement, $\beta$, has to be adopted. To account for the continuity of a ship structure, the second derivative of the displacement, $\beta_{xx}$, has to be zero at the ends of the stiffener ($x = 0$ and $x = a$). The simplest formulation that holds is $\beta = \beta_0 * \sin\frac{m\pi x}{a}$ and can be adopted for axial compression. However, the buckling shape for the lateral pressure results in a high stress, $\sigma_x$, around the mid-length of the stiffener. The simple formulation for $\beta$ results in relatively large errors when comparing the assumed and actual buckling shapes. Therefore, the buckling shape formulation has to be updated by including the next higher mode along with the primary buckling mode shape. The improved formulation is given below.

$$\beta = \beta_0\left[K\sin\frac{m\pi x}{a} + (K-1)\sin\frac{(m+2)\pi x}{a}\right] \tag{4.9}$$

In the formulation, $m$ is the primary mode number and $K$ is an introduced unknown coefficient. The appropriate value for $K$ is selected by minimizing the tripping load, because the Rayleigh-Ritz principle is applied it results in the true load being greater than the minimized value for $K$.

Equation 4.8 is updated for the high stress at the mid-length by implementing Equation 4.9. Resulting in Equation 4.10 to determine the internal strain energy for flanged stiffener and Equation 4.11 for flat bar stiffeners.

$$V = \frac{1}{4} a \beta_0^2 \left(\frac{\pi}{a}\right)^2 GJ \mathrm{H}_m(\mathrm{K}) \tag{4.10}$$

Where:

$a$ = Length of the stiffeners between the (transverse) support;

$E$,$G$ = Young's and shear modulus;

$C$ = Rotational spring constant per unit length of support structure;

$I_z$ (=$\frac{1}{12}(t_f f_w^3 + d_w t_w^3)$ = Moment of inertia about the web plane;

$\bar{s}$ (=$\frac{1}{2}[d_w + \frac{d_w + t_f}{1+(d_w/t_f)(t_w/f_w)^3}]$) = Height of centroid above toe;

$\Gamma$ (=$\frac{1}{36}(t_w^3 d_w^3 + \frac{1}{4} t_f^3 f_w^3)$) = Longitudinal warping constant;

$J$ (=$\frac{1}{3}(d_w t_w^3 + f_w t_f^3)$) = St. Venant's torsion constant.

$$V = \frac{1}{12} d_w a d B_0^2 \left(\frac{\pi}{a}\right)^2 \bar{H}_m(K) \tag{4.11}$$

The quadratic functions for tripping under lateral pressure are given by $H_m(K)$ and $\bar{H}_m(K)$ and made explicit below.

$$\begin{aligned} H_M(K) =& [(m^2K^2 + (m+2)^2(K-1)^2) + (m^4K^2 \\ &+ (m+2)^4(K-1)^2)(\frac{\pi}{a})^2(\frac{E}{GJ})(I_z s^{-2} + \Gamma) \\ &+ (K^2 + (K-1)^2)(\frac{a}{\pi})^2 \frac{C}{GJ}] \end{aligned} \tag{4.12}$$

$$\begin{aligned} \bar{H}_M(K) =& [(\frac{\pi d}{a})^2(m^2K^2 + (m+2)^2(K-1)^2) \\ &+ 6(1-v)(m^2K^2 + (m+2)^2(K-1)^2) \\ &+ \frac{2C}{d_w d_c}(\frac{a}{\pi})^2(K^2 + (K-1)^2)] \end{aligned} \tag{4.13}$$

Ultimately, the internal strain energy $V$ is set equal to the external work $W$. The critical pressure $q$, introduced in the stress field in Equations 4.5, 4.6 and 4.7, is found by solving the set of equations for the buckling coefficient $K$. The lowest pressure obtained from is the approximated critical pressure for the onset of tripping failure.

## 4.2. Shahabian and Roberts' formulation

As the pre-buckling stress field of Adamchak covers load cases with uniform lateral pressure, Shahabian and Roberts found the stress field for the patch load. They proposed a stress field for a patch load on a web of a bridge girder. The stress field formulation is also applicable to a stiffener web in a ship hull under a patch load, like a fender load. The stress field of Shahabian and Roberts is split into three parts: underneath the patch load plus the two sides. The work done by a patch load is obtained by considering three separate integrals for these parts. The stress field of Shahabian and Roberts

corresponds to a simply supported web without a flange. The proposed pre-buckling stress field Shahabian and Roberts proposed for the web of the stiffener is shown below. A schematic representation of the stress field adopted by Shahabian and Roberts is presented in Figure 2.2.

For $0 \leq x \leq \frac{a-c}{2}$

$$\sigma_x = \frac{6P}{d_w^3 t_w}\left(y - \frac{d_w}{2}\right)x$$
$$\sigma_y = 0$$
$$\tau_{xy} = \frac{3P}{d_w^3 t_w} y\,(d_w - y)$$

For $\frac{b_w - c}{2} \leq x \leq \frac{b_w + c}{2}$

$$\sigma_x = \frac{6P}{d_w^3 t_w}\left(y - \frac{d_w}{2}\right)\left(-\frac{x^2}{c} + \frac{b_w x}{c} + \frac{b_w}{2} - \frac{c}{4} - \frac{b_w^2}{4c}\right)$$
$$\sigma_y = -\frac{P}{t_w c}\left(1 - 3\frac{y^2}{d_w^2} + 2\frac{y^3}{d_w^3}\right)$$
$$\tau_{xy} = \frac{3P}{d_w^3 t_w} y\,(d_w - y)\left(\frac{b_w - 2x}{c}\right)$$

For $\frac{b_w + c}{2} \leq x \leq b_w$

$$\sigma_x = \frac{6P}{d_w^3 t_w}\,(b_w - x)\left(y - \frac{d_w}{2}\right)$$
$$\sigma_y = 0$$
$$\tau_{xy} = \frac{-3P}{d_w^3 t_w} y\,(d_w - y)$$

The maximum allowable value for the total force $P$ with the related patch dimension $c$ is obtained using the Rayleigh-Ritz approximation. The pre-buckling stress field for Adamchak and Shahabian and Roberts is visualized in Figure 4.1 and the coordinate system is shown in Figure 2.2.

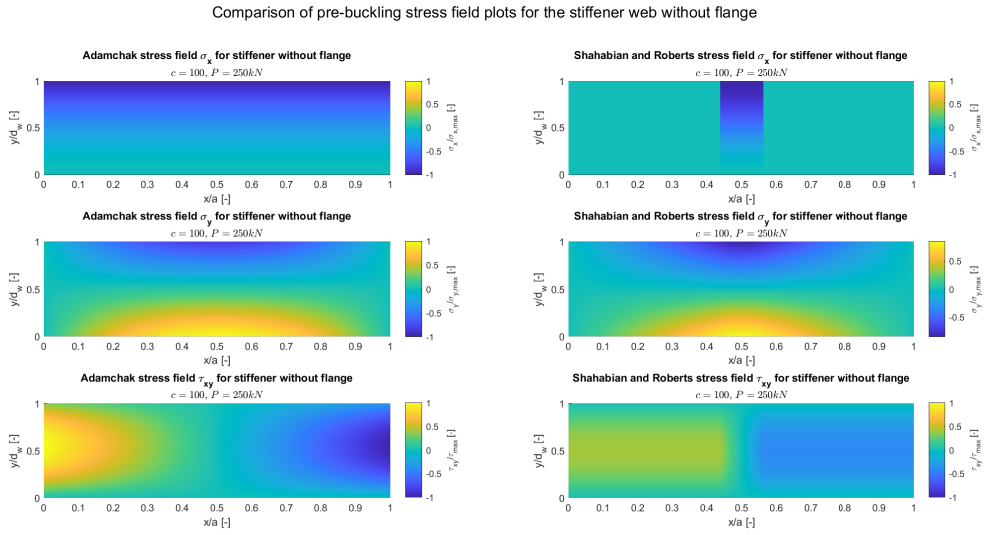


Figure 4.1: Comparison of the analytical pre-buckling stress field proposed by Adamchak [1] and Shahabian and Roberts [25].

Depending on the size of the patch load in relation to the web frame spacing, either Adamchak or Shahabian and Roberts is a good representation of fender panel stiffeners in stiffened hull panels. However, the main shortcoming of Shahabian and Roberts is that no equilibrium is reached for a web with a flange attached.

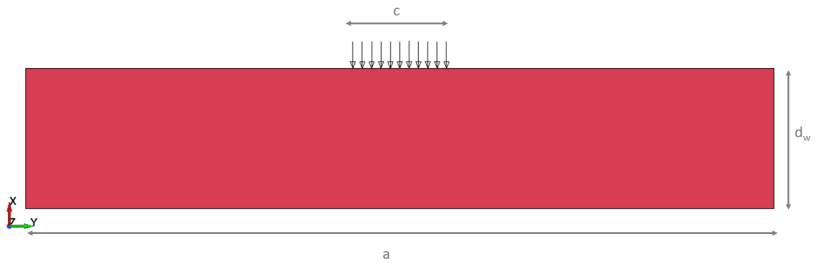


Figure 4.2: Stiffener web with load to validate analytical pre-buckling stress fields.

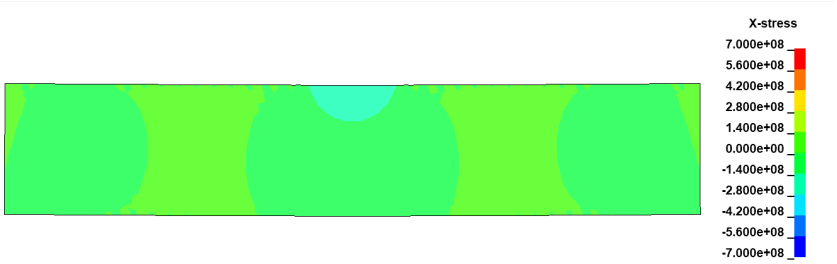


Figure 4.3: FEA stiffener web $\sigma_x$ pre-buckling stress field [Pa].

## 4.3. Validation of pre-buckling stress fields

To determine whether the method of Adamchak or Shahabian and Roberts shows a better representation of a pre-buckling stress field of a web under patch load, both are compared to a Finite Element Model (FEM). The FEM model of a simply supported stiffener is presented in the following figure.

To validate the stress fields from Figure 4.1, the simply supported web from Figure 4.2 is loaded with 22.5 kN over 11 nodes in the middle of the web. The same load is applied to the analytical pre-buckling stress fields and the results are compared with the FEM result.

The stress field from the FE analysis is presented in the three stress components in the following figures.

Table 4.1 summarizes the results. It shows that Shahabian and Roberts stress field extreme values lie closer to the FEM model. Furthermore, the distribution of the stress from Figures 4.3, 4.4 and 4.5 correspond better to the stress field representation of Shahabian and Roberts in figure 4.1.

However, one of the shortcomings of the pre-buckling stress field from Shahabian and Roberts is that it does not satisfy the equilibrium equations, Equation 4.4, for a configuration with a stiffener. To study the influence of that, the next section proposes a modified pre-buckling stress field for a configuration with a stiffener. Then, the original formulation is compared to the modified configuration and both are compared to two configurations with flange in FEM.

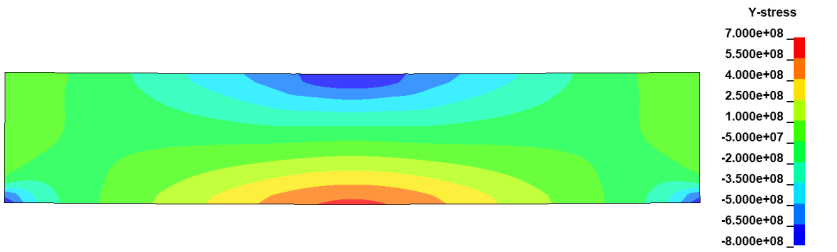


Figure 4.4: FEA stiffener web $\sigma_y$ pre-buckling stress field [Pa].

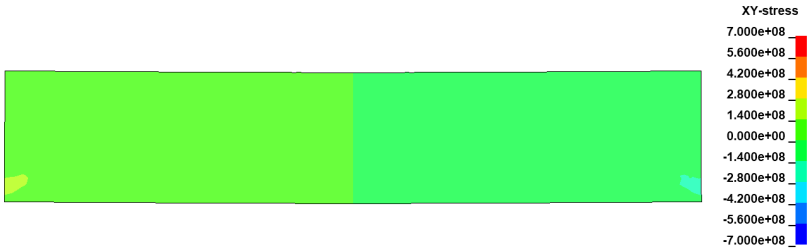


Figure 4.5: FEA stiffener web $\tau_{xy}$ pre-buckling stress field [Pa].

Table 4.1: Comparison of the pre-buckling stress field without a flange.

| Solution without flange | $\sigma_{x,top}$ [MPa] | $\sigma_{x,bottom}$ [MPa] | $\sigma_{y,top}$ [MPa] | $\sigma_{y,bottom}$ [MPa] | $\tau_{xy,top}$ [MPa] | $\tau_{xy,bottom}$ [MPa] |
|---|---|---|---|---|---|---|
| Adamchak [1] | -166.5 | -0.5 | -792 | 968 | -199.5 | 199.5 |
| Shahabian and Roberts [25] | -165 | 0 | -825 | 825 | -82.5 | 82.5 |
| LS-DYNA model | -195 | 0 | -800 | 586 | -230 | 230 |
| Euler-Bernoulli approximation | -152 | 0 | -406 | 406 | -165 | 165 |

## 4.4. Modified Shahabian and Roberts' formulation

The pre-buckling stress field for a patch-loaded stiffener shows agreement with some components of the FEM for a configuration without a flange. In this section, the formulation of Shahabian and Roberts is modified for a configuration with a flange. The effect of the force equilibrium, that is not reached, is identified with two FEM configurations. The modified formulation is based on the derivations of Adamchak in 1979 [1] and Shahabian and Roberts in 1999 [25].

The axial stress, $\sigma_y$, is adapted by redefining the effective vertical moment of inertia of the stiffener, web and flange combination, with the associated effective width of plating. For the effective width, the commonly applied formulation by Von Kármán is used [13].

$$b_{eff} = \frac{\pi \cdot t}{2\sqrt{3\,(1-\nu^2)}}\sqrt{\frac{E}{\sigma_Y}} \tag{4.14}$$

In the original formulation of Shahabian and Roberts the standard equation for an inertia moment for a rectangular cross-section is applied, for a configuration with a flange, the inertia moment is modified. Additionally, the neutral axis is redefined in case a flange is present in the stiffener configuration. Moreover, the total patch load $P$ is rewritten to the equivalent load per unit length $q$ with the patch dimension $c$.

Below the redefined formulation, derived for the three considered sections of the stiffener, is shown. Where $x$ and $y$ indicate the position of the stress in the stiffener web, $h$ is the neutral axis of the plate-stiffener-flange combination from the mid-plane of the attached plating and $t$ is the thickness of the attached shell plate. The moment of inertia around the connection point of the stiffener to the plate is indicated by $I$ and $q$ is the force over a unit of length of the patch with dimension $c$.

For the stress in the x-direction, $\sigma_x$, the following is derived, with a contribution of the internal force over the area of the cross-section and the initiated moment due to the force. It is assumed that the flange transfers the load to the web of the stiffener.

For $0 \leq y \leq \frac{a-c}{2}$

$$\sigma_x = 0 \tag{4.15}$$

For $\frac{a-c}{2} \leq y \leq \frac{a+c}{2}$

$$\sigma_x = -\frac{q}{t_w} + \frac{q}{t_w}\left(3\frac{x^2}{d_w^2} - 2\frac{x^3}{d_w^3}\right) \tag{4.16}$$

For $\frac{a+c}{2} \leq y \leq a$

$$\sigma_x = 0 \tag{4.17}$$

The formulation of Shahabian and Roberts assumes that outside the loaded region, no stress acts in the x-direction. However, the reaction force on the ends of the stiffener web does show stress in the x-direction in the FEM results.

The stress in the y-direction is imposed by the bending moment due to the patch load on the stiffener.
For $0 \leq y \leq \frac{a-c}{2}$

$$\sigma_y = \frac{1}{2}\frac{q}{I}(x - h + \frac{t}{2})cy \tag{4.18}$$

For $\frac{a-c}{2} \leq y \leq \frac{a+c}{2}$

$$\sigma_y = \frac{1}{2}\frac{q}{I}(x - h + \frac{t}{2})(-y^2 + ay + \frac{ac}{2} - \frac{c^2}{4} - \frac{a^2}{4}) \tag{4.19}$$

For $\frac{a+c}{2} \leq y \leq a$

$$\sigma_y = \frac{1}{2}\frac{q}{I}(a - y)c(x - h + \frac{t}{2}) \tag{4.20}$$

For the stress in the shear stress, $\tau_{xy}$, the following is derived.
For $0 \leq y \leq \frac{a-c}{2}$

$$\tau_{xy} = \frac{1}{4}\frac{q}{I}xc(d_w - x) \tag{4.21}$$

For $\frac{a-c}{2} \leq y \leq \frac{a+c}{2}$

$$\tau_{xy} = \frac{Q\bar{y}A}{It} = \frac{1}{4}\frac{q}{I}(\frac{A_f(d_c - h + \frac{t}{2})}{t_w} + \frac{1}{2}d_w^2 - \frac{1}{2}x^2)(a - 2y) \tag{4.22}$$

For $\frac{a+c}{2} \leq y \leq a$

$$\tau_{xy} = -\frac{1}{4}\frac{q}{I}xc(d_w - x) \tag{4.23}$$

The pre-buckling stress field of the original and modified formulation of Shahabian and Roberts are presented in Figure 4.6. The applied load is similar to those applied in the previous section.

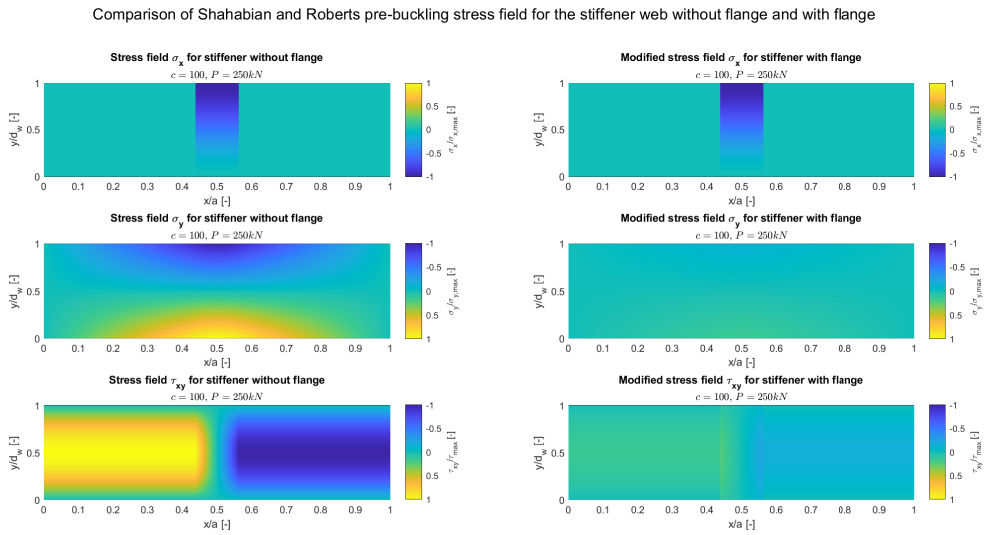


Figure 4.6: Comparison of the analytical pre-buckling stress field of Shahabian and Roberts [25] and the modified formulation for a flanged stiffener.

As the moment of inertia increases with the configurations, it is expected that the stress in the stiffener web decreases. With the addition of the flange, a uniform shear stress distribution in the stiffener web is expected, while for a single web configuration the shear stress has a parabolic distribution. The following two configurations are used to gain insight into the applicability of the modified pre-buckling stress field to patch loads on flanged stiffeners.

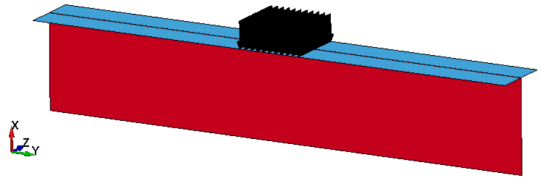

Figure 4.7: Stiffener web and flange combination with load to validate analytical pre-buckling stress fields.

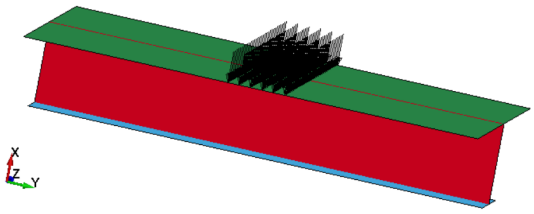

Figure 4.8: Stiffener web with plate and flange with load to validate analytical pre-buckling stress fields.

The figures below show the results of the FEM configurations and are compared to the formulation by Shahabian and Roberts [25] and the modified formulation for a stiffener web with a flange.

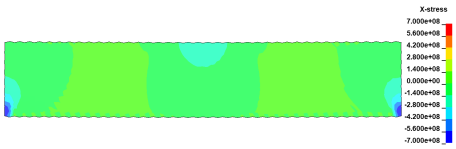

(a) FEA stiffener web-flange combination $\sigma_x$ pre-buckling stress field [Pa].

(b) FEA stiffener web-flange-plate combination $\sigma_x$ pre-buckling stress field [Pa].

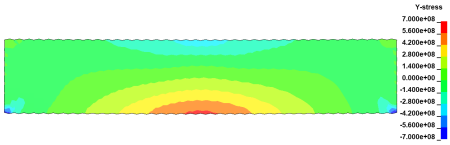

(c) FEA stiffener web-flange combination $\sigma_y$ pre-buckling stress field [Pa].

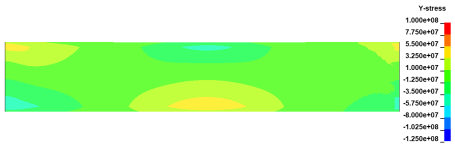

(d) FEA stiffener web-flange-plate combination $\sigma_y$ pre-buckling stress field [Pa].

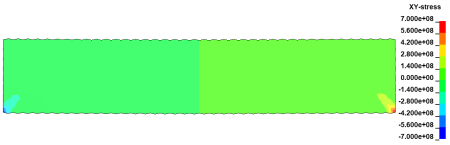

(e) FEA stiffener web-flange combination $\tau_{xy}$ pre-buckling stress field [Pa].

(f) FEA stiffener web-flange-plate combination $\tau_{xy}$ pre-buckling stress field [Pa].

Figure 4.9: Pre-buckling stress fields for two configurations of a stiffener web in LS-DYNA.

The results from the pre-buckling stress fields from the configurations in Figures 4.7 and 4.8 and the analytical stress field in Figure 4.9 are summarized in Table 4.2.

Table 4.2: Comparison of the pre-buckling stress field with patch load with and without a flange.

| Solution with and without flange | $\sigma_{x,top}$ [MPa] | $\sigma_{x,bottom}$ [MPa] | $\sigma_{y,top}$ [MPa] | $\sigma_{y,bottom}$ [MPa] | $\tau_{xy,top}$ [MPa] | $\tau_{xy,bottom}$ [MPa] |
|---|---|---|---|---|---|---|
| Shahabian and Roberts [25] | -165 | 0 | -825 | 825 | -82.5 | 82.5 |
| Modified Shahabian and Roberts | -165 | 0 | -108.5 | 132.5 | -20 | 20 |
| LS-DYNA flange-web configuration | -140 | 0 | -280 | 420 | -100 | 100 |
| LS-DYNA flange-web-plate configuration | -70 | 0 | -55 | 80 | -32.5 | 32.5 |
| Euler-Bernoulli approximation | -49.5 | 0 | -140 | 145 | -24.8 | 24.8 |

From the table, it can be concluded that the stresses decrease when the flange is taken into account in the configuration. However, there is a discrepancy in both methods compared to the FEM results. The FEM results for the flange-web configuration result in higher $\sigma_y$ and $\tau_{xy}$ stresses, while the stress in

the x-direction shows good agreement. However, the results of the configuration of the flange-web-plate show lower stresses in all directions. Nevertheless, the modified configuration can be used to describe load cases for panels that are narrower than the web frame spacing. If the panel engages with the whole width of the stiffened panel between the web frames, Adamchak's formulation is preferred. The schematic representation of these panel dimensions in relation to the stiffened panel is given in Figure 4.10.

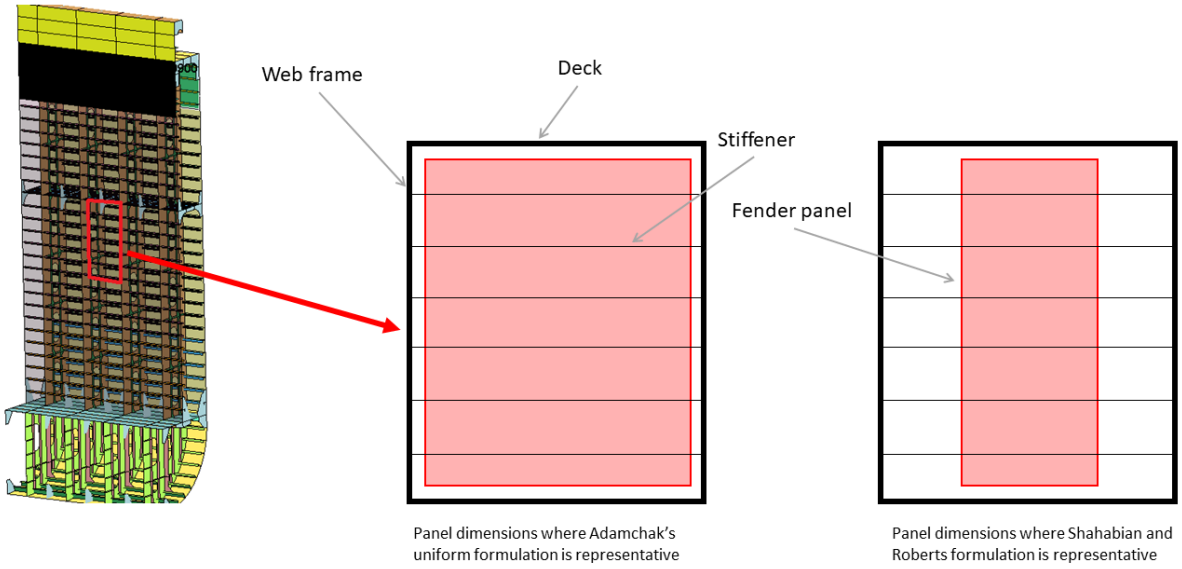


Figure 4.10: Schematic representation of panel dimensions in relation to a stiffened panel in ship hull where Adamchak [1] or Shahabian and Roberts [25] is representative.

## 4.5. Parametric study

In practice, there are indications that tripping occurs due to fender loading [3]. To obtain insight into the structures sensitive to tripping failure in fender contact, a parameter study is executed. The parametric sensitivity study focuses on ratios and non-dimensional formulations from the literature. Sheikh et al. determined two parametric ratios that influence the occurrence of tripping in stiffened panel elements [26]. First, the plate transverse slenderness ratio, $\beta_1$, formulated as

$$\beta_1 = \frac{B}{t}\sqrt{\frac{f_{yp}}{E}}. \tag{4.24}$$

Secondly, the ratio of stiffener torsional slenderness to plate transverse flexural slenderness,$\beta_4$, is given as

$$\beta_4 = \frac{(\frac{s_{wf}}{r})\sqrt{\frac{f_{ys}}{E}}}{(\frac{B}{t})\sqrt{\frac{f_{yp}}{E}}} \tag{4.25}$$

where $f_{yp}$ and $f_{ys}$ indicate the yield strength of the plate and stiffener and $E$ is the material modulus. $B$ is the stiffener spacing, $t$ is the plate thickness, $s_{wf}$ is the length of the stiffened plate panel between the web frames and $r$ is the radius of gyration of the stiffener.

Stiffened panels with higher structural capacities to tripping were found to have low $\beta_1$ and $\beta_4$ values. For $\beta_1$ below 1.5, stiffener tripping is expected. A more complete formulation was proposed by Sheikh et al. to identify stiffener tripping of stiffened steel panels.

$$\text{Stiffener tripping occurs if } (\beta_1 - 2.8)^2 + \beta_2^4 > 1.3^2; \tag{4.26}$$

It is expected that the parameters identifying sensitivity to tripping failure contain information about the properties of the stiffener and the attached plating of the stiffener.

For the parametric study, two grillages are studied that are also used later on in Chapter 5. The first one is the grillage between two web frames of a large container carrier with a layout similar to Figure 4.12. Secondly, the single shell of a large bulk carrier is considered, which is presented in Figure 4.11. To conclude upon the analytical solutions, both Adamchak and also the Shahabian and Roberts solutions are considered. Adamchak is shows to be applicable when a stiffened panel between two web frames is considered to be fully loaded by a fender panel. The uniform pressure load cases then correspond with the load case. However, Adamchak underlined the discrepancy with numerical results as describing the pre-buckling stress field is complex. Furthermore, the modified stress field of Shahabian and Roberts gives a better representation of stiffeners with flanges. Finally, Sheikh's parameters $\beta_1$ and $\beta_4$ describe sensitivity to tripping of panel configurations.

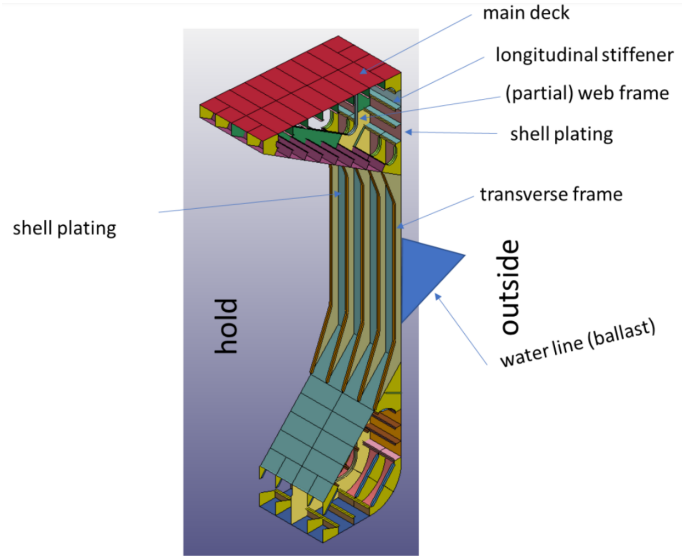


Figure 4.11: Layout of a single shell structure parallel ship hull [32].

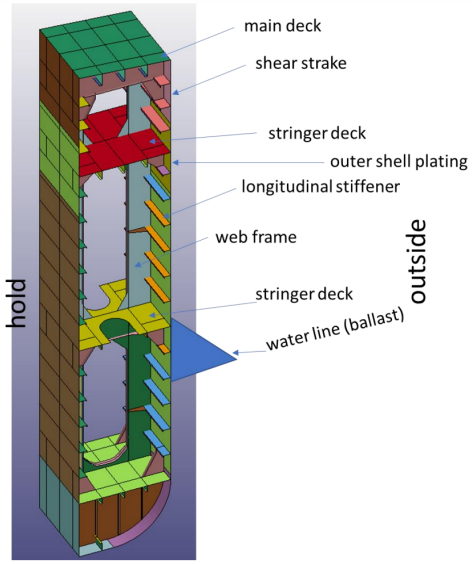


Figure 4.12: Layout of a cell structure parallel ship hull [32].

# 5

# Numerical simulations

In this chapter, numerical simulations with parallel hull sections in contact with a fender panel are presented. The goal is to quantify the allowable loading of fender panels on different parallel hulls. Bulk carriers, tankers and container vessels are tested for their structural capacities. The fender system is simplified to a rigid panel. The first objective is to determine the influence of the compliance of the ship in contact with the fender panel. Then, the hull pressure capacities are quantified and the parametric sensitivity is studied. First, different modelling options for ship-fender contact are explored. Next, the main assumptions and components of the numerical models are presented and the validation of the model is explained. Afterwards, it is described how to obtain a force-displacement curve for the coupled system. Then, the onset of plasticity is elaborated on. Finally, the parametric study for the simulations is presented.

## 5.1. Dynamic and deformation modelling

To gain insight into the structural capacities of the vessel when subjected to a fender panel or similar load, two different modelling options are explored. For both modelling options, only a section of the vessel is considered. It is assumed that in multiple fender contact, the distance between the fenders is sufficiently large that the influence of the fenders is independent.

The two modelling options in LS-DYNA Finite element software that are explored, are as follows:

1. Model the ship by constraining the section to a node with the ship's mass and moment of inertia. The fender is simulated by moving a rigid quay wall and rigid panel with an initial velocity into the parallel hull section. The rubber buckling fender between the quay wall and rigid fender panel is a spring with assigned non-linear properties. The dynamical behaviour and the structural response of the ship are both determined by LS-DYNA.

2. The section of the parallel hull is clamped on the front and aft. A rigid fender panel with imposed constant velocity is moved through the hull. The deformation behaviour and reaction force of the structure are determined by LS-DYNA. Afterwards, an analytical formulation is used to determine the maximal reaction force that occurs in the dynamical behaviour of the coupled fender-ship system.

The advantage of the first method is that it captures the dynamic behaviour of the fender-ship response during berthing impact. However, the complex model makes it numerically expensive and time-consuming to simulate. Taking into account the diversity of both fenders and ships, a larger number of simulations is beneficial. Furthermore, the mass of the ship, the added mass of the water and the inertia heavily influence the dynamic and deformation behaviour of the simulation. An advantage of the second modelling approach is the possibility to account for and study the compliance of the ship in low-speed impact problems. Furthermore, the resulting simulation time is manageable for a parametric study. A disadvantage is the simplification of the dynamic behaviour of the system during and after the impact. After simulating both models in an early stage of the research, the second method is selected.

As the goal of the study is to determine the structural response of the ship's parallel hull and the influence of the impact location, area and ship structural components. Consequently, the advantages of isolating the cross-section with the rigid fender panel make the method preferable for this research.

## 5.2. Components and assumptions

As the simulation set-up is now selected, the components and assumptions in the simulations are elaborated on. The modelling components can highly influence the results of the simulations and are thoroughly tested to specify the limitations and assumptions in the results.

### 5.2.1. Material model

The ship is modelled with Belytschko-Tsay four-node shell elements, where the shell thickness is the plate thickness of the structural component. The selected material for the shell elements is MAT_024 from the LS-DYNA library. It is an elasto-plastic material, where the stress-strain curve and strain rate dependency can be defined arbitrarily. Strain rate effects are implemented with the scaled yield stress using the total strain rate. The plasticity is based on J2, also known as von Mises equivalent stress, yield criterion as shown in the equation below.

$$\Phi(\sigma) = \bar{\sigma} - \sigma_y\left(\varepsilon^p\right) = 0 \tag{5.1}$$

Where $\bar{\sigma}$ is the effective stress, $\sigma_y$ is the yield stress of uniaxial tests and $\varepsilon^p$ is the effective plastic strain. The lowest steel grade, Grade A with a minimum yield strength of 235 $MPa$, approved by class society is applied to the sections [15]. Similar material properties were adopted in previous studies [12, 32].

For the material, linear hardening is assumed. The material is selected as it is a very efficient material model for the application and is typically applied for contact problems in the elastic region. The validation of the material behaviour and yielding are discussed in further detail in Sections 5.3 and 5.5.

### 5.2.2. Boundary conditions and prescribed motion

The parallel side hull of the vessels is limited to a section of the hull [32]. As described in Section 5.1 the section is isolated and clamped in the simulation. The clamped boundaries are imposed at the front and aft plan of the section. The fender panel is not fully constrained to move and rotate in all directions apart from the y-direction translation [18]. In practice, fender panels are partly constrained to rotate by chains but could move in constrained directions as well, see figure below. However, for this research, only the y-translation is considered.

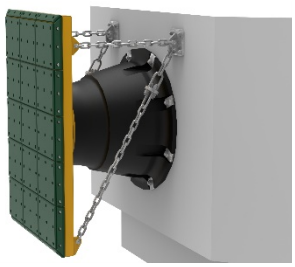

Figure 5.1: Cone fender equipped with panel that is constrained by chains [19].

A constant velocity of 20 $cm/s$ is imposed in the 'moderate' region of berthing speeds in ports [24]. To test the influence of the velocity, two more velocities were analysed as shown below.

- Constant velocity of 20 $cm/s$ (base model);
- Constant velocity of 10 $cm/s$;
- Velocity decreasing from 20 $cm/s$ to 10 $cm/s$ after initial contact.

The reaction force where plasticity occurs is more or less the same for the constant imposed velocities. For the decreasing velocity, the capacity increases by 2.5%.

### 5.2.3. Contact

To indicate the regions in contact in the simulation, a segment-based surface-to-surface contact is selected from the LS-DYNA library. The contact is divided into a master and slave side of the contact. In the fender impact face, the rigid fender panel is the master surface and the ship hull is the slave surface. The advantage of this contact type is that it can be used when the orientation of parts relative to each other can not be predicted. For impact simulations, this is a sensible contact. The contact is treated symmetrically, both the master segments and slave segments are checked for penetration throughout the simulation. The penetration is checked for either side of the shell elements.

Based on PIANC typical design values of coefficients of friction between the fender system and the hull, a value of 0.5 is adopted [19]. Most fender panels have polyethylene facings, and the related friction coefficient against a steel hull is $\geq 0.4$. To account for rough surface, temperature and dry contact, a higher value is advised and adopted.

On the contact card, friction properties are defined. The friction coefficient is varied between 0 and 0.6 to determine the influence on the maximum reaction force before plasticity occurs. For the analysis, the friction coefficient $\mu_s = 0$ and $\mu_s = 0.6$ resulted in the reaction forces being within 1% of each other. Therefore, the influence of friction is negligible in the simulations.

In the early stage of the research, force-time curves showed a large spike at the initial contact time. Afterwards, the force moved to a much lower value and steadily progressed with the increase of deformation. The spike is a numerical effect of the rigidity of the fender panel and the constant imposed velocity. The panel is modelled as rigid and cannot deform at the first contact with the ship. However, the panel moves with a constant speed and in the simulation, the hull is imposed with an acceleration in the initial contact with the panel. As a result, the reaction force becomes relatively large. This is overcome by implementing a soft constraint to the contact. Using the SOFT = 2 determines the first is contact does not produce a large force, which corresponds better with fender panels in contact with the ships in real cases. After applying the A-card, the force increases steadily with the displacement of the fender panel into the ship's hull. The influence of the peak at the initial contact was found to be in a range of 1 to 2.5% lower maximum allowable reaction force.

### 5.2.4. Structural layout hulls

For this research, eight vessels are analysed for their structural properties and the impact resistance related to them. Bulk carriers, tankers and container vessels of different sizes are included in the study. An overview and detailed properties of the vessels are summarized in Appendix A. Later on in Section 5.6.3, the representative hulls are selected. In the literature, several indications were found that the structural layout influences the structural capacity to resist transverse loading [14, 34]. Roughly two structural layouts are observed in the vessels for this research, single and double, or cell, shell hulls [32]. The single shell consists of shell plating with stiffeners attached, Figure 4.11. The cell structure is built up of two shell plates with stiffeners and those are connected with web frames, Figure 4.12. Depending on if the load acts in the middle of a plate with stiffeners in between web frames, partly on a web frame or centred on a web frame, different structural behaviour is expected. The panel with stiffeners is identified as the weak spot in the ship structure in most literature. To test this hypothesis in concentrated transverse impact, the impact is simulated at different locations of the hull.

## 5.3. Calibration and validation

The numerical simulations are executed to represent the ship's structural response to fenders and should behave realistically. Some assumptions are done in the previous section regarding the behaviour. Furthermore, the sensitivity to input parameters such as friction and speed have been addressed. In this part, the calibration and validation steps of the model are discussed.

At first, the influence of the boundary conditions and the deformation behaviour of the structure when impacted by the panel are checked visually. No unexpected local stress concentrations were found near the boundaries. With the increasing displacement of the fender panel, the vessel hull deforms.

Looking at the deformation to force behaviour, first the effect of the rigidity of the fender panel is observed. The rigid panel influences the reaction force unnaturally at the initial contact. The panel imposes a constant velocity on the hull. Therefore, it is accelerated from zero to the velocity in one time step. The force is the result of the acceleration and the mass. After an A-card, or SOFT-card, was added to the simulations, the reaction force increased steadily with the displacement of the panel. The

reaction force to impose deformation decreases after the ship's structure has failed in such a way that structural capacity is lost.

To validate the onset of plasticity, the equivalent von Mises stress and the strain of the hull are validated with the following procedure. The validation is executed for a 19,000 TEU container vessel impacted by a 6m × 2m rigid fender panel. For the material applied in the base model simulation, the following properties hold.

- Yield strength: $\sigma_y = 235MPa$
- Material modulus: $E = 206GPa$

Similar material properties are adopted as in prior studies by Vredeveldt and Rhijsburger in 2018 [32] and IJzerman in 2021 [12] to allow for comparison of the results of this study to results of their studies.

At 13 $mm$ displacement of the fender panel into the hull, the onset of plasticity starts in the numerical model at a mean effective strain of $\varepsilon = 1137\mu m/m$. For the theoretical elastic strain at the onset of plasticity it is known to be $\varepsilon_e = \frac{\sigma_y}{E}$. The theoretical effective elastic strain is $\varepsilon_e = 1140\mu m/m$.

In LS-DYNA, at the onset of plasticity, the effective elastic strain corresponds closely to the theoretical elastic strain. The plastic strain at the onset of plasticity is zero and increases in the first time step after the onset of plasticity to $\varepsilon_p = 10\mu m/m$. All strain values are extracted per element and averaged over the three integration points over the thickness of the element. The first element showing plastic strain at the validation point also has a von Mises stress exceeding the yield stress of the material.

The last validation that is executed is the validation of the contact behaviour. As the contact should be symmetric, the reaction force for the slave- and master segments are studied. The reaction force is equal and shows a similar course over time. Lastly, the panel is restricted to move in the translational y-direction and the main proportion, 98%, of the reaction force originates from the y-component.

No full validation of the numerical model behaviour was reached during the project. It was too numerically expensive to do a full convergence study using a mesh sensitivity analysis in LS-DYNA for very large geometries. Furthermore, no experimental data was found in the literature that could validate the models. However, the simulations were executed according to the DNV recommended practice for determination of structural capacity by non-linear FEA [**DetNorskeVeritas2013DDNV-RP-C208Methods**]. Therefore, the author argues that the outcomes of the model are trustworthy as analytical validations, and deformation validations were executed and the simulations are performed according to DNV-RP-C208.

## 5.4. Coupled system force-displacement behaviour

The influence of the elastic energy absorbing capacity by the ship in fender-ship contact has not been taken into account before. The study by Li questions the NORSOK N-004 rule, which assumes that the ships take no energy absorbing capacity [14, 20]. As proposed by Li et al. and in the NORSOK N-004 rules, the components are represented by force-displacement (F/d) curves. The elastic energy absorbing capacity, or the buffering effect, is expected to be a relatively small portion compared to the fender. To determine the proportion added by the compliance of the ship, this section examines the elastic structural response of the fender, ship and the coupled system.

### 5.4.1. Fender force-displacement curves

The fender force-displacement curve is provided by the manufacturer and is based on a design situation with an initial velocity of 0.15 m/s, a temperature of 23 degrees$\pm 5^{\circ}C$ and $0^{\circ}$ compression angle [27, 31]. Depending on the type of buckling fender, the maximum deflection as a percentage of the dimension of the fender varies.

Previous research implemented cylindrical rubber fenders with linear force-displacement behaviour. The fender panel and the associated buckling fender correspond with non-linear force-displacement curves.

The fenders considered for this study are [27]:

- SPC Cone Fender 1200 G2.9
- FE Element Fender 1600x2000 G1.4

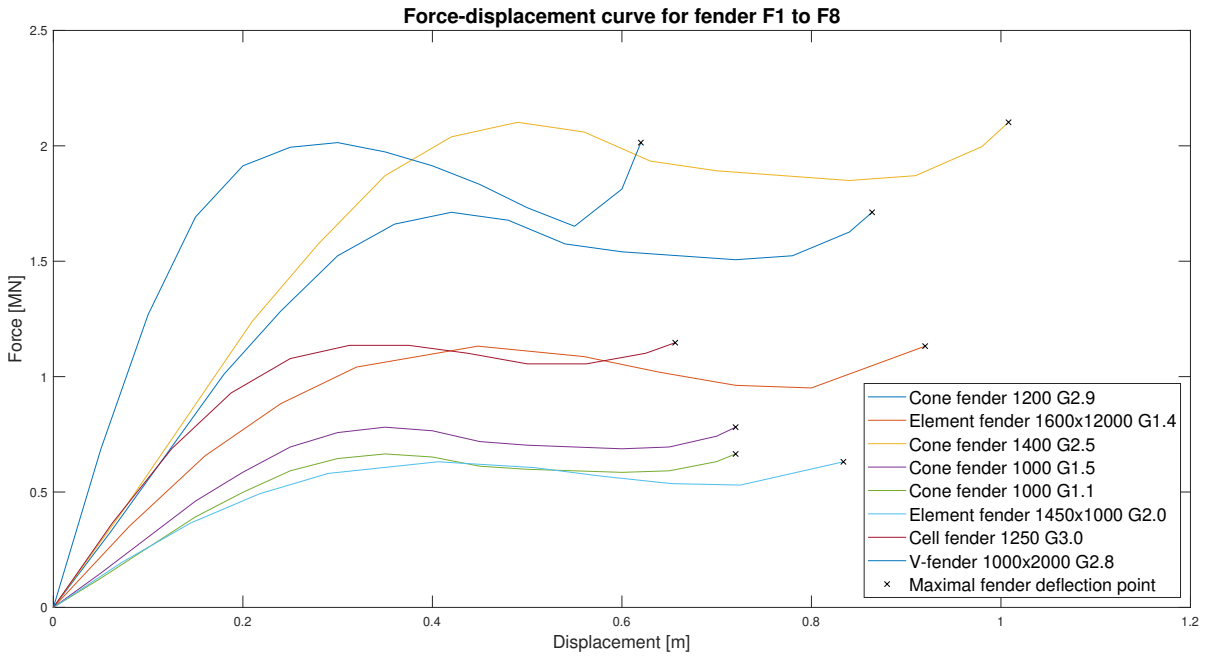


Figure 5.2: Force-displacement curves for the fenders included in the research [27].

- SPC Cone Fender 1400 G2.5
- SPC Cone Fender 1000-S G1.1
- SPC Cone Fender 1000 G1.1
- FE Element Fender 1450x1000 G2.0
- CSS Cell Fender 1250 G3.0
- SX-P V-Fender 1000x2000 G2.8

### 5.4.2. Ship force-displacement curves

The F/d-curve of the ship is established by imposing a displacement by a rigid panel to ultimately determine the influence on the energy-absorbing capacity of the system. In Appendix A, general information and properties of the ships included in the numerical simulations are presented. The displacement is imposed by moving a rigid panel at a constant velocity into the hull. The total reaction force on the ship and the displacement of the related displacement are extracted from the simulation. As the assigned contact between the fender panel and the ship hull is symmetric, the total reaction force and displacement can be extracted from the rigid fender part. Since the area of the panel is known, it is possible to convert the reaction force to an equivalent hull pressure. The curve covers both the elastic and the plastic section of the deformation. In Section 5.5, it is explained how this can also be related to the onset of plasticity.

The reaction force over time (F-t) and the displacement over time (d-t) are combined and result in the desired force-displacement curve of the ship. The F-d curves for the vessels in this study are presented in Figure 5.3.

The small tanker vessel (1) and the large bulk carrier (3) are tested for their energy-absorbing capacity. As the large bulk carrier shows different F/d-behaviour and shows to be relatively weak.

### 5.4.3. Coupled force-displacement curve

In Chapter 2, the energy absorbing capacity of ship and fender is related to the relative stiffness of the bodies. The hypothesis is that the fender absorbs the largest part, however, to determine the share the ship's compliances take, the force-displacement (F/d) curves are obtained separately. The F/d-curve of the coupled system of the fender and ship is obtained by using the springs-in-series theory. For

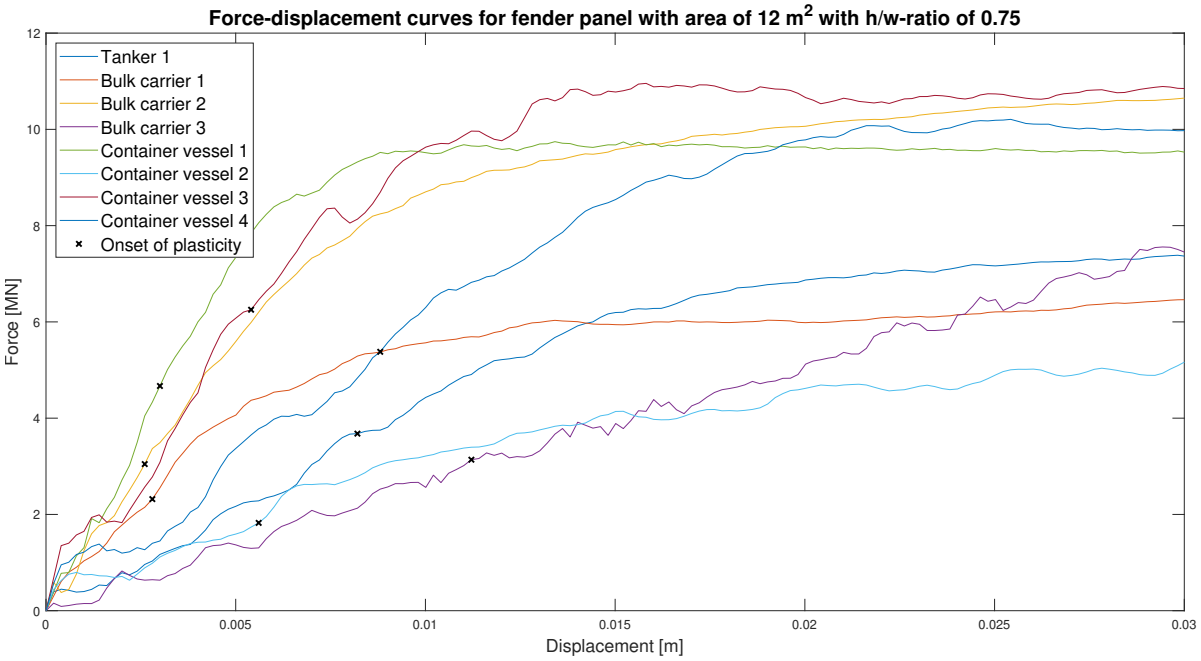


Figure 5.3: Force-displacement curves for the vessels included in this research.

springs in series, the equivalent F/d-curve is derived. Using the following set of equations leads to the maximum reaction force occurring in the system. In the simulations retrieving the F/d-curves, the other body acts as rigid. The relative stiffness is determined using the formulations below.

$$F_{reaction} = k_{coupled} * (\Delta_{fender} + \Delta_{ship}) = k_{fender} * \Delta_{fender} = k_{ship} * \Delta_{ship} \tag{5.2}$$

Analysing the dynamics of the interaction, the deceleration, is to be equal to the force over the mass. With the set of equations below, the maximal displacement and corresponding maximum reaction force is obtained.

$$F = m * \ddot{\Delta} \tag{5.3}$$

$$\ddot{\Delta} = \frac{F}{m} \tag{5.4}$$

$$\dot{\Delta} = \frac{1}{m} \int F dt + \dot{\Delta_0} \tag{5.5}$$

$$\Delta = \frac{1}{m} \iint F dt + \int \dot{\Delta}_0 dt = \frac{1}{m} \iint F dt + \dot{\Delta}_0 t \tag{5.6}$$

The initial velocity $\dot{\Delta}_0$ is constant, and therefore the formulation is simplified to the right-hand equation.

$$\dot{\Delta} = 0 \Rightarrow \Delta_{max} \tag{5.7}$$

$$F_{max} = \Delta_{max} \cdot k_{coupled} \tag{5.8}$$

Using the properties of the ship, like mass, and the initial velocity, the maximum force that occurs in the ship-fender system can be determined. The maximum force occurs at the point in the F/d-curve that corresponds to the point where all berthing energy is absorbed by the system and the ship is fully decelerated. The maximum force can be compared to the maximal capacity before plasticity occurs in the ship's side structure.

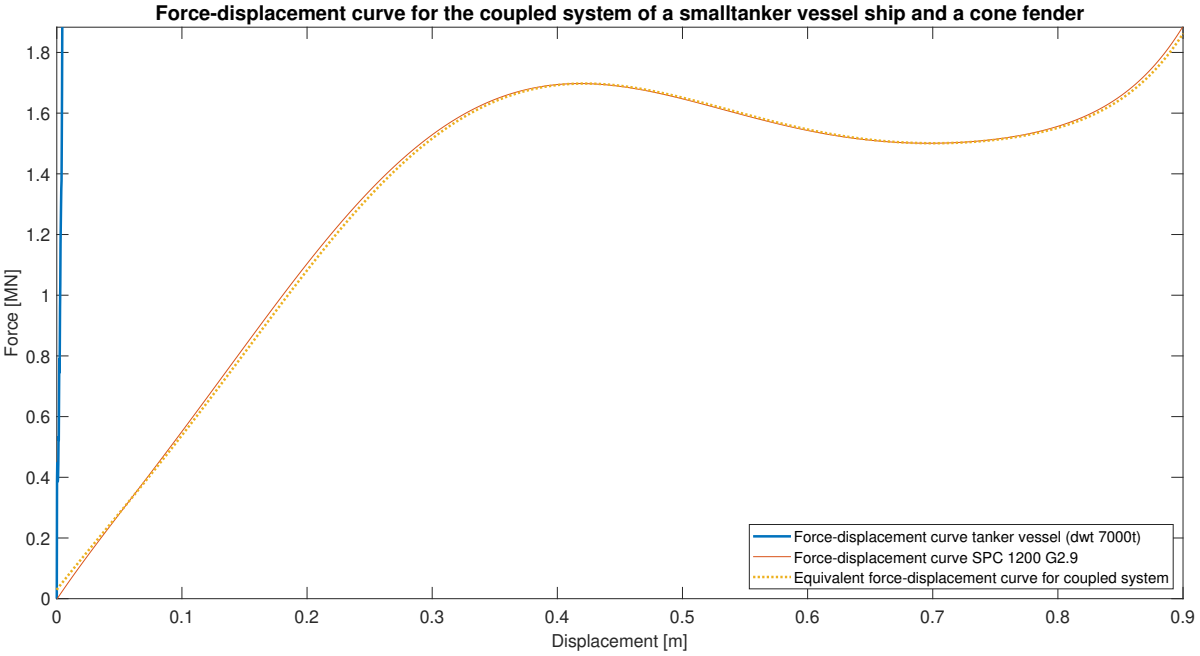


Figure 5.4: Coupled force-displacement curve of small tanker vessel and SPC cone fender 1200 G2.9.

Next, the algorithm that defines the coupled F/d-curve is described. Coupling these gives the equivalent F/d-behaviour and allows the use of the equations above to determine the maximum reaction force occurring in the coupled system. A simple algorithm is used to retrieve the combined curve. First, a fourth-order polynomial fit that is forced to have zero force at zero displacements is made for the ship and fender F/d-curves. Next, the fitted functions of ship and fender are generated for two vectors with the same length. It is known that the reaction force on both ship and fender is the same as a result of force equilibrium, and the equivalent displacement is the sum of the displacement of the ship and fender at the corresponding reaction force. The algorithm constructs a new set of vectors, where the displacement for the F/d-curve is the sum of the displacement of the ship and the displacement of the fender. The new equivalent displacement vector and the reaction force vector are presented in the figure below.

From the F/d-curve of the coupled system, the energy contribution of the ship is derived. As can already be seen in Figure 5.4 the fender F/d-curve and the coupled curve are very close. The additional energy contribution for the small tanker vessel is at the largest 9 kJ on 1400 kJ deformation energy. That is only a little over 0.6%.

For the lighter vessel structure, the large bulk carrier, a similar analysis is executed. This results in a contribution at most of 1% on the energy absorbing capacity. Looking back at the literature that was found on this subject, it can be concluded that there is a certain 'elastic buffering capacity. The contribution is, however, very low compared to the fender contribution to absorb energy. Since the fender is designed to absorb the energy, this could have been expected to be the case. However, in the PIANC guidelines the softness factor, $C_s$, accounts for the ship's compliance to account for 10% of the elastic energy absorption. Based on the findings regarding the softness factor presented in Figure 5.4, it is advised to eliminate the $C_s$ factor in the kinetic design energy in Equation 2.6 from the PIANC guidelines.

The previously described analytical dynamics that are applied to determine if the plasticity criterion is reached in the ship's hull in contact with the fender are now simplified. The fender F/d-curve is sufficient to apply this and examples of this are available in the PIANC guidelines. Later on, in Chapter 6, this is incorporated into the results from the numerical simulations on the structural capacities.

In addition, after overloading of the fender, the contribution of the ship will most likely increase as the fender system becomes rigid. However, the focus of this research is on the Ultimate limit state design of the vessel and determining whether the maximum rated fender force exceeds the vessel's capacities. The overloading of the fender is out of the scope of this research. The information from the

numerical simulations of the compliance of the ship is used in Section 5.6 for parametric studies to the (elastic) energy absorbing capacity for different configurations of fenders and layouts.

## 5.5. Onset of plasticity

In this section, the onset of plasticity in the numerical simulations is discussed. The main objective is to quantify this onset and identify what governs the failure. The plasticity in the model is included in the material properties assigned to the ship section. It is an isotropic elasto-plastic material. The onset of plasticity can be extracted from the numerical simulations by seeking elements that have plastic strains above zero or Von Mises stresses over the yield strength. The extracted onset of plasticity is based on the effective plastic strain. As discussed in section 5.2.1 the yielding of the material is $J_2$-based.

The effective plastic strain is available in the post-processing software of LS-DYNA. Different criteria are discussed below before an appropriate criterion for the onset of plasticity is selected.

Criteria for the onset of plasticity using the numerical simulations:

1. As soon as the first element has an equivalent plastic strain that is non-zero.
2. When yielding flows over the element boundary and two adjacent elements have a non-zero equivalent plastic strain.
3. Recommendation for local permanent deformation of 0.2 % of the stiffener span by IACS [23].

The second criterion is opted for. The third criterion is not applicable, because only deformation is considered while the fender panel moves with a constant velocity. Therefore, it can not be concluded what state 0.2 % local permanent deformation is induced. The first criterion is not selected because, in numerical simulations, stress concentrations do occur in single elements. When the strain yields over the boundaries of two elements connected, it is flagged as the onset of plasticity.

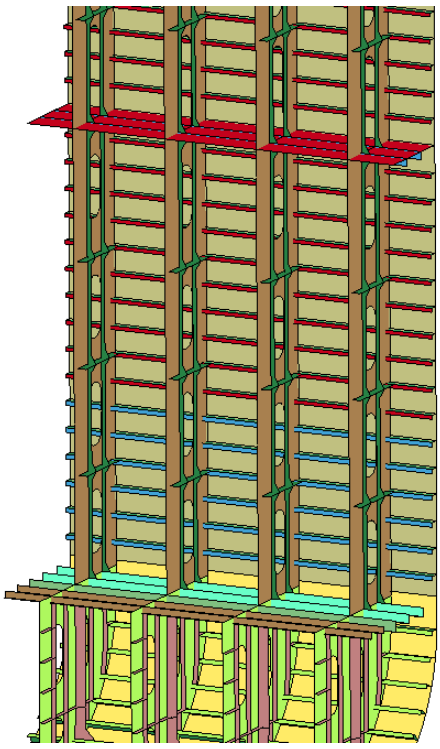

(a) Considered section of the container vessel hull for the onset of plasticity. The inner hull and inner flanges are deactivated for animation purposes.

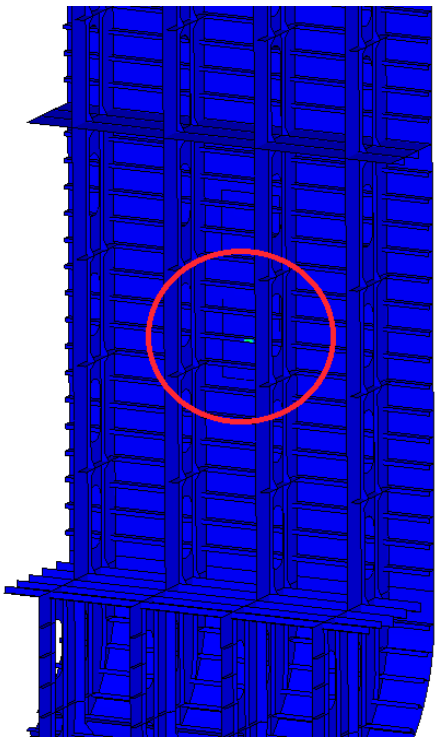

(b) The red circle identifies the onset of plasticity and the black rectangle indicates the panel location.

Figure 5.5: Visualizing the onset of plasticity in LS-DYNA software with example hull large container vessel and 6m x 2m panel.

The fringe range in the software is not averaged over the elements, but considered per element. The average of the equivalent plastic strain over the three through-thickness integration points is leading.

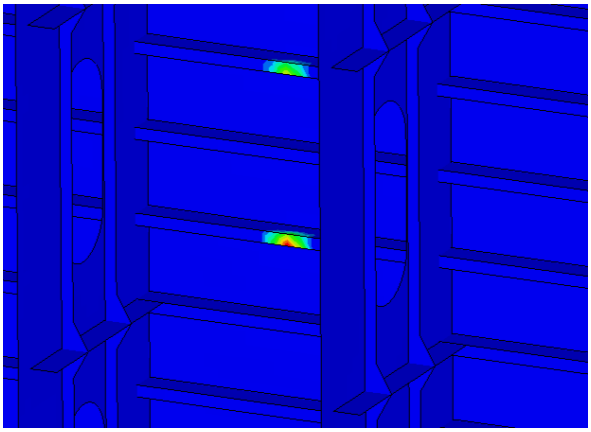

(a) Local detail of the MinMax-nodal averaged effective plastic strain at the onset of plasticity in the hull section. The $\varepsilon_p$ is between 0 $\mu m$ (blue) and 260 $\mu m$ (red).

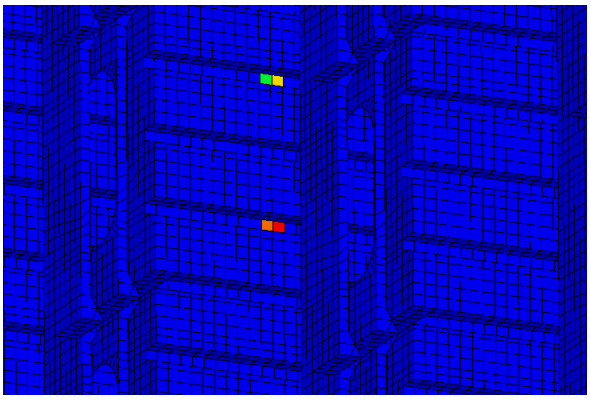

(b) Local detail of the plasticity criterion of the effective plastic strain of the elements. The $\varepsilon_p$ is between 0 $\mu m$ (blue) and 260 $\mu m$ (red)

Figure 5.6: Local details of the onset of plasticity in stiffened panel in LS-DYNA software in large container vessel (C4) and 6m × 2m fender panel. The local detail shows L-profile stiffeners ($275mm \times 12mm$ + $125mm \times 12mm$) with stiffener spacing $b = 850mm$ and HIP ($900mm \times 2000mm$) web frames with $3160mm$ spacing.

### 5.5.1. Post-processing of the simulations

Further post-processing of the simulations consists of the extraction of the Force-time diagrams (F/t). The F/t-curve is used to determine the reaction force at the time step where the onset of plasticity is observed. The allowable reaction force for all simulations is collected and visualised to study the trends occurring.

Moreover, after the plasticity is observed, the corresponding failure mechanism is visually determined. The failure modes that are expected to occur in the simulations are the failure of the stiffener and plate, tripping failure and failure in the web frames. In the next paragraph, the simulations are discussed for which the maximum reaction force and failure mode have to be obtained.

## 5.6. Parametric sensitivity

It is mentioned numerous times that the contact between the ship and the fender panel is highly subjective to the dimensions of both the ship and the panel. Therefore, it is crucial to determine what the influence is of these different parameters. In this section, the parameter studies for the numerical simulations are presented.

### 5.6.1. Panel location

As was mentioned by Sheikh et al. the location of impact induces failure in different structural components [26]. Based on his findings, three simulations are executed for the panel impact location on the parallel side hull. The structural components impacted are a stiffened panel in between two web frames and on a web frame. The impact on the stiffened panel is simulated for a symmetric and asymmetric impact. The selected panel is a 6 m high panel and 0.5 m wide. With the fairly narrow panel, the impact is concentrated on the structural component under investigation.

### 5.6.2. Panel dimension

In Chapter 2, the pressure-area relation to the maximum capacity of ships in ice floe impact is discussed. In the current guidelines of PIANC, a constant value is used for the hull pressure to the fender area. Consequently, the maximum allowable reaction force with the area is linearly increasing. In this section, this relation is tested by varying the fender panel area and dimensions. Buckling fenders are equipped with a fender panel, and the panel does not change in size during the simulations. The force over time behaviour is also quickly related to the current equivalent allowable hull pressure capacities. The panel sizes vary from 6 $m$ to 0.5 $m$, and both high and wide panels are considered. The fender panel dimensions are based on panels used in daily practice [27, 31]. In the table below, the simulations are specified.

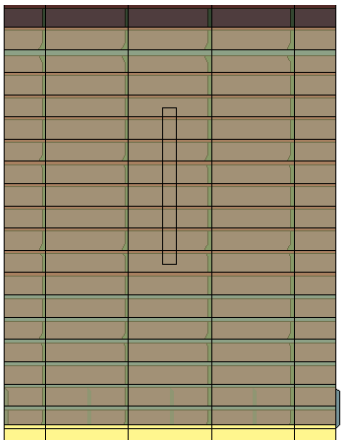

Figure 5.7: Fender panel located on the middle of a stiffened panel, the shell plate is transparent to indicate the structural components behind the plate.

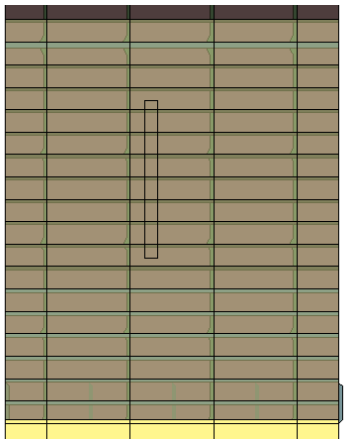

Figure 5.8: Fender panel located asymmetrically on stiffened panel, the shell plate is transparent to indicate the structural components behind the plate.

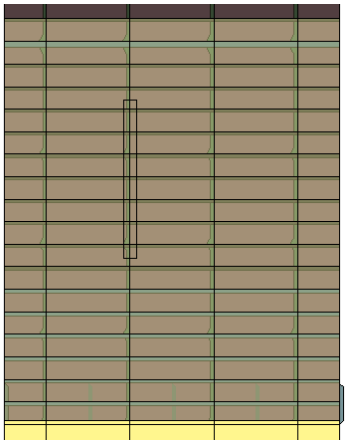

Figure 5.9: Fender panel located on a web frame, the shell plate is transparent to indicate the structural components behind the plate.

Table 5.1: Numerical simulations to determine influence of fender panel dimensions.

| **Simulation** | **Height [$m$]** | **Width [$m$]** | **Area [$m^2$]** |
|---|---|---|---|
| **1** | 6 | 2 | 12 |
| **2** | 6 | 1 | 6 |
| **3** | 6 | 0.5 | 3 |
| **4** | 3 | 2 | 6 |
| **5** | 3 | 1 | 3 |
| **6** | 3 | 0.5 | 1.5 |
| **7** | 2 | 6 | 12 |
| **8** | 1 | 6 | 6 |
| **9** | 0.5 | 6 | 3 |
| **10** | 2 | 3 | 6 |
| **11** | 1 | 3 | 3 |
| **12** | 0.5 | 3 | 1.5 |
| **13** | 6 | 6 | 26 |
| **14** | 6 | 4 | 24 |
| **15** | 4 | 6 | 24 |

The sizes of the panel with respect to the hull of a 19,000 TEU container vessel of the ULVC class are shown in Figure 5.10. In the figure, the horizontal black lines indicate where the stiffeners and decks are and the vertical black lines indicate where the web frames are located. The simulations are post-processed by extracting the onset of plasticity and the corresponding reaction force as described above.

### 5.6.3. Ship type

In this last section, the governing ship types for the study and the corresponding layout and structural components are discussed. At the end of this section, three governing vessels are specified. An overview of the vessels and their properties is presented in Table 3.1. These vessels are selected as representative vessels in the study of Vredeveldt and Rhijsburger to cylindrical fenders [32]. The 3D models of small sections of these ships are available, they are modified to be applicable to fender panels as larger panels also occur.

To give an upper and lower limit to the capacities of vessels with a cell structure, the largest and smallest vessel is used for the parametric study. The New Panamax ULVC container vessel is the first opted ship, it is an ultra-large container vessel. For those vessels, the hull pressure capacities have been decreasing over the years, so the limitations to this are important to study. For a very small

vessel, the hull pressure capacities are larger according to the PIANC WG33 guidelines. However, if the maximal reaction force also increases linearly with the panel area size, it means a small vessel could carry larger impact forces than a large vessel. Therefore, a small vessel is also included in the parametric study. The last vessel that is subjected to the fender panels is the Capesize VLBC bulk carrier, as this vessel has a fairly different structural layout. The other vessels have a cell structure with an inner- and outer hull, whereas the Capesize bulk carrier in this study is single-skinned. In the literature in Chapter 2, it was indicated that different behaviour and structural capacities arise for these types of vessels [3]. Figure 4.12 shows the typical components in the cell parallel side hull, and Figure 4.11 shows the layout for a single shell that is more typical for bulk carriers.

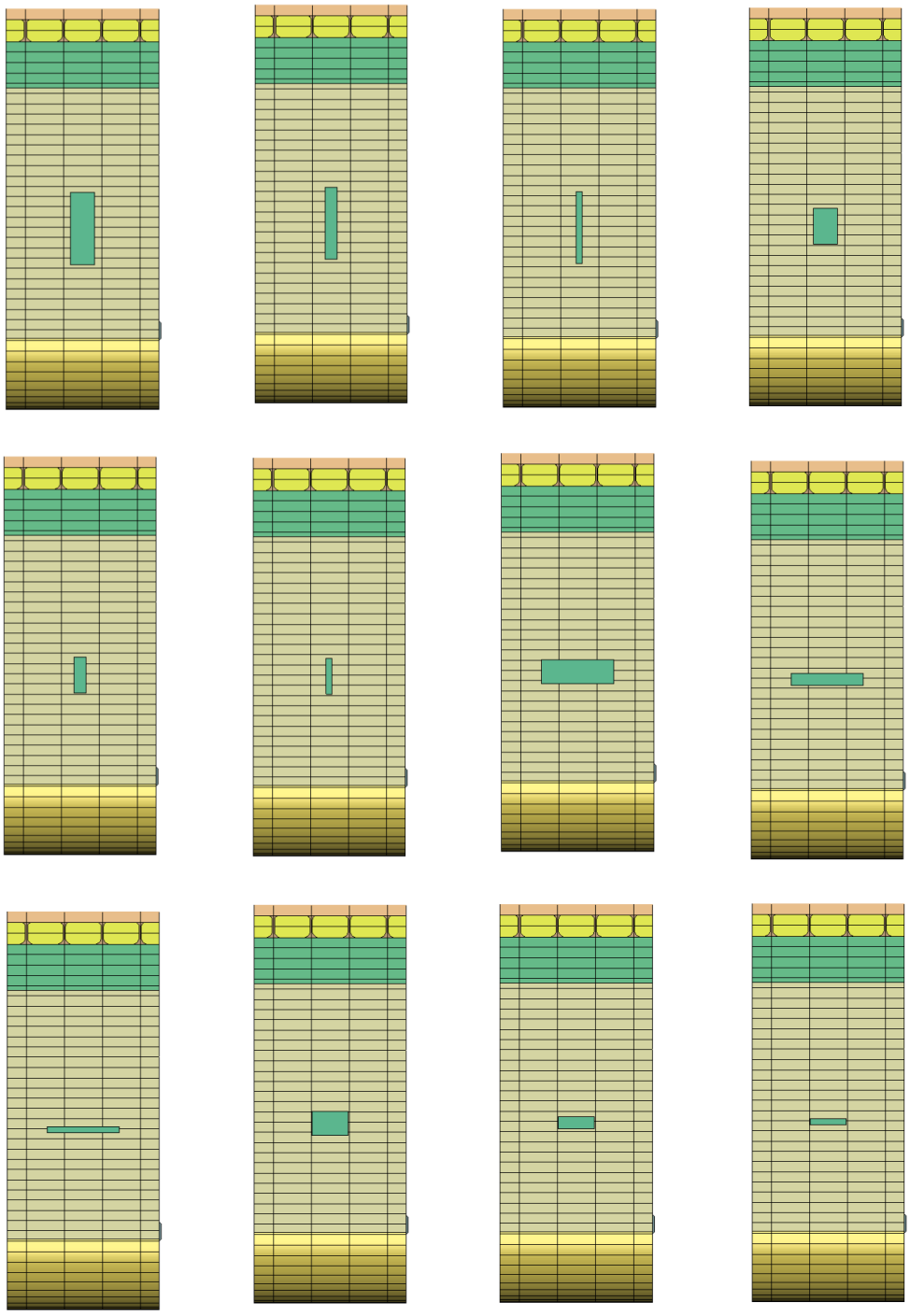

Figure 5.10: Overview of the panel dimensions in relation to 19,000 TEU container parallel hull section (12.6m wide).

# 6

# Results

This chapter reviews the results of the analytical models and the numerical simulations. Moreover, a comparison is made with the prior studies discussed in Chapter 2. First, the results of the three governing vessels, a coaster-size tanker vessel, a ULVC container vessel and a Panamax bulk carrier, are presented. In the previous parts of the study, the selection of these vessels is substantiated. After the other vessel's results are shown.

## 6.1. Analytical model

Several analytical tripping models are discussed in Chapter 4. The modified pre-buckling stress field is generated and used to determine the critical tripping pressure for the two large vessels, as they were identified to be sensitive to tripping. The occurrence of tripping and other failure response is discussed in Section 6.3. The critical tripping load for the stiffened panel of the large container vessel of a panel of 3×1 m engaging with three stiffeners is analysed. For the bulk carrier, a section with five stiffeners is considered with a 6m × 4m panel.

Table 6.1: Analytically determined critical distributed load to induce tripping in investigated stiffened panels.

| Stiffened panels studied for tripping | Stiffener panel | Number of stiffeners | Maximum reaction force per stiffener | Maximum reaction force total |
|---|---|---|---|---|
| Large container vessel | 3m x 1m | 3 | 25.58 kN | 127.9 kN |
| Large bulker | 6m x 2m | 5 | 42.7 kN | 128.1 kN |

The corresponding PIANC equivalent hull pressures for the container ship and bulker is 200 $kN/m^2$. The outcome of the tripping capacities is much lower. As addressed in Chapter 4, the tripping model still has shortcomings in correctly representing the pre-buckling stress field. The parametric approach that is proposed by Sheikh et al. is applied to the vessel hulls to determine whether tripping is probably governing [26]. To obtain these results, Equations 4.24, 4.25 and 4.26 are used. The results are presented in table 6.2.

Table 6.2: Sheikh et al. influential parameters to tripping failure for investigated stiffened panels [26].

| Stiffened panels studied for tripping | $\beta_1$ | $\beta_4$ | Sensitive to tripping according to Sheik et al. method? [26] |
|---|---|---|---|
| Large container vessel | 2.42 | 1.25 | Yes |
| Large bulker | 2.29 | 3.19 | Yes |

The results of the analytical formulations in relation to the numerical simulations and the observed failure behaviour are elaborated on in Chapter 8.

## 6.2. Numerical simulations

The results of the numerical simulations, that are discussed in Chapter 5, are presented in this part. The numerical simulations are analysed in two different categories, wide and high panels. The early results showed different trends for wide and high panels and therefore, they are split. For the three vessels, a small tanker, a large container carrier and a large single shell bulker, the equivalent allowable hull pressure from the simulations is compared to the PIANC criterion. Next, a total allowable reaction force is introduced for a better understanding of the structural response and capacities. After, the failure mechanism arising at the onset of plasticity is presented.

### 6.2.1. Impact location

As addressed in Section 2.4, the impact location results in different governing failure. Furthermore, the different structural components influence the capacity of the hull to withstand berthing and other transverse loads. In Chapter 5, the impact location simulations are discussed, and the large container vessel is selected for these simulations. The results of the simulations are presented in table 6.3.

Table 6.3: Maximum hull capacities to determine the influence of the impact locations with different structural components on a container vessel.

| Contact location 6m x 0.5m panel | Maximum allowable reaction force [MN] | Allowable equivalent hull pressure [kN/m$^2$]] | Additional capacity compared to centered on grillage. |
|---|---|---|---|
| Centered on stiffened panel (base case) | 1.71 | 569 | - |
| Asymmetric on stiffened panel | 1.71 | 569 | 0% |
| On a web frame | 2.93 | 974 | 71% |

The impact simulation on the web frame clearly resulted in a larger reaction force of the fender panel to trigger the onset of plasticity in the ship section. The stress concentration for the impact on the web was located in the web frame, while the stress concentration in the other simulations occurred in the stiffeners. The results are in line with prior studies on plastic deformation and capacity as discussed in the literature. The structural capacity for the same fender panel configuration increases by more than 70% when the panel engages with a web frame instead of the stiffened panel in between two web frames. The PIANC criterion for this vessel type is 200 $kN/m^2$ equivalent hull pressure. All simulations show that more than double the capacity is reached in the configuration of these small panels.

### 6.2.2. Rated fender reaction force

In Section 5.4, the contribution of the ship's compliance to the energy absorption behaviour of the ship-fender system is elaborated on. It was concluded that the ship contribution is very small and, if designed correctly, the fender should absorb 99% of the berthing energy. The corresponding maximum rated fender reaction force for the three governing vessels is derived, using analytical dynamics, are presented in Table 6.4.

Table 6.4: Maximal fender reaction force from analytical dynamics.

| $F_{fender,max}$ **[MN]** | **Small tanker vessel** |
|---|---|
| Small tanker vessel (T1) | 2.2 |
| Large bulk carrier (B3) | 3.4 |
| Large container vessel (C4) | 5.2 |
| Container vessel 1 | 1.0 |
| Container vessel 2 | 2.8 |
| Container vessel 3 | 2.1 |
| Bulk carrier 1 | 2.4 |
| Bulk carrier 2 | 3.8 |

The maximum rated fender reaction force is obtained to determine whether the maximum allowable pressure is reached for the ship. For the whole considered group of vessels, the outcome of the analytical dynamic analysis is found in Appendix A. The capacity to withstand berthing loads, like fender impact, of the three governing ships is discussed in the following part.

### 6.2.3. Large container vessel

Numerical simulations are executed for a large container vessel for the impact of different fender panel dimensions. The onset of plasticity is determined, and the corresponding equivalent hull pressure is presented in Figure 6.1. The hull pressure is presented in relation to the current PIANC hull pressure criterion. The allowable equivalent hull pressure for the small panel areas is far from the PIANC criterion, while the large panel areas show an onset of plasticity under the safe line according to the PIANC criterion. The relation for the tall and high panels is a second-order exponential with a horizontal asymptote. The details on the second-order exponential trend line for this, and all other vessels, are documented in Appendices B and C.

Table 6.5: Maximum hull pressure for a large container vessel to determine the influence of the direction of the dimensions of the fender panel.

| **Panel** | **1** | **2** | **3** | **4** | **5** | **6** | **7** | **8** | **9** | **10** | **11** | **12** | **13** | **14** | **15** |
|---|---|---|---|---|---|---|---|---|---|---|---|---|---|---|---|
| **Height [m]** | 6 | 6 | 6 | 3 | 3 | 3 | 2 | 1 | 0.5 | 2 | 1 | 0.5 | 6 | 4 | 6 |
| **Width [m]** | 2 | 1 | 0.5 | 2 | 1 | 0.5 | 6 | 6 | 6 | 3 | 3 | 3 | 4 | 6 | 6 |
| **Area [m$^2$]** | 12 | 6 | 3 | 6 | 3 | 1.5 | 12 | 6 | 3 | 6 | 3 | 1.5 | 24 | 24 | 36 |
| **Maximal equivalent hull pressure [kN/m$^2$]** | 272 | 468 | 567 | 321 | 537 | 571 | 432 | 737 | 1087 | 529 | 495 | 867 | 169 | 230 | 238 |

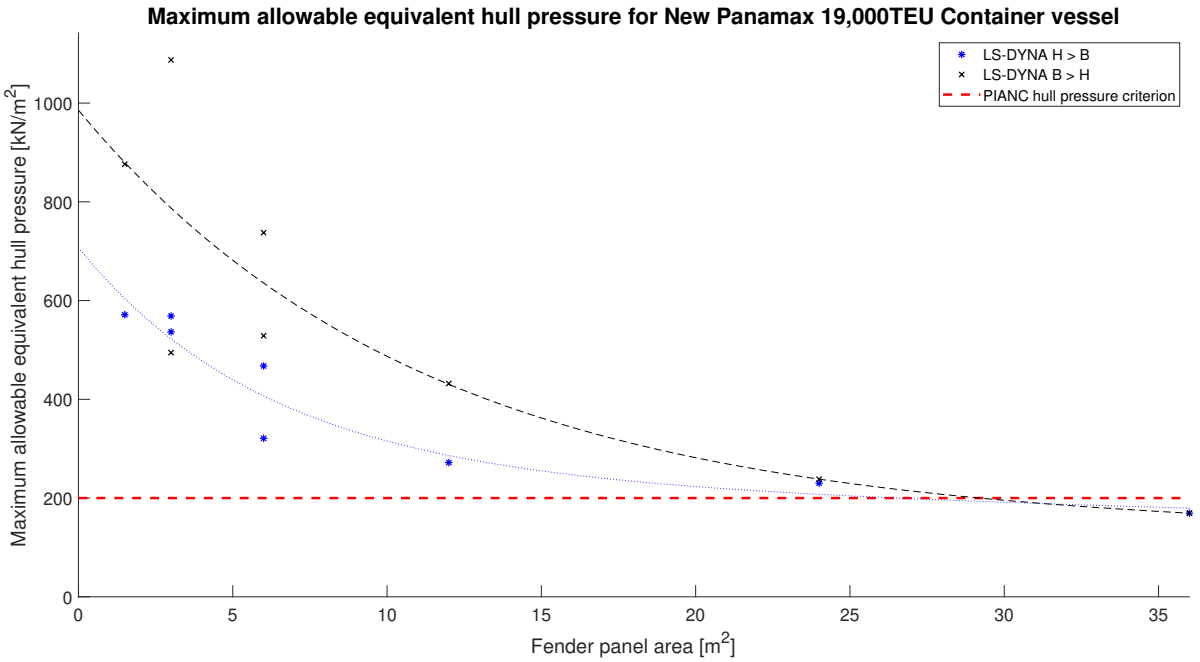


Figure 6.1: Allowable equivalent hull pressure on a large container vessel.

To gain more insight into the limit to the safe application of the PIANC criterion, the total allowable reaction force in relation to the panel area is shown in Figure 6.2. It is visible that the large panels do not show safe application in relation to the PIANC criterion. Furthermore, making panels larger does not necessarily yield more total allowable fender reaction force capacity. Based on the second-order exponential trend lines, the lowest intersection between one of the trend lines and the constant PIANC hull pressure criterion is around 5.5 $MN$.

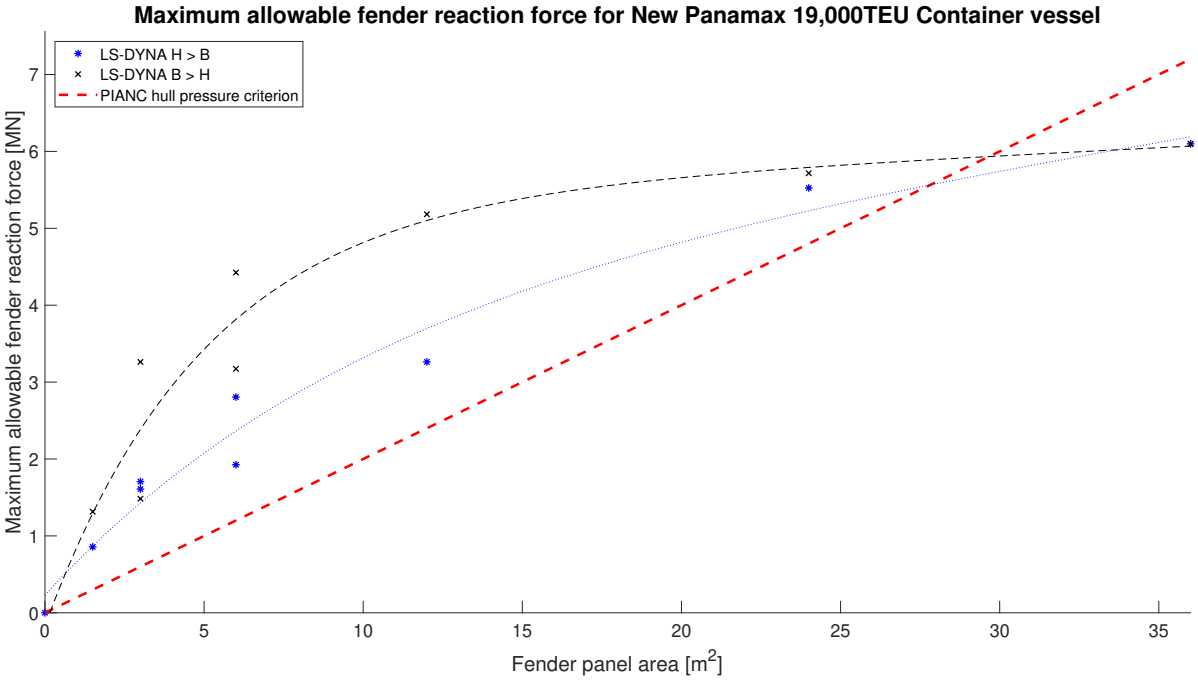


Figure 6.2: Allowable total reaction force on the parallel hull of a large container vessel.

### 6.2.4. Small tanker vessel

For the small tanker vessel, the allowable equivalent hull pressure is presented in relation to the fender panel area in Figure 6.3. The figure shows that the PIANC criterion overestimates the capacity of the small vessel at a much smaller fender panel area than for the large container vessel. Furthermore, the wide panels outperform the tall panels only to an area of 15 $m^2$. Nevertheless, a second-order exponential trend is also applicable to the results of the small tanker vessel.

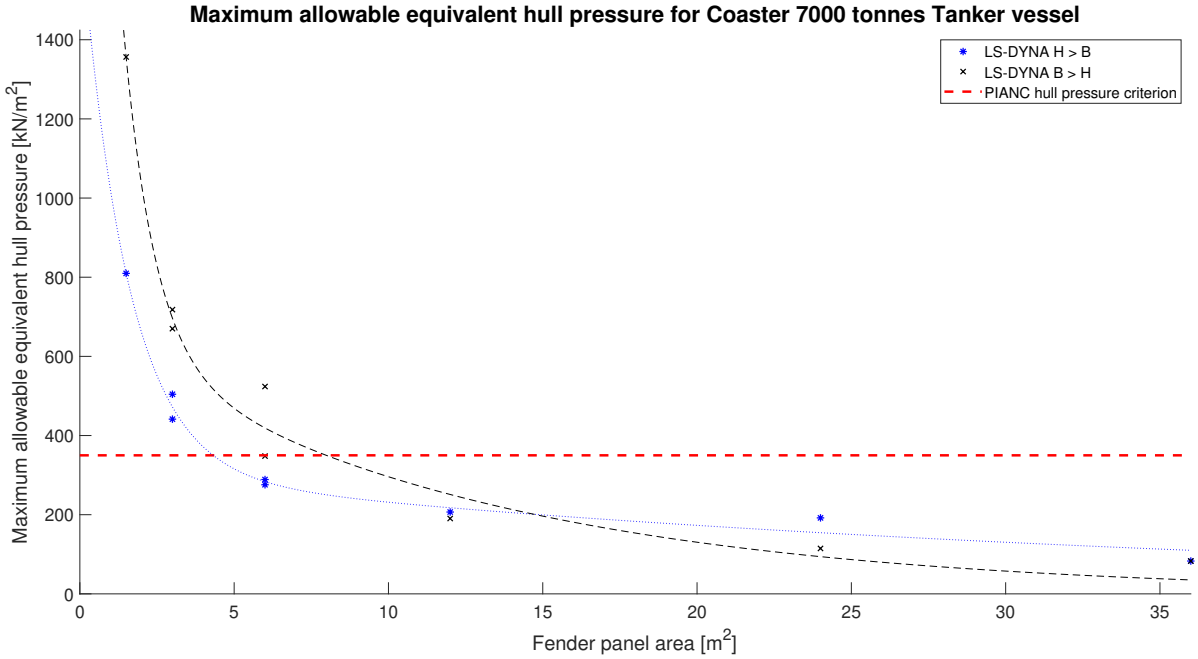


Figure 6.3: Allowable equivalent hull pressure on a small tanker vessel.

In Figure 6.4, the allowable reaction force in relation to the area of the fender panel is plotted. It is observed that after the upper limit of the total reaction force for a small tanker vessel is reached, the allowable reaction force capacity remains constant with an increase in the panel area. The reason that the capacity does not increase further exponentially with the width is that the web frame spacing is smaller than for large vessels. Therefore, the web frames are activated at an earlier stage. In addition, high panels may lead to the activation of a deck and thus increase the allowable load for high panels on small vessels. For the wide panels, the constant total reaction force is approached from a panel area of 5 $m^2$. When observing the intersection of the trend lines and intersection with the PIANC criterion is found around 1.8 $MN$.

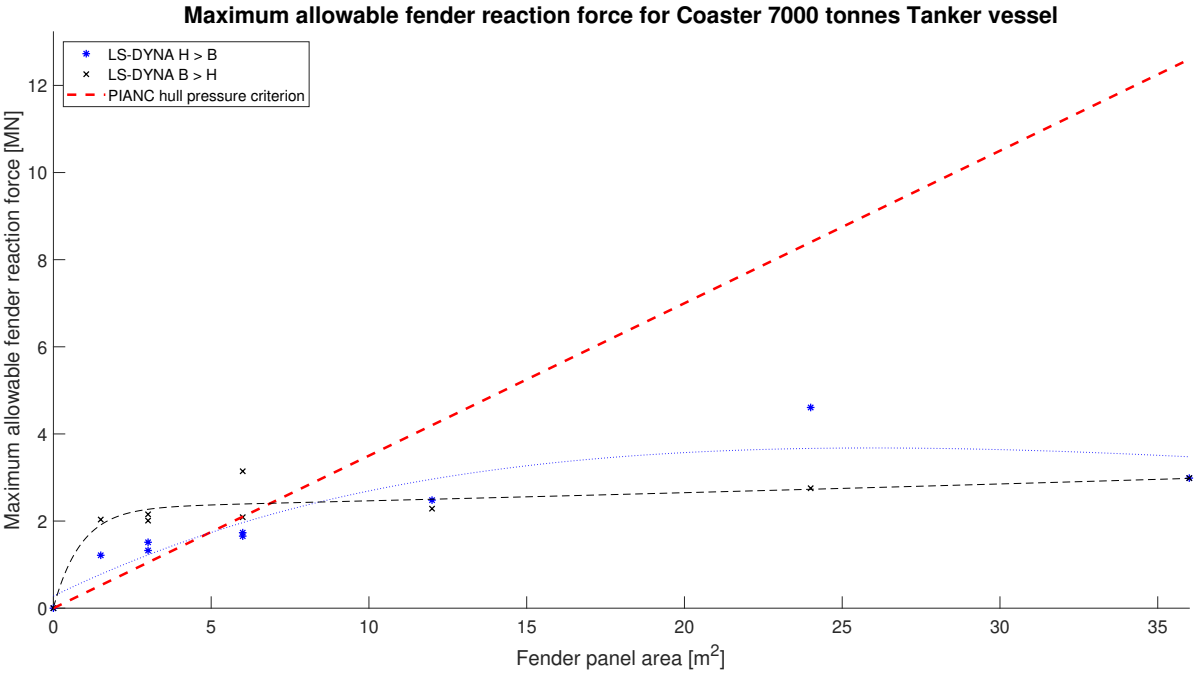


Figure 6.4: Allowable total reaction force on the parallel hull of a small tanker vessel.

### 6.2.5. Single shell bulk carrier

The last governing vessel is the large single-shell bulk carrier, and the results are presented in this section. The allowable equivalent hull pressure for this Capesize bulk carrier is presented in Figure 6.5. An exponential decreasing trend is again observed with an increase in the panel area. Due to the structural layout of these single-shell hulls, the high panels outperform the wide panels. As the high panels engage with more stiffeners, while wide panels can not activate web frames in these hulls. The lower PIANC criterion is rather low, but it is met for all panel areas. It is found that tripping does occur for these vessels for large areas, especially high, panels.

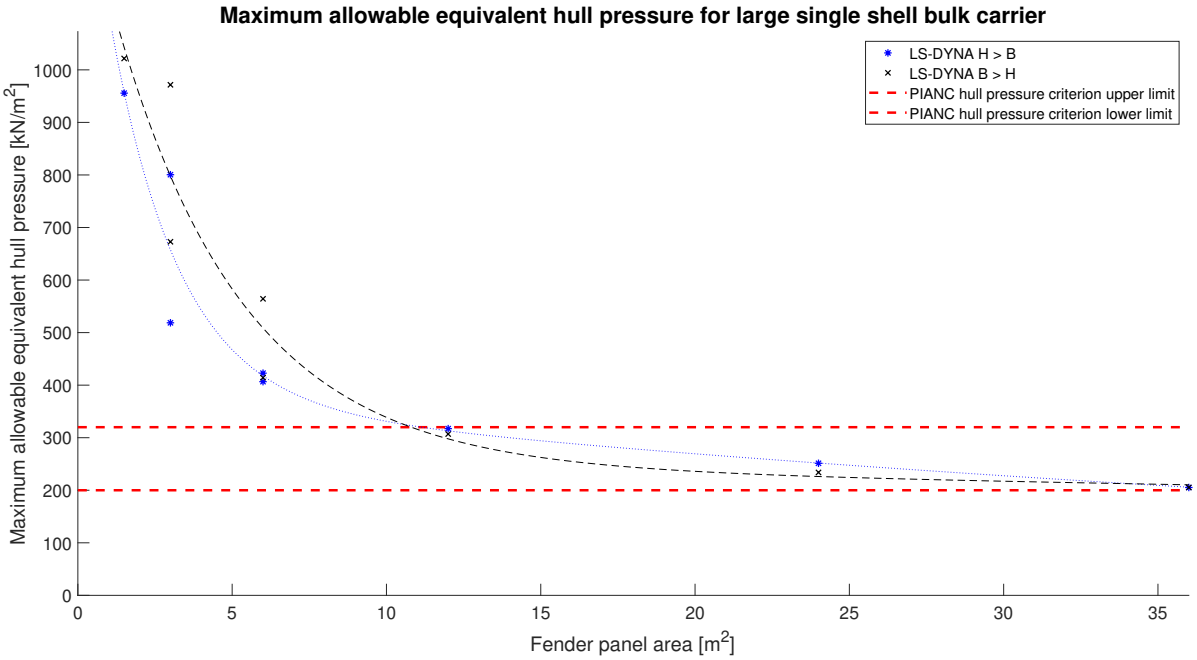


Figure 6.5: Allowable equivalent hull pressure on a large bulk carrier.

The allowable reaction force for the bulk carrier is presented in Figure 6.6. No clear horizontal limit is observed, but a slow linear increase is seen after the intersection with the 320 $kN/m^2$ line is crossed. If the 320 $kN/m^2$ equivalent pressure is adopted, a total reaction force limit of 3.8 $MN$ should be adopted to ensure safe loading. For the lower PIANC limit, no total reaction force limit is necessary.

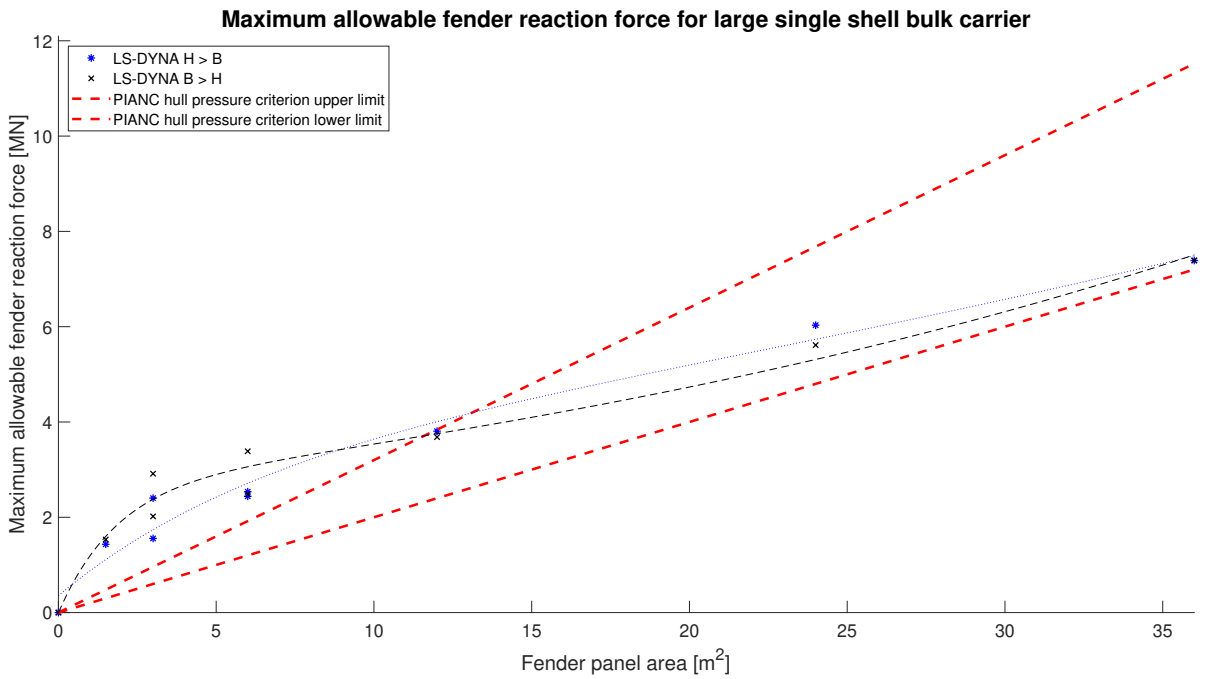


Figure 6.6: Allowable total reaction force on the parallel hull of a large bulk carrier.

## 6.2.6. Container vessel 1

The smallest vessel considered for this study is a 754 TEU feeder vessel. The simulations of the vessel were limited to a total fender area of 12 $m^2$ because the larger fender panels activated the boundary conditions. The high and wide panels are plotted together, and the relation to the equivalent hull pressure is presented in Figure 6.7. It shows a linearly decreasing relation with the panel area. The capacity is higher than the current PIANC criterion. One relation is shown as the limited amount of simulations does not allow for separate trend lines.

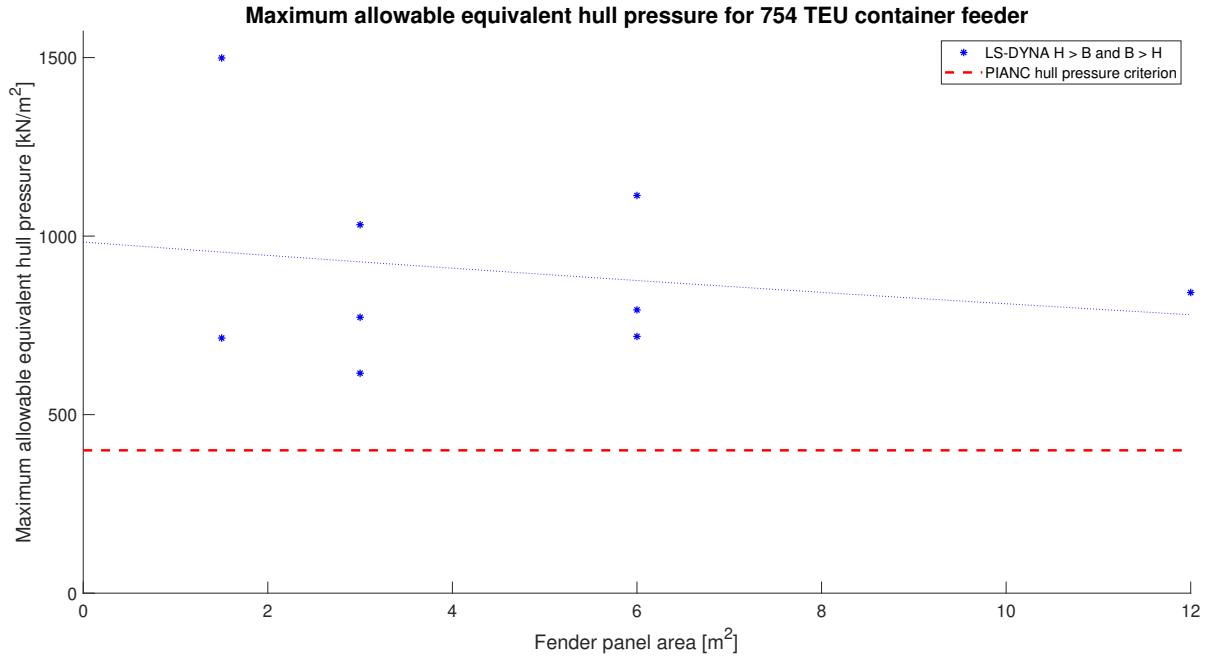


Figure 6.7: Allowable equivalent hull pressure on a container feeder.

The linear trend is also visible in Figure 6.8. A criterion of 500 $kN/m^2$ is safe for all the incorporated simulations. There is no indication of a limit in total reaction force in this region. The limiting factor here is the area where the hull can engage sufficiently.

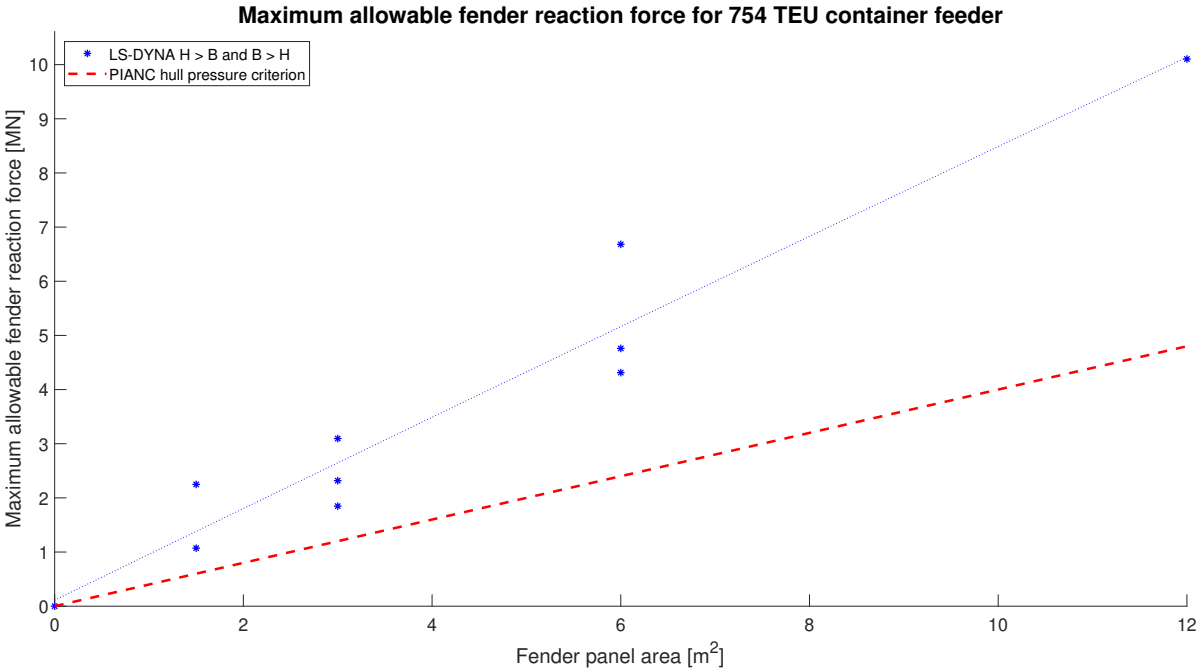


Figure 6.8: Allowable total reaction force on the parallel hull of a container feeder.

### 6.2.7. Container vessel 2

A small container coaster was used in the numerical simulations to verify the allowable hull pressure for first and second generation container vessels. The 7,500 TEU coaster vessel has a length over all of 146 $m$. The allowable equivalent hull pressure capacities of the container coaster are presented in figure 6.9. The relation for the high (blue) and wide (black) panel areas with the pressure are described with a second-order exponential trend. The equivalent hull pressure capacities are overestimated for a large part of the numerical simulations by the PIANC criterion. The three blue stars in the left-bottom of the figure represent the high panels that do not activate a web frame or deck. It illustrates that the stiffened panel in between the web frames and decks does not have sufficient capacity to resist fender-induced load that is acceptable according to the PIANC criterion.

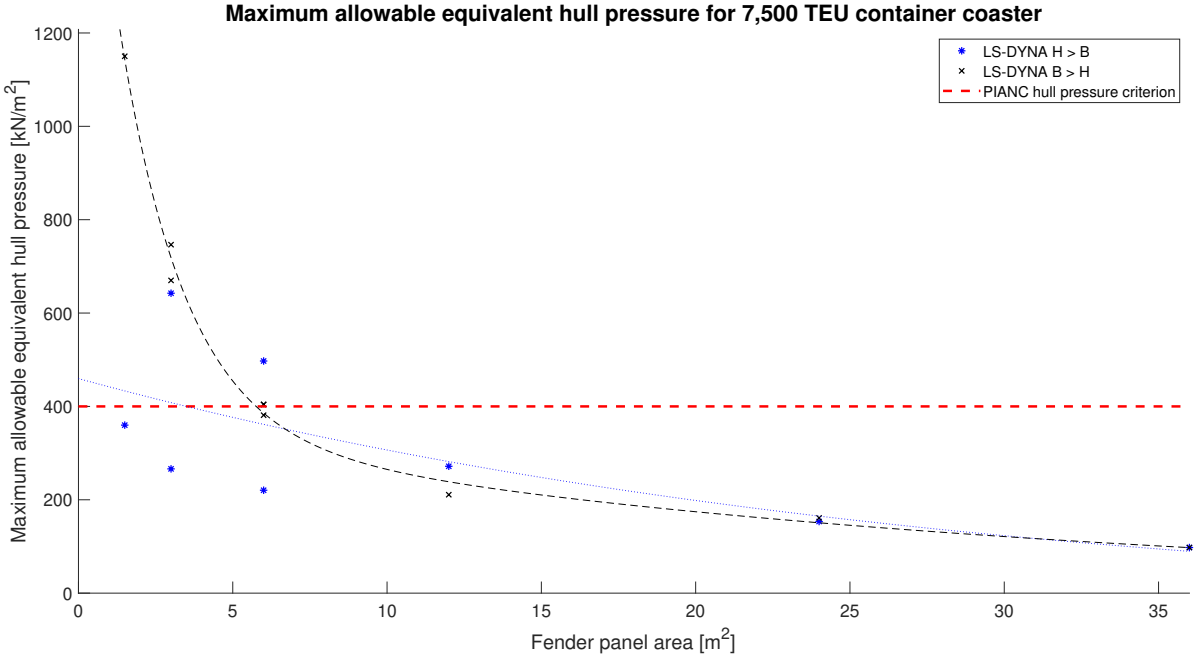


Figure 6.9: Allowable equivalent hull pressure on a container coaster.

Figure 6.10 presents the relation between the total allowable reaction force and the fender panel area. It is again visible that the three high and small panels show bad capacities. The panels with a similar area that engages with a deck activate more capacity in the hull. The other simulations follow a slow linear increase with the area as more structural elements are engaged. The exponential trend lines are heavily influenced by the zero areas, zero force point. The three lowest simulations lie above the 240 $kN/m^2$ line, all other points could be covered by maintaining the 400 $kN/m^2$ criterion with a limit of 1.5 $MN$ maximum allowable reaction force.

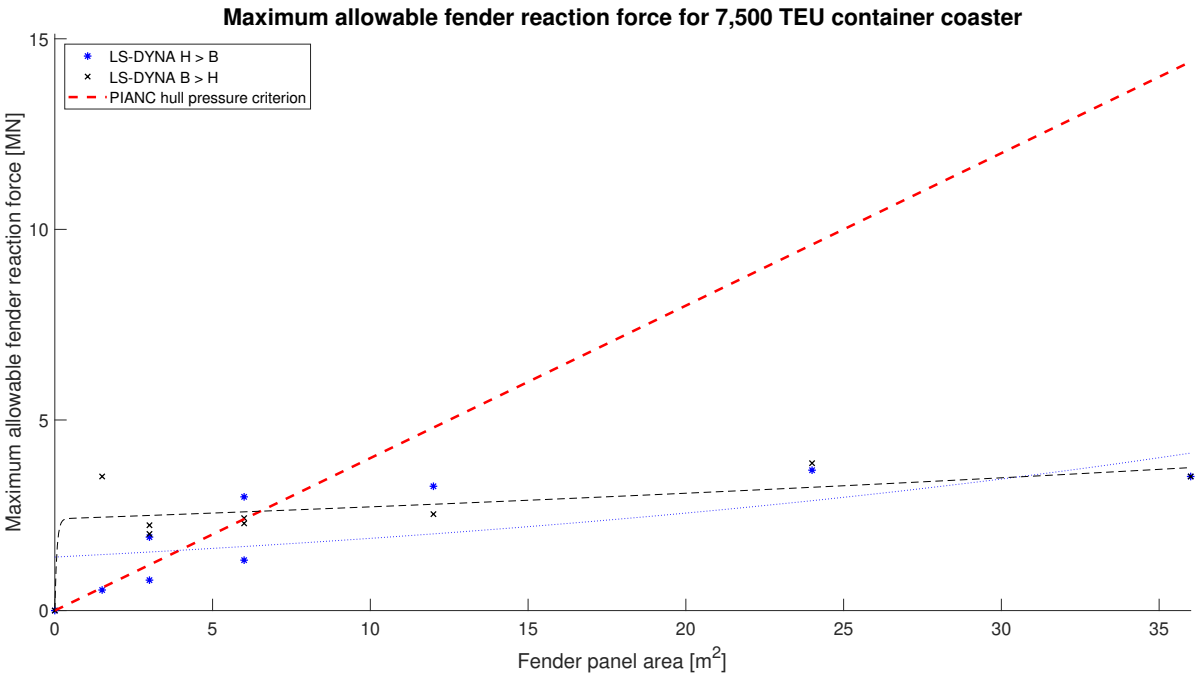


Figure 6.10: Allowable total reaction force on the parallel hull of a container coaster.

### 6.2.8. Container vessel 3

To gain insight into the structural behaviour and capacities of the third generation container vessels, a Post-Panamax was submitted to 15 fender panels. The equivalent hull pressure capacities are presented in figure 6.11. The equivalent hull pressure for both high and wide panels is one and a half times the allowable pressure according to PIANC for the small panels. Around 20 $m^2$ fender panel area, the second-order exponential trend lines intersect with the PIANC constant hull pressure criterion.

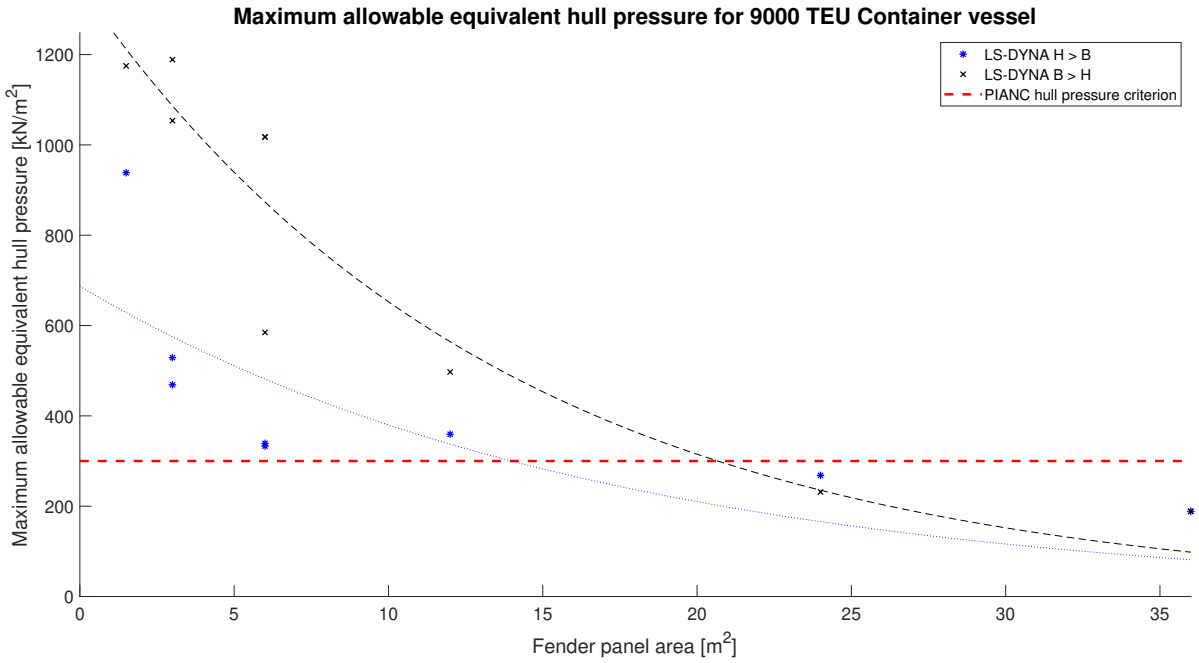


Figure 6.11: Allowable equivalent hull pressure on a Post-Panamax container vessel.

The force-area relationship is presented in Figure 6.12 for the Post-Panamax vessel. It shows a similar intersection point as the equivalent hull pressure, Figure 6.11. The wide panels are performing

better than the high panels over the whole region up to 24 $m^2$. The current criterion of 300 $kN/m^2$ is safely applicable to 24$m^2$ or with a total allowable reaction force of 5.5 $MN$. The rated reaction fender force for this vessel is around 2.1-2.5 $MN$. There was no relation found in the simulations for the height over the width of the fender panel and the allowable total reaction force.

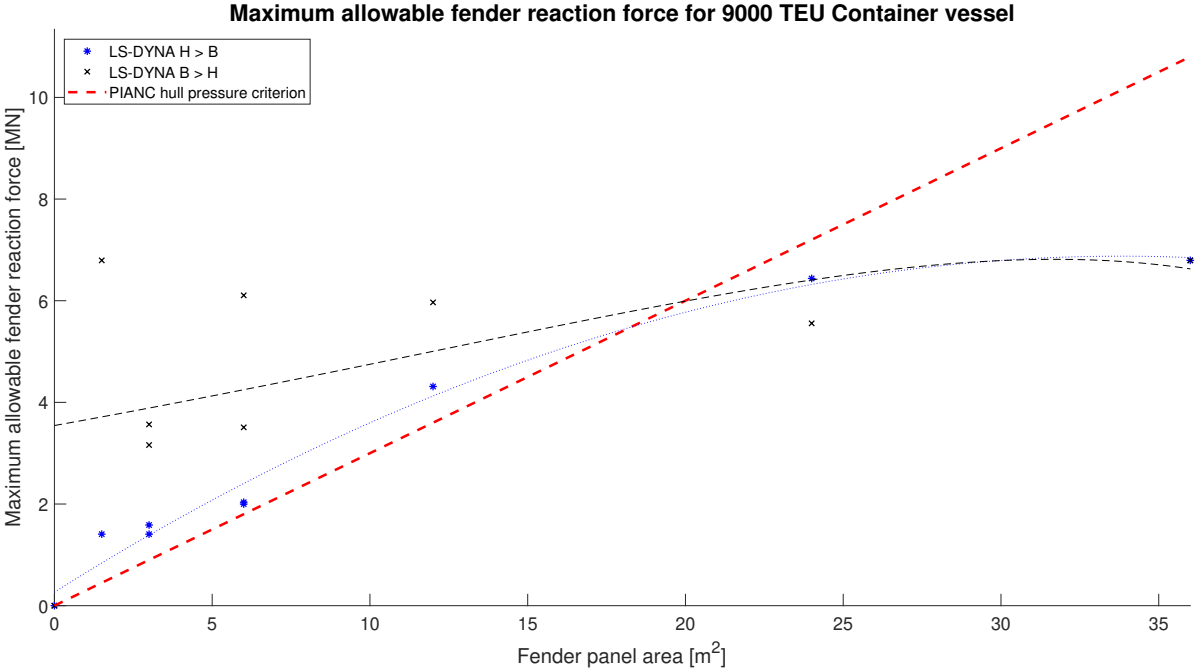


Figure 6.12: Allowable total reaction force on the parallel hull of a Post-Panamax container vessel.

### 6.2.9. Bulk carrier 1

A handysize bulk carrier is also considered. Again, the numerical simulations with different panel dimensions were executed. The wide panels show higher capacities than the small panels. The relatively small web frame spacing influences the capacities largely in these small panel simulations. The 6m x 2m and 6m x 4m high panels show very large capacities as they engage with a web frame and a deck. Due to these high capacities, the results are strongly influenced.

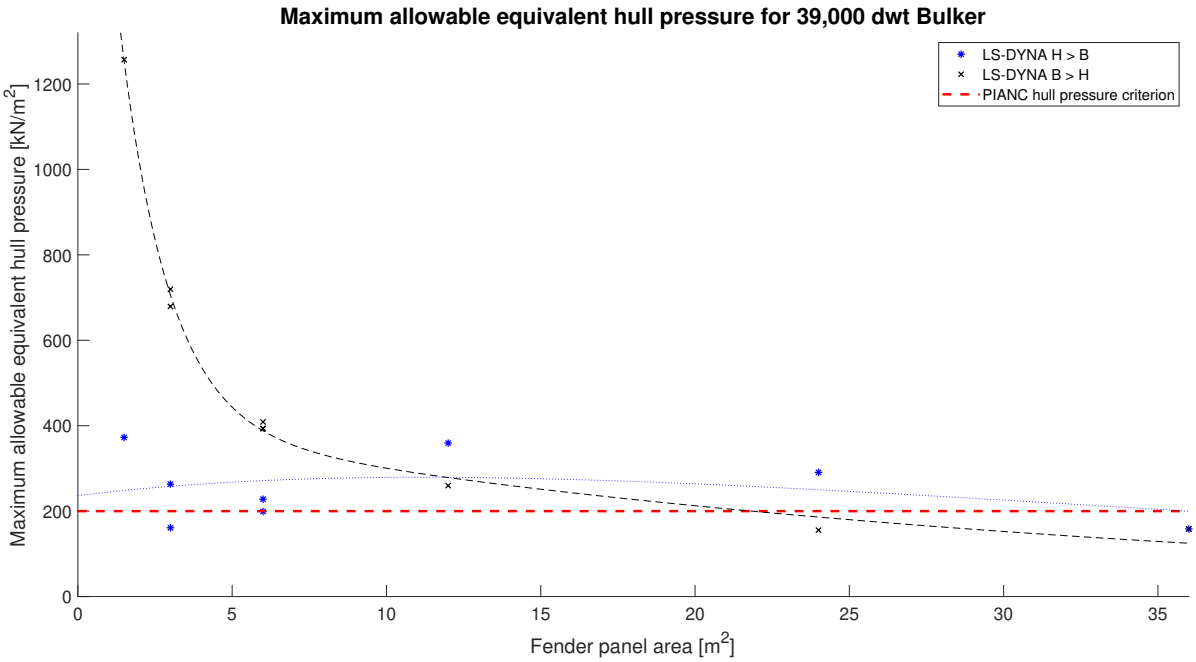


Figure 6.13: Allowable equivalent hull pressure on a Handysize bulk carrier.

The outcomes of the simulations are safe with the current PIANC lower limit hull pressure criterion until 2.2 $MN$ from where the exponential trend line intersects with the PIANC linear force criterion. The trend line for the high panels does not show a strong trend to any horizontal asymptote. The high capacities reached for the 6m × 2m panel and the 6m × 4m are the cause of this discrepancy.

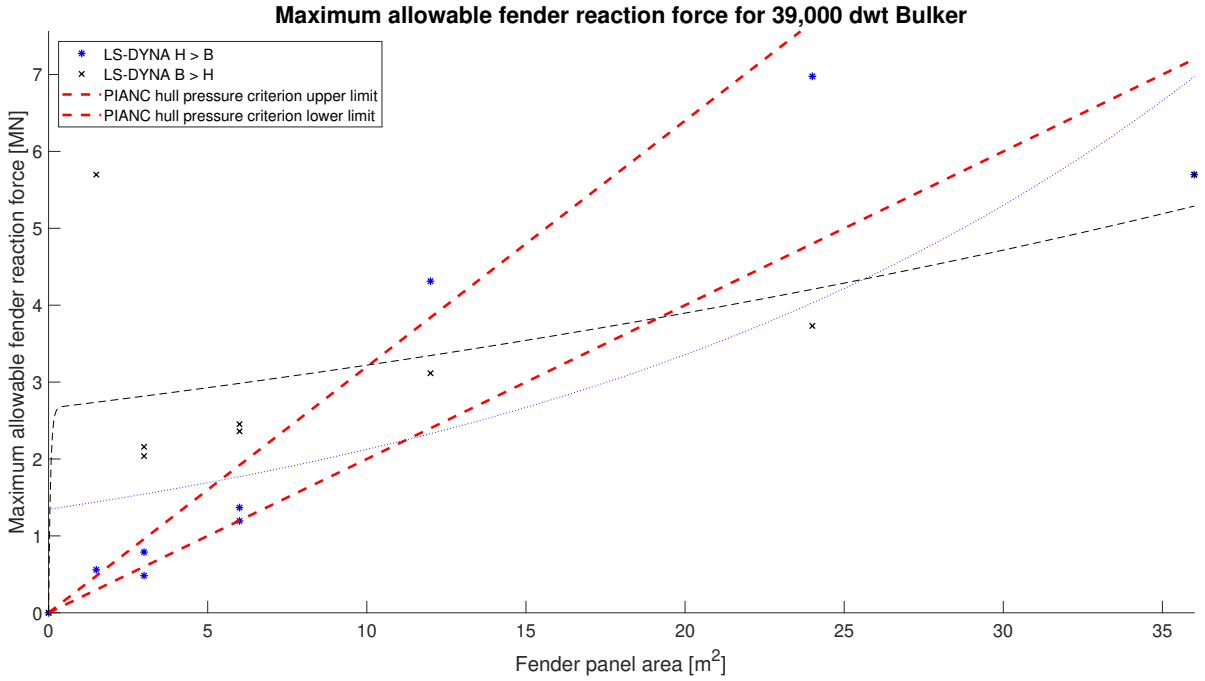


Figure 6.14: Allowable total reaction force on the parallel hull of a Handysize bulk carrier.

## 6.2.10. Bulk carrier 2

For the ultra-large bulk carrier (ULBC) the results show different force-area relations than the previous results. For both high and wide panels, relatively high equivalent hull pressure capacities are reached.

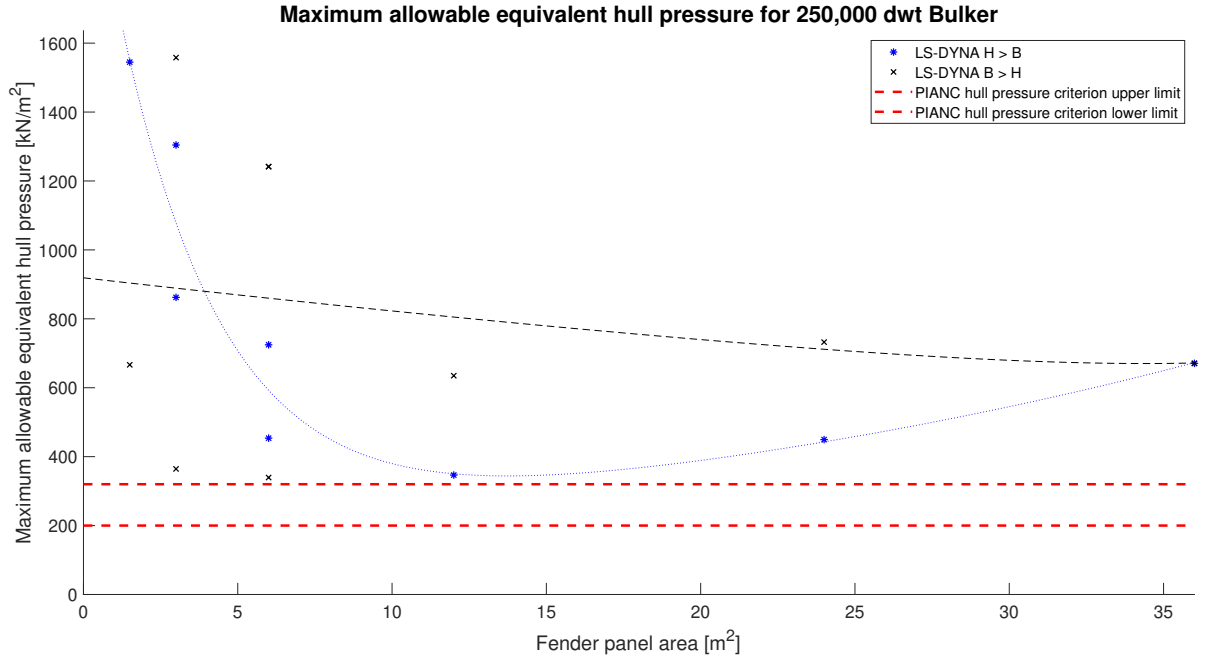


Figure 6.15: Allowable equivalent hull pressure on a Capesize bulk carrier.

The allowable total reaction force for the large bulk carrier increases with the fender panel area. For this size bulk carrier, no horizontal asymptote is visible in the force-area relation. It is important to note that the impact location of the fender panels is at the large web frame for the bulk carrier. For the large bulk carrier at the impact location of the fender both 200 $kN/m^2$ and 320 $kN/m^2$ would be acceptable as all simulations point lie above the 320 $kN/m^2$ limit.

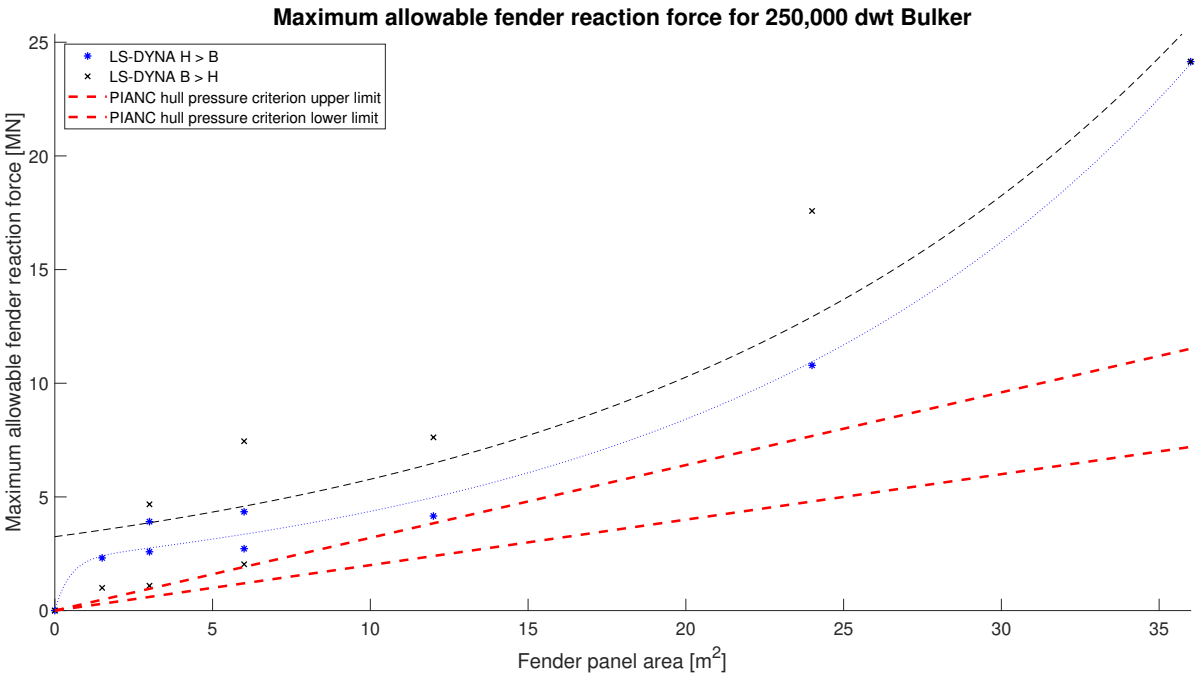


Figure 6.16: Allowable total reaction force on the parallel hull of a Capesize bulk carrier.

## 6.3. Observed failure modes

In Section 4.5, the sensitivity of the large single shell bulk carrier and the large container carrier to tripping failure are explored. Indications were found for both that tripping failure is a possible governing failure mode. In this part, the observed failure response at the onset of plasticity is presented. Small and slim panels in between web frames result in stiffener-plate failure in the container vessel. Tripping happens in the case of a panel that almost spanned the width between the web frames. For the large bulk carrier, high and slim panels result in stiffener tripping of the low part of the very long stiffeners. High and slim panels also result in tripping in the container structure. As soon as the stiffener panel covers one or several web frames, the web frame failure is the governing failure response. However, the onset of plasticity then occurs in a much higher reaction force. The failure behaviour is in most situations not one single mode of failure that is observed, but in general stiffener-plate failure happens for small panels in between web frames and tripping occurs for higher but slim panels. Web frame failure was governing in all cases where the panel engaged with a web frame.

## 6.4. Comparison to prior results

The outcomes of the numerical simulations are presented in relation to prior research on fender impact by Vredeveldt and Rhijsburger [32] and IJzerman [12] discussed in Chapter 2.

### 6.4.1. Systematic cylindrical fender study by Vredeveldt and Rhijnsburger

In table 6.6, a comparison is presented between the results obtained from the numerical simulations of cylindrical impact on a single stiffener [32] and the small panels of the simulations executed in Chapter 5. The cylindrical fenders are rubber elements without a fender panel, therefore, the contact area is not constant. The contact area is at the largest at the maximum deflection of the cylindrical fender and is stated in the table below. Furthermore, only the wide panels for the numerical simulations in Chapter 5, are included in the comparison, as these correspond to the contact area of the cylindrical fender. The significantly higher capacities obtained from the panel impact, suggest that the additional activation of web frames and more stiffeners improve the capacity significantly.

Table 6.6: Comparison of hull capacities according to numerical single stiffener cylindrical fender impact study [32] and LS-DYNA simulations.

| Vessel (Appendix A) | Fender type* [32] | Full compression cylindrical fender contact area $m^2$[32] | Numerical single stiffener allowable reaction force [kN][32] | LS-DYNA fender panel contact area [m] | Numerical simulations allowable reaction force [kN] |
|---|---|---|---|---|---|
| Tanker coaster (T1) | ⌀1000-600-1000 | 0.94 | 134 | 1.5 | 2035 |
| Tanker coaster (T1) | ⌀1400-800-2200 | 2.76 | 232 | 3.0 | 2155 |
| Container Panamax (C3) | ⌀1400-800-2200 | 2.76 | 623 | 3.0 | 3160 |

**Fender dimensions (⌀1000-600-1500) is outer diameter - inner diameter - width.*

Only a limited number of numerical simulations were executed in the study by Vredeveldt and Rhijnsburger. All vessels included in this study were incorporated into an analytical model. A full comparison of the analytical results obtained in the study by Vredeveldt and Rhijnsburger is presented in Appendix D. The analytical results underestimate the capacity for cylindrical fender impact in comparison to the numerical capacities obtained by TNO. The differences were reported in a range of 58% to 99%.

### 6.4.2. Plate- and stiffener-induced failure formulations by IJzerman

The study of IJzerman resulted in a generic semi-analytical formulation for the allowable equivalent hull pressure [12]. The formulation is presented in the background of this study in Chapter 2. In the following sections, the outcomes of the numerical simulations of the governing vessels are set side by side with the semi-analytical formulation of IJzerman.

### Small tanker vessel

First, the results for the small tanker vessel are compared to the results of IJzerman in Figures 6.17 and 6.18. The allowable loads and equivalent pressure of the semi-analytical equation are conservative compared to the numerical simulations. The capacity of the ship to resist fender loads is higher for small panels. The upper limit for the formulation by IJzerman lies close to the outcomes of the numerical simulations and is well under the PIANC hull pressure criterion.

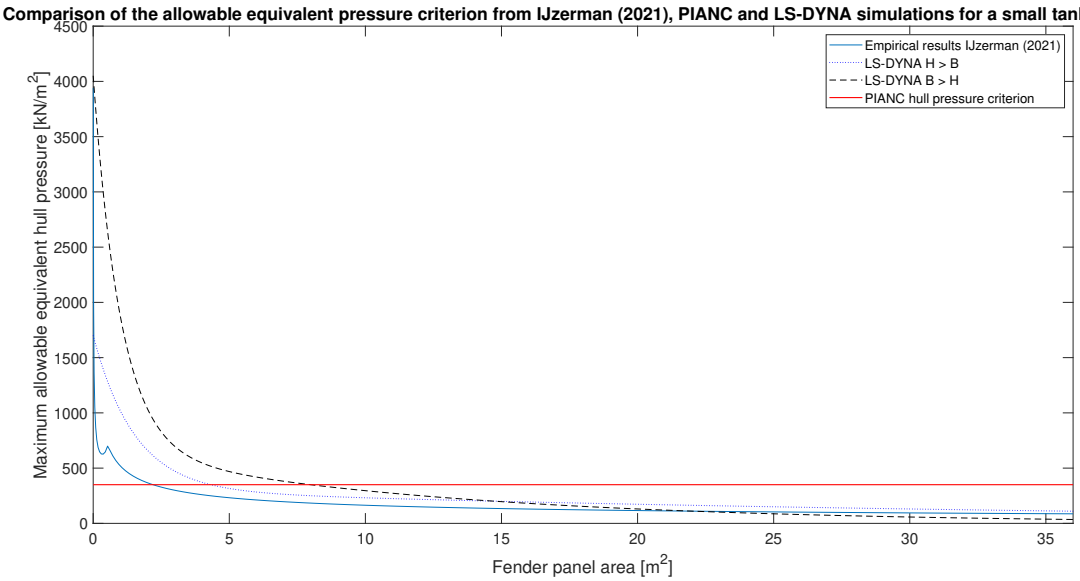


Figure 6.17: Comparison of the safe equivalent hull pressure for a small tanker according to prior research by IJzerman [12], the numerical simulations and PIANC.

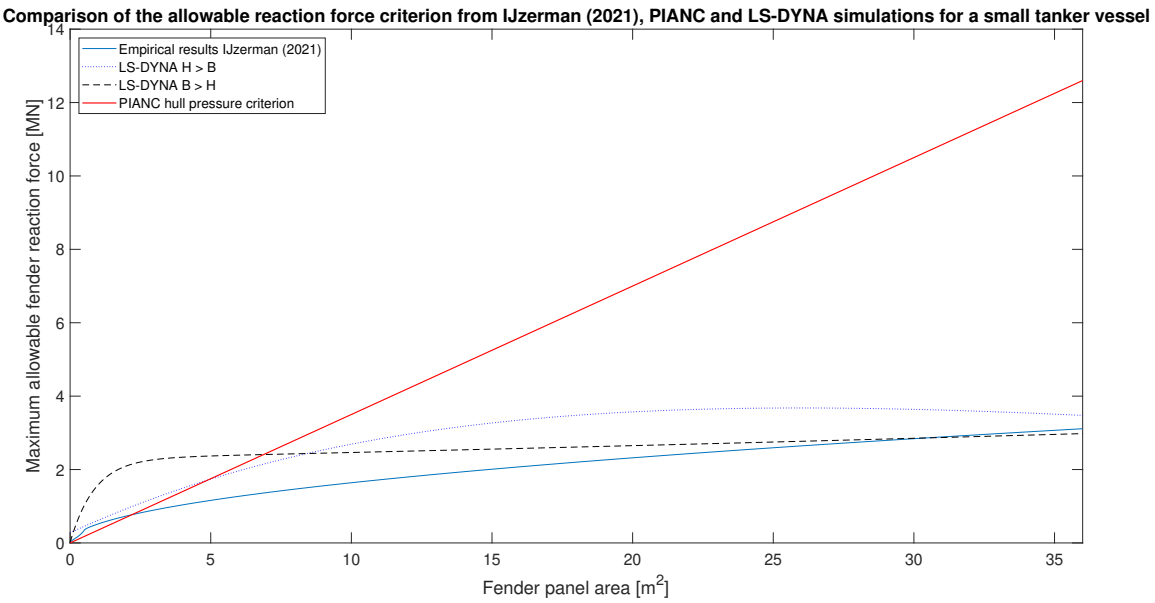


Figure 6.18: Comparison of the safe reaction force for a small tanker according to prior research by IJzerman [12], the numerical simulations and PIANC.

### Large bulk carrier

Next, the results of the large bulk carrier are compared to the outcomes of IJzermans formulation in Figures 6.19 and 6.20. According to the study of IJzerman, the capacities of the large bulk carrier to withstand fender loads are safe for the complete range of the PIANC lower limit and most of the upper limit for bulkers. This is in contrast with the numerical simulations, where the allowable total reaction force does not increase rapidly after a panel area of 10 $m^2$.

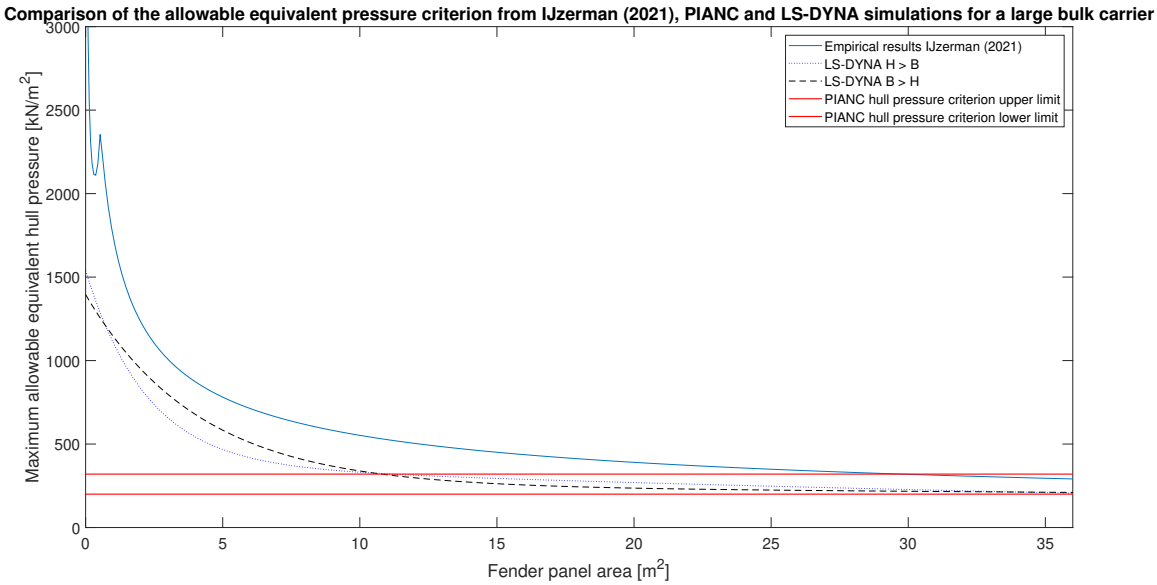


Figure 6.19: Comparison of the safe equivalent hull pressure for a large bulk carrier according to prior research by IJzerman [12], the numerical simulations and PIANC.

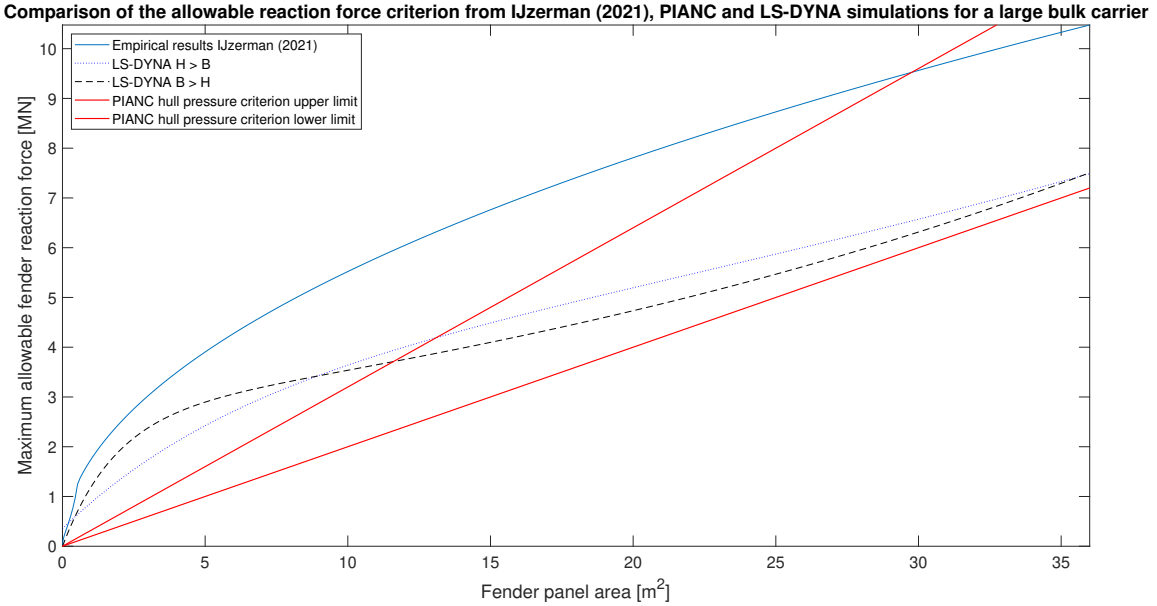


Figure 6.20: Comparison of the safe reaction force for a large bulk carrier according to prior research by IJzerman [12], the numerical simulations and PIANC.

### Large container vessel

Lastly, the large container vessel is studied in relation to the semi-analytical results in Figures 6.21 and 6.22. For the large container vessel, the numerical simulations show a clear limitation to the maximum allowable fender reaction force. In contrast, the formulation of IJzerman shows a linear increase in the capacity with the fender panel area. This is also visible in the equivalent hull pressure figure, where the formulation of IJzerman takes an almost constant value for higher fender panels.

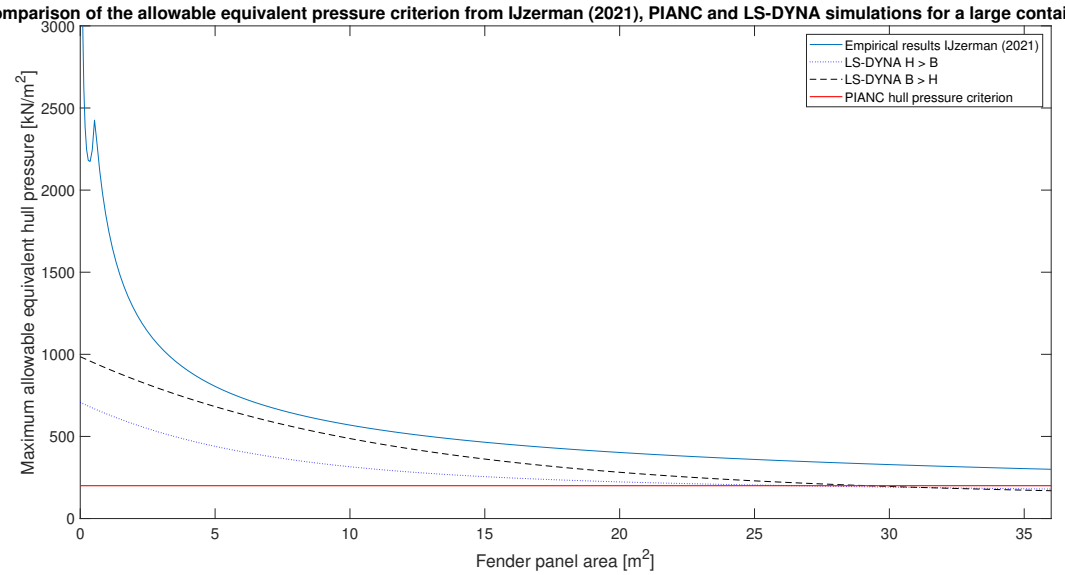


Figure 6.21: Comparison of the safe equivalent reaction force for a large container carrier according to prior research by IJzerman [12], the numerical simulations and PIANC.

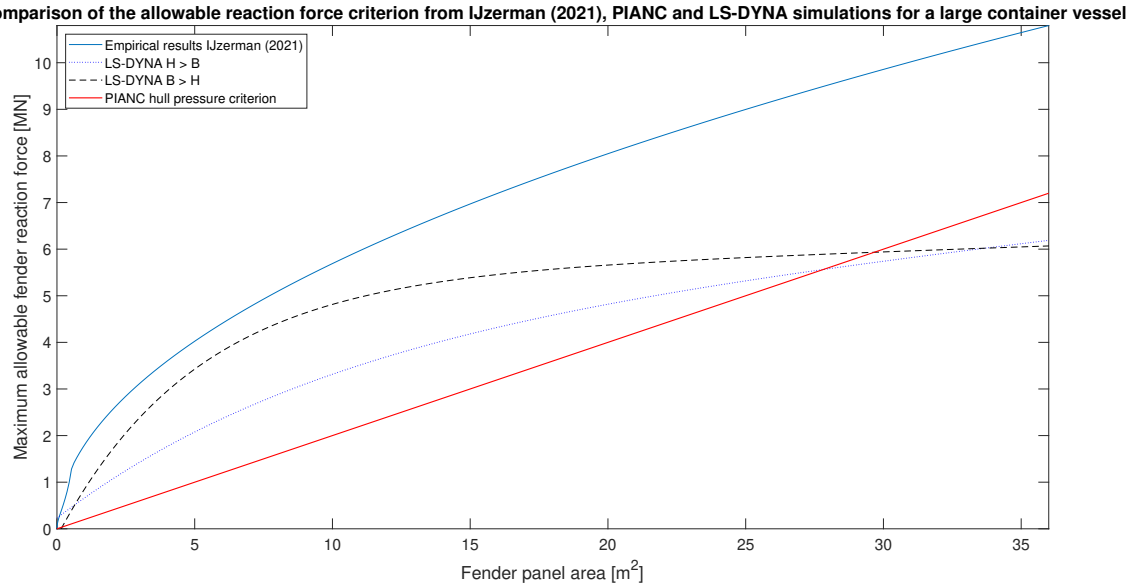


Figure 6.22: Comparison of the safe reaction force for a large container carrier according to prior research by IJzerman [12], the numerical simulations and PIANC.

The semi-analytical formulation of IJzerman shows agreement in some regions of the results. However, the pressure-area relationship and limitations that are visible from the numerical simulations and the interaction of and with different structural components do lead to variance in the results with large fender panels for large vessels. The wide panels in the numerical simulation give a very high response capacity for the small tanker vessel in comparison to the study of IJzerman and TNO and underline the

difference in engagement with different structural components for wide panels. In general, the formulation of IJzerman overestimates the capacities that were found for the large vessels in the numerical simulations. This suggests that the numerical simulations account for the concentration of stress in certain components, which results in yielding to occur at an earlier state. However, for the small vessel, even lower capacities than retrieved from the numerical simulations were found. This aligns with what was found in literature, that the activation of web frames and decks results in additional capacity for the small vessel.

# 7

# Discussion and recommendations

## 7.1. Interpretation of the results

When the results from Chapter 6 are carefully examined, it is noticed that the governing vessels show a second-order exponential relation between total allowable reaction force and fender panel area. This results in the linear fender-area relationship proposed by the PIANC criterion is too optimistic for large fender panels. Consequently, the PIANC criterion has to be updated for safe berthing. Furthermore, the allowable fender load is strongly influenced by the structural geometry of the vessel. This is illustrated by the allowable reaction force for the smaller vessels. The total allowable capacity is reached at a much lower total reaction force. Furthermore, for small vessels, the wide panels do not outperform the high panels in all dimensions. As web frames are activated at an earlier stage and the stress concentration remains in these web frames, the capacity does not increase exponentially with the width. In some cases, high panels on small vessels activate a deck and generate an additional increase in allowable load. Therefore, the correct sizing of fender panels results in more efficient use of the vessel's capacity. Moreover, the small bulk carriers capacity is overestimated in the very low panel region. This range of panels only engages with the stiffened panel in between the web frames. It is important because this specific vessel is built in grade A steel, this means that the implementation of the current PIANC guidelines could result in yielding. For this specific vessel type, small bulk carriers, it is advised to always engage with a web frame or deck. In the results, there is no clear answer to what the allowable reaction force for a point load is. This means that the trend line is influenced by this value, which is currently 0, following from the PIANC criterion. It is observed that small contact areas, e.g. cylindrical fenders, allow for hull pressure much higher than the PIANC criterion. It endorses the findings of Vredeveldt and Rhijsburger that cylindrical allow for safe berthing in moderate berthing condition ports. For the analytical formulation, the uniform distribution of Adamchak shows similar agreement as the modified Shahabian and Roberts stress field. Both are in different regions, but it can be ascribed to the fender panel dimensions concerning the web frame spacing.

## 7.2. Relevance

Verifying and validating the allowable fender-induced load is relevant to ensure safe berthing. Every vessel berths in its lifetime, and there still was uncertainty about the structural behaviour and capacities to these berthing loads. As vessels keep growing, the berthing energy and loads increase. Therefore, it was important to identify the mechanisms influencing the structural capacities to resist berthing loads in this study. Quantifying these capacities and the influence of the fender design ensures safe hull criteria for new fender design guidelines. Moreover, analysing the parallel hull of different vessels give insight into the parametric influence and the identified trend led to an update of the current criterion. Furthermore, the analytical formulation of tripping is not only relevant to describe tripping failure due to fender loading but also to other cases resulting in transverse concentrated loads stiffeners. The findings of this study can also be used by classification societies to write rules for the patch-loading strength of ships. The pre-buckling stress fields and tripping formulations can also be applied to web girders in bridges and other civil structures.

## 7.3. Limitations

One of the important limitations of this research is that in the numerical simulations perfect geometries without residual stresses or initial imperfections were used. In case initial imperfections or residual stresses exist in the ship section the threshold to the onset of plasticity is expected to be lower. Furthermore, the initial deformation influences the observed failure behaviour and makes the structure more sensitive to failure in a shape similar to the initial deformations. Considering the reduced capacity in case of initial deformation the current simulations may overestimate the ship's capacity. However, the lowest steel grade, Grade A with a minimum required yield strength of 235 $MPa$, is used to define the lower limit for the onset of plasticity and to be able to compare to prior results. Other steel grades with higher yield strengths are more widely applied and the influence of this is not covered in this study. It is important to take this hidden safety into account when interpreting the results of this research. It is argued that the incorporation of Grade A steel to the perfect geometry of the ship section makes it acceptable as a limit to apply in the PIANC guidelines. A limiting factor in the analytical approach was the inaccuracy in describing the pre-buckling stress fields of the stiffener web in the analytical tripping formulation. In this study, it is concluded that the modified stress field shows better agreement but is still not completely in line with the numerically observed behaviour. One of the recommendations to overcome this is to incorporate the rotational restrain in tripping caused by the connected structural components to the stiffener, for example, web frames. Another limitation in the numerical model is the required time to prepare and simulate the different scenarios of fender panels and vessels. Methods like kriging show the potential to describe the trend of the onset of plasticity more accurately. Another consequence of the computational time is the limitation of the results to the considered vessel types and sizes for quantification. The practical finding can be applied more widely. Lastly, the dynamic behaviour is not incorporated in the numerical simulations. The reaction force only builds up and the contact remains. In practice, it is expected that it builds up, but the ship also rotates, and the reaction force builds up according to the fender force-displacement behaviour. As discussed in Chapter 5, the isolated model is expected to give a conservative approach.

## 7.4. Recommendations for future research

Following from the research, some recommendations are given for future research. First, the pre-buckling stress fields should be improved in the analytical model in further research. The accuracy of these stress fields highly influences the outcome of the analytical model and the obtained results show a discrepancy between the numerical simulations and failure in practice. It is also suggested to determine the influence of the rotational restrain of structural components attached to the ends of the stiffener. In the numerical simulations, web frames and decks restricted the ends of the stiffener to tripping and the allowable loads were significantly higher than the outcome of the analytical solutions. Furthermore, the equations should be updated with residual stresses and initial deformation, the solution proposed by Danielson can be applied for this [6]. One of the most promising recommendations for the short term is to determine the point load capacity of the vessel hulls. This allows to determine the yielding point for the point where the area is zero in the force-area and pressure-area relationship figures. A kriging methodology could be implemented in numerical models in further research. It will help to construct a more accurate allowable impact criterion over the full range of available fender panels and vessel dimensions. Furthermore, this will facilitate an optimisation algorithm to determine the optimal fender panel dimension for corresponding vessels. More information should be obtained about correlations of the maximum allowable reaction force or equivalent hull pressure to other variables than the fender panel area. Another practical recommendation is to do statistical research on web frame and deck spacing for the range of vessels visiting berths that require new fenders. This will discretize the required minimal fender panel width or height to ensure the activation of the structural capacity of the web frames. To further complement the PIANC hull pressure criterion table, research on belting and the impact of belting is necessary. Belting is regularly governing in fender panel design, for example, ferry terminals.

## 7.5. Recommendations for PIANC WG211

This study showed that the typical hull pressure table from WG33 needs to be updated. Based on the results of this study, it is advised to adjust the current linear hull pressure criterion with the equivalent contact area by adding the limit to the allowable reaction force. The efficient fender panel dimensions are related to the size of the vessel. Moreover, as the large bulk carriers clearly outperform the small bulk carrier (B1), it is advised to adopt a different criterion for small and large bulk carriers in the criterion. Furthermore, it is concluded from the numerical simulations that wider panels are more effective than high panels in most applications. Therefore, it is important to underline this in the fender design guidelines. If the results are compared to the rated fender reaction force for the vessels in Table 6.4, it can be noted that the reaction force-area graphs should be limited. The outcomes of this study are summarized in Table 7.1. At last, based on Figure 5.4, it is advised to eliminate the current softness factor of $C_s = 0.9$. It is found that the contribution of the ship hull is 1% at most for the vessels included in this research. Therefore, the $C_s$ factor approaches one and should be taken out.

Table 7.1: Recommendation for the update of the PIANC hull pressure criterion for WG211.

| Type of vessel | Vessel in this study | Allowable hull pressure WG33 [$kN/m^2$] | Recommended allowable hull pressure [$kN/m^2$] | Recommended allowable total fender impact load [$MN$] |
|---|---|---|---|---|
| Container vessel 1st and 2nd generation | C1 and C2 | <400 | 400* | 1.5 |
| Container vessel 3rd generations | C3 | <300 | 300 | 5.5 |
| Container vessel 5th and 6th generation | C4 | <200 | 200 | 5.6 |
| Small bulk carriers | B1 | <200 | 200 | 2.2 |
| Large bulk carriers | B2 and B3 | <200 | 320 | 3.8 |
| Oil tankers =/< 60.000 DWT | T1 | <300 | 300 | 1.8 |

** 240 $kN/m^2$ has to be adopted if activation of web frame or deck can not be guaranteed.*

# 8

# Conclusion

Due to the increase in the size and capacity of vessels, the current PIANC guidelines for the design of fender systems have to be updated in 2023. The main objective of this thesis has been to validate and verify the current PIANC hull pressure criterion for the new guidelines. To obtain an updated generic formulation for the capacity of ships to withstand the fender-induced load, numerical simulations of detailed parallel hull geometries have been executed. A parametric approach was adopted to include the diversity of both vessels and fenders. Furthermore, an additional governing failure mode has been examined and included.

This chapter provides the answers to the research questions.

1. What is the governing failure mode in loading of the ship's side hull by fenders equipped with panels?
2. How can the critical failure load for the governing failure mode be analytically formulated?
3. To what extent are the critical fender-induced loads influenced by the impact location and the dimensions of the fender panel?
4. What is the influence of the vessel's dimensions and type on the critical fender-induced loads?
5. Which structural components can be identified as the weakest link(s) in contact between fenders and vessels?
6. What is the optimal fender panel dimension, considering critical failure mechanism and vessel diversity?

To conclude, the main research question is answered by summarizing the main findings of this study at the end of the chapter.

The first objective was to gain insight into the structural response for fenders engaging with several structural elements. It was found that the governing failure mode in the ship-fender panel contact largely depends on the dimensions of the fender panel. The dimensions of the fender panel in relation to the ship's structural components activate different failure modes. For panels narrower than the web frame spacing, the highest stresses occur in the stiffeners. Consequently, either plate-stiffener failure or tripping failure occurs. Numerical simulations showed that for small and narrow panels the plate- and stiffener-induced failure is governing, while high and slim panels result in stiffener tripping. The parallel hull showed to be even more sensitive to tripping failure if the stiffeners have a long span. As soon as the fender panel activates a web frame or a deck, the stresses concentrate in those larger structural components. The stress in the plate and stiffeners are no longer governing in failure. Therefore, yielding occurs in the web frame and the risk of tripping decreases. When a fender panel activates one or more web frames in the structure, the capacity to fender-induced loads rise and the parallel structure can safely carry higher reaction forces from the fender panel.

As concluded above three main failure modes were observed, plate-stiffener-induced failure, tripping of stiffeners and yielding in web frames (or decks). The second objective of this study was to obtain

an analytical solution for these critical failure loads. A formulation of the first failure response was found in literature: IJzerman suggested a lower-bound fit to analytical solutions to quantify plate- and stiffener-induced failure [12]. To describe tripping failure, a modification of the existing pre-buckling stress field formulations, defined by Adamchak [1] and Shahabian and Roberts [25], was proposed. In this research, a new solution for the pre-buckling stress field is formulated that shows better agreement with numerical pre-buckling stress fields retrieved from different web frame configurations in LS-DYNA. The corresponding critical failure patch load for single stiffeners could be derived using these pre-buckling stress fields with the Rayleigh-Ritz approximation. However, this analytical formulation underestimates the capacity of the hull structure to withstand berthing loads by fenders. And needs to be improved with additional rotation restrain by web frame, before it can be used to estimate the critical fender-induced loads to tripping. Moreover, the web frame failure occurs at larger induced loads, because the structural capacity of the web frame is much larger than the stiffened panel. It is, therefore, not necessary to provide an analytical formulation, as it is not considered to be the critical failure mode.

To determine the influence of the impact location and dimension of the fender on the critical fender-induced loads, numerical simulations were performed for eight vessels with fifteen fender panel sizes. The results show that the impact location and contact area indeed influence the capacity of the ship's structural response. The impact location largely influences how the stress is distributed in the stiffeners, plate, and web frames. This result is in alignment with those of accidental impact resulting in plastic deformation in studies on arctic engineering [14, 33, 34]. Consequently, fender contact areas activating a web frame or deck significantly increases the load resisting capacities. However, when the fender panel dimensions increase, a limiting value was found for the total fender-induced load. This indicates that the constant hull pressure criterion adopted by PIANC can not be safely applied to all panel dimensions. The relation between the fender panel area and the maximal reaction force follows a non-linear, exponential trend. A limit to the total allowed fender reaction force is proposed as an addition to the hull pressure criterion to ensure safe berthing.

Bulk carriers, container vessels and tankers were tested for their load-carrying capacity to quantify the influence of a vessel's dimension, and it's type on the critical fender-induced loads. It was found that the structural layout of the vessel strongly influences the capacity. The capacity of the cell structure, generally found in container vessels and tankers, showed to be influenced by the web frame spacing. Because of the web frame, it can carry higher fender-induced loads as the stress concentrates in this larger component. The wide panels clearly outperformed the high panels for these large vessels as they activate with web frames. For small vessels, the correlation of the allowable pressure with the height/width ratio of the fender panels was less clear. Because the smaller web frame spacing in these ships results in an earlier activation of web frames. For all the examined ship sizes, the areas engaging with web frames and decks outperformed similar areas that engaged with either one. However, for smaller vessels, the stress also concentrates in the web frame and remains governing, and the increase of the contact area does not result in additional capacity. Therefore, for a small container vessel, the total reaction force capacity is lower than for larger vessels of a similar type. Additionally, for large container vessels and single-shell bulk carriers, the numerical simulations proved that tripping failure is a possible governing failure mode. These vessels have long stiffeners, which makes them vulnerable to rotation around the line of attachment. This corresponds with the claim of Barber that single shell bulkers are sensitive to tripping failure [3] and are confirmed by applying an analytical tripping sensitivity formulation [26]. To conclude, the vessel's dimensions largely influence the critical fender-induced loads.

Base on the findings in this research, an update for the current PIANC hull pressure criterion is suggested. The equivalent hull pressure can be maintained, however, it should be limited with a total allowable reaction force on the parallel hull. Moreover, the distinction between small and large bulk carriers needs to be considered in the hull pressure capacities of the update of the guidelines. With respect to the fender design stated in the PIANC guidelines, it is recommended that the weakness of the stiffened panels between web frames is addressed. Consequently, fender panels should be dimensions to sufficiently activate the available structural capacity in the ship's hull, i.e. engage with either a web frame or a deck.

Finally, the main research question: *"How can critical fender-induced loads acting on the parallel side hull be quantified, accounting for the diversity of vessel and fender?"* can be answered. This research shows that the critical fender-induced load is largely influenced by the structural layout of the ship, particularly the web frame spacing and the size of the fender panel in relation to the vessel's di-

mensions. The constant hull pressure criterion implemented in the current guidelines for fender design of PIANC overestimates the ship's structural capacities. Instead, this research indicates it should be limited to the total allowable reaction force of the fender. Moreover, in general, wide panels outperform high panels, because they activate the web frames. However, making the panels much wider than the web frame does not necessarily result in higher allowable loads, as the stress is mainly concentrated in the web frames. This is in contrast to the findings for small vessels, where wide panels do not always outperform high panels. Additionally, for small vessels, high panels regularly engage with decks, which increases the fender-induced load-carrying capacity. This research includes large and small vessels and quantifies the allowable equivalent pressure and total reaction force. By implementing the design recommendations to dimension panels, such that the fender engages with a web frame or deck, efficient use of the vessel's capacity can be ensured. The outcomes of this study are not only interesting for the update of the fender design guidelines but can also be implemented for rules on the patch load's resistance of ships by classification societies.

# A

# Ship properties and structural layout

For the research to the impact capacity of the parallel hull of the ship to fender-induced loads, three vessel types are considered: tankers, bulk carriers and container vessels. To cover the range of vessels considered in the current PIANC hull pressure criterion several sizes are considered. The following vessels are considered in the body of this research:

- Tanker 1: Coaster (T1)
- Container vessel 4: ULCV (C4)
- Bulk carrier 3: Panamax (B3)
- Container vessel 1: Feeder (C1)
- Container vessel 2: Coaster (C2)
- Container vessel 3: Panamax (C3)
- Bulk carrier 1: Handysize (B1)
- Bulk carrier 2: Capesize/VLBC(B2)

The first three vessels are elaborated on in Section 5.6.3 as the governing hulls and therefore, presented first. Table A.1 presents the current PIANC hull pressure criterion and the corresponding vessel in this study to verify and validate the current criterion.

Table A.1: Vessel types covered in study for update of the PIANC hull pressure criterion for WG211.

| Type of vessel | Vessel in this study | Allowable hull pressure WG33 [$kN/m^2$] |
|---|---|---|
| Container vessel 1st and 2nd generation | C1 and C2 | <400 |
| Container vessel 3rd generations | C3 | <300 |
| Container vessel 5th and 6th generation | C4 | <200 |
| Bulk carriers | B1, B2 and B3 | <200 |
| Oil tankers =/<60.000 DWT | T1 | <300 |

## A.1. Tanker 1

Table A.2 states the main properties of the small tanker vessel.

Table A.2: Vessel properties of tanker coaster (T1).

| Property | Value |
|---|---|
| **Vessel type** | Tanker coaster |
| **Length over all (LOA)** | 104.52 m |
| **Breadth (B)** | 17 m |
| **Depth (T)** | 9.5 m |
| **Draught (D)** | 6.3 m |
| **Deadweight tonnage (DWT)** | 7072 t |
| **Capacity** | 8363 $m^3$ |
| **PIANC hull pressure** | 350 $kN/m^2$ |
| **Rated reaction force fender** | 1.4 MN |
| **Web frame spacing** | 2.66 m |

Figure A.1 shows the structural layout of a parallel hull section of the tanker vessel. The section that is used for the numerical simulations is 10.6m wide.

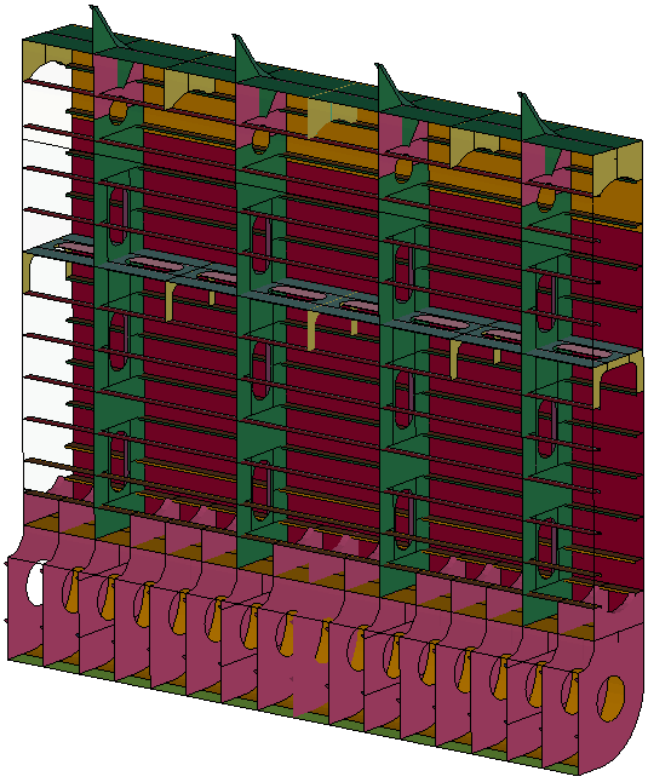

Figure A.1: Structural layout of tanker coaster, where the inner hull is transparent for visual purposes.

## A.2. Container vessel 4

Table A.3 states the main properties of the Ultra Large Container vessel (ULVC).

Table A.3: Vessel properties of ULVC (C4).

| Property | Value |
|---|---|
| **Vessel type** | ULCV/New Panamax |
| **Length over all (LOA)** | 400 m |
| **Breadth (B)** | 58.6 m |
| **Depth (T)** | 30.5 m |
| **Draught (D)** | 14.5 m |
| **Deadweight tonnage (DWT)** | 156,200 t |
| **Capacity** | 19,000 TEU |
| **PIANC hull pressure** | 200 $kN/m^2$ |
| **Rated reaction force fender** | 5.3 MN |
| **Web frame spacing** | 3.16 m |

Figure A.2 shows the structural layout of a parallel hull section of the tanker vessel. The section that is used for the numerical simulations is 12.6 m wide.

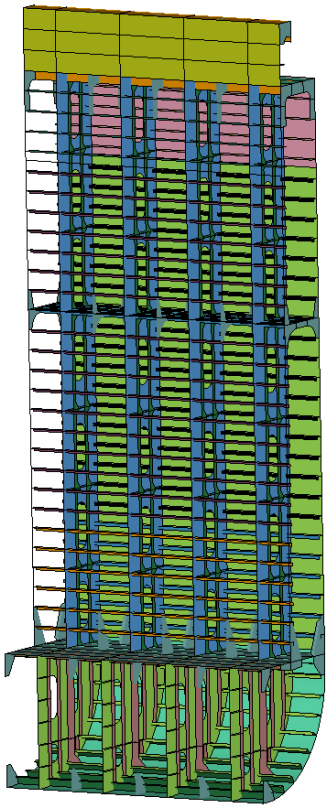

Figure A.2: Structural layout of ULCV, where the inner hull is transparent for visual purposes.

## A.3. Bulk carrier 3

Table A.4 states the main properties of the Panamax bulk carrier. For bulkers the PIANC hull pressure criterion is 200 $kN/m^2$, but in some cases a upper limit of 320 $kN/m^2$ is adopted.

Table A.4: Vessel properties of Panamax bulk carrier (B3).

| Property | Value |
|---|---|
| **Vessel type** | Panamax |
| **Length over all (LOA)** | 196 m |
| **Breadth (B)** | 32.26 m |
| **Depth (T)** | 18.5 m |
| **Draught (D)** | 13 m |
| **Deadweight tonnage (DWT)** | 58,608 t |
| **Capacity** | 58,609 t |
| **PIANC hull pressure** | 200 $kN/m^2$ |
| **Rated reaction force fender** | 3.4 MN |
| **Web frame spacing** | 3.2 m |

Figure A.3 shows the structural layout of a parallel hull section of the tanker vessel. The section that is used for the numerical simulations is 12.8 m wide.

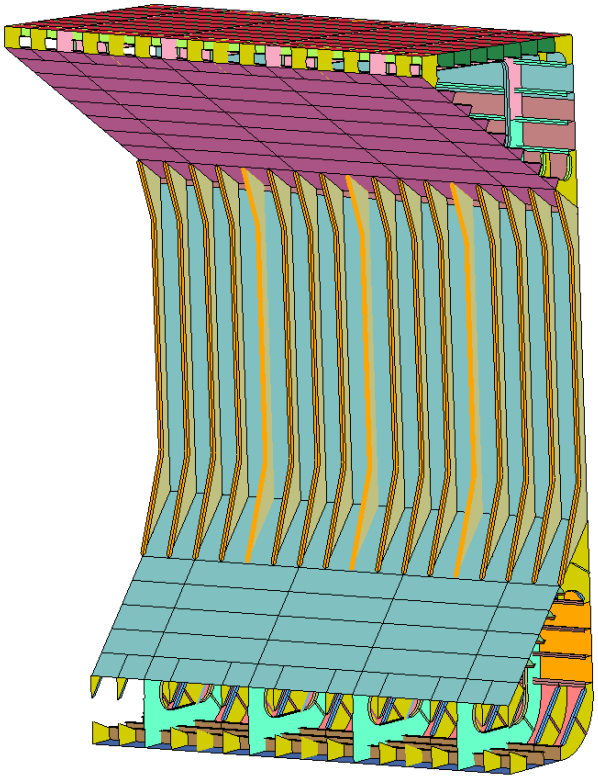

Figure A.3: Structural layout of Panamax bulk carrier.

## A.4. Container vessel 1

Table A.5 states the main properties of the feeder size container.

Table A.5: Vessel properties of container feeder (C1)

| Property | Value |
|---|---|
| **Vessel type** | Feeder |
| **Length over all (LOA)** | 118.24 m |
| **Breadth (B)** | 15.9 m |
| **Depth (T)** | 8.8 m |
| **Draught (D)** | 7.21 m |
| **Deadweight tonnage (DWT)** | 8300 t |
| **Capacity** | 754 TEU |
| **PIANC hull pressure** | 400 $kN/m^2$ |
| **Rated reaction force fender** | 1.0 MN |
| **Web frame spacing** | 1.995 m |

Figure A.4 shows the structural layout of a parallel hull section of the tanker vessel. The section that is used for the numerical simulations is 8.0 m wide.

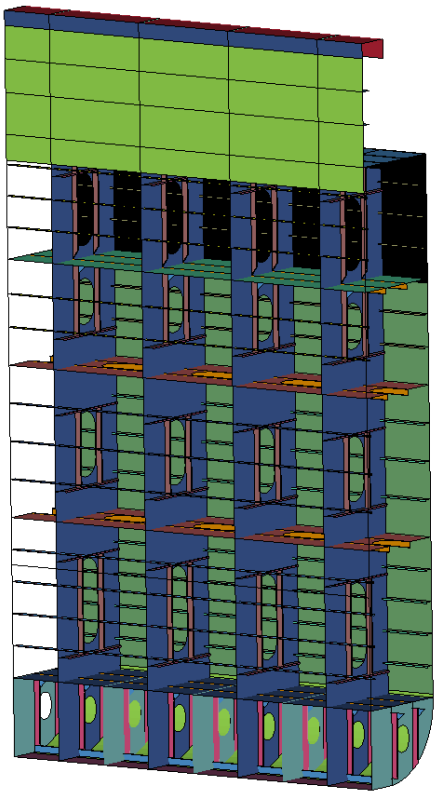

Figure A.4: Structural layout of container feeder, where the inner hull is transparent for visual purposes.

## A.5. Container vessel 2

Table A.6 states the main properties of a second generation container vessel.

Table A.6: Vessel properties of container coaster (C2)

| Property | Value |
|---|---|
| **Vessel type** | Coaster |
| **Length over all (LOA)** | 146.25 m |
| **Breadth (B)** | 19.7 m |
| **Depth (T)** | 11.45 m |
| **Draught (D)** | 8.25 m |
| **Deadweight tonnage (DWT)** | 13,500 t |
| **Capacity** | 7500 TEU |
| **PIANC hull pressure** | 400 $kN/m^2$ |
| **Rated reaction force fender** | 1.1 MN |
| **Web frame spacing** | 2.8 m |

Figure A.5 shows the structural layout of a parallel hull section of the tanker vessel. The section that is used for the numerical simulations is 11.35 m wide.

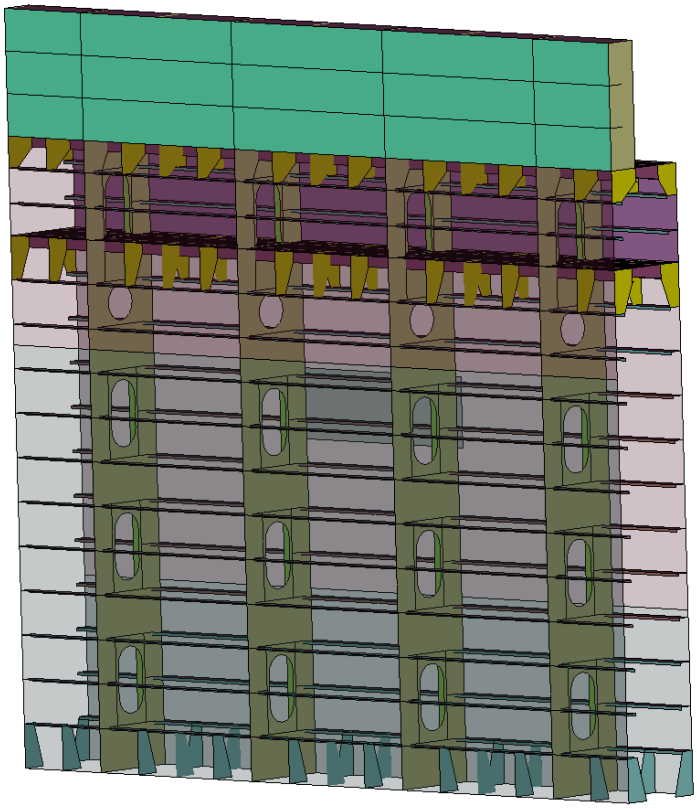

Figure A.5: Structural layout of container coaster, where the inner hull is transparent for visual purposes.

## A.6. Container vessel 3

Table A.7 states the main properties of Post-Panamax container vessel.

Table A.7: Vessel properties of Post-Panamax container vessel (C3)

| Property | Value |
|---|---|
| **Vessel type** | Post-Panamax |
| **Length over all (LOA)** | 229.92 m |
| **Breadth (B)** | 48.20 m |
| **Depth (T)** | 24.80 m |
| **Draught (D)** | 14.50 m |
| **Deadweight tonnage (DWT)** | 112,171 t |
| **Capacity** | 9000 TEU |
| **PIANC hull pressure** | 300 $kN/m^2$ |
| **Rated reaction force fender** | 2.1 MN |
| **Web frame spacing** | 3.16 m |

Figure A.6 shows the structural layout of a parallel hull section of the tanker vessel. The section that is used for the numerical simulations is 12.16 m wide.

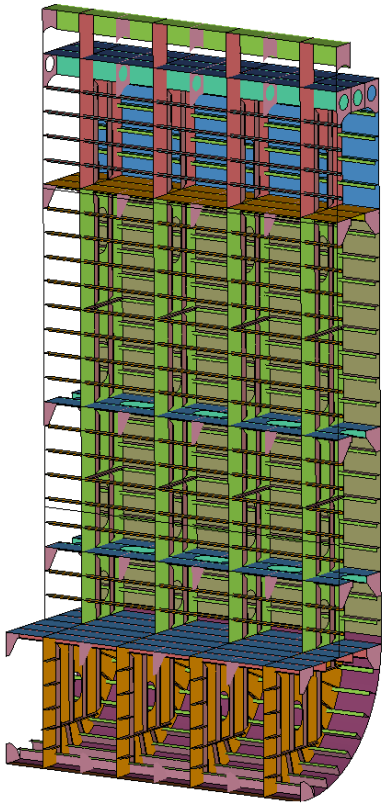

Figure A.6: Structural layout of Post-Panamax container vessel, where the inner hull is transparent for visual purposes.

## A.7. Bulk carrier 1

Table A.8 states the main properties of the Handy size bulk carrier. For bulkers the PIANC hull pressure criterion is 200 $kN/m^2$, but in some cases a upper limit of 320 $kN/m^2$ is adopted.

Table A.8: Vessel properties of Handysize bulk carrier (B1)

| Property | Value |
|---|---|
| **Vessel type** | Handy |
| **Length over all (LOA)** | 179.9 m |
| **Breadth (B)** | 30 m |
| **Depth (T)** | 14.8 m |
| **Draught (D)** | 10.6 m |
| **Deadweight tonnage (DWT)** | 39,000 t |
| **Capacity** | 39,000 t |
| **PIANC hull pressure** | 200 $kN/m^2$ |
| **Rated reaction force fender** | 1.4 MN |
| **Web frame spacing** | 2.4 m |

Figure A.7 shows the structural layout of a parallel hull section of the tanker vessel. The section that is used for the numerical simulations is 9.6 m wide.

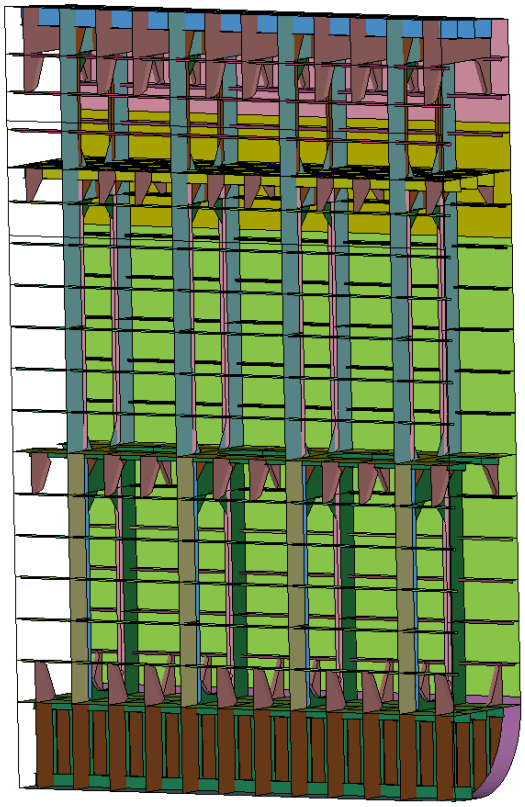

Figure A.7: Structural layout of Handysize bulk carrier, where the inner hull is transparent for visual purposes.

## A.8. Bulk carrier 2

Table A.9 states the main properties of the Very Large Bulk Carrier (VLBC) bulk carrier. For bulkers the PIANC hull pressure criterion is 200 $kN/m^2$, but in some cases a upper limit of 320 $kN/m^2$ is adopted.

Table A.9: Vessel properties of Capesize bulk carrier (B2)

| Property | Value |
|---|---|
| **Vessel type** | Capesize |
| **Length over all (LOA)** | 330.07 m |
| **Breadth (B)** | 57 m |
| **Depth (T)** | 25.10 m |
| **Draught (D)** | 18 m |
| **Deadweight tonnage (DWT)** | 250,000 t |
| **Capacity** | 250,000 t |
| **PIANC hull pressure** | 200 $kN/m^2$ |
| **Rated reaction force fender** | 3.8 MN |
| **Web frame spacing** | 4.95 m |

Figure A.8 shows the structural layout of a parallel hull section of the tanker vessel. The section that is used for the numerical simulations is 19.8 m wide.

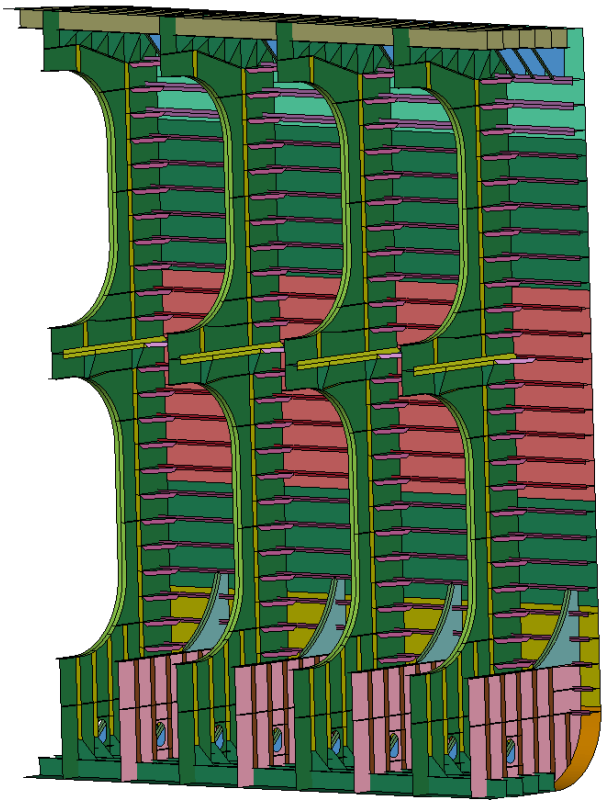

Figure A.8: Structural layout of Capesize bulk carrier.

# B

# Trend lines allowable equivalent hull pressure fender

The following part presents the obtained equivalent hull pressure trend lines for different vessels for wide and high panels in the body of this research. The trend lines are divided into two categories: panels with a height/width ratio above or equal to one and panels with a height/width ratio below one. The visual representation of these trend lines in comparison to the outcomes of the numerical simulations, the PIANC criterion and prior studies are presented in Chapter 6.

## Tanker 1

Trend line high fender panels:

```
General model Exp2:
     val(x) = a*exp(b*x) + c*exp(d*x)
     Coefficients (with 95% confidence bounds):
       a =        1396  (675.2, 2117)
       b =     -0.6611  (-1.052, -0.27)
       c =       304.9  (157.6, 452.2)
       d =    -0.02831  (-0.05636, -0.0002697)
```

Trend line wide fender panels:

```
 General model Exp2:
     val(x) = a*exp(b*x) + c*exp(d*x)
     Coefficients (with 95% confidence bounds):
       a =        3381  (-1310, 8071)
       b =     -0.9927  (-2.163, 0.1772)
       c =       670.6  (67.2, 1274)
       d =    -0.08186  (-0.1799, 0.01619)
```

## Container vessel 1

Trend line all fender panels:

```
 General model Exp1:
     val(x) = a*exp(b*x)
     Coefficients (with 95% confidence bounds):
       a =       983.3  (540, 1427)
       b =    -0.01933  (-0.1061, 0.06739)
```

## Container vessel 2

Trend line high fender panels:

```
General model Exp2:
     val(x) = a*exp(b*x) + c*exp(d*x)
     Coefficients (with 95% confidence bounds):
       a =   -1.11e+06  (-1.546e+16, 1.546e+16)
       b =    -0.02471  (-4.206e+04, 4.206e+04)
       c =   1.111e+06  (-1.546e+16, 1.546e+16)
       d =    -0.02471  (-4.205e+04, 4.205e+04)
```

Trend line wide fender panels:

```
General model Exp2:
     val(x) = a*exp(b*x) + c*exp(d*x)
     Coefficients (with 95% confidence bounds):
       a =        1628  (1289, 1967)
       b =     -0.4715  (-0.6604, -0.2826)
       c =       360.1  (165.6, 554.5)
       d =    -0.03629  (-0.06575, -0.006827)
```

## Container vessel 3

Trend line high fender panels:

```
General model Exp2:
     val(x) = a*exp(b*x) + c*exp(d*x)
     Coefficients (with 95% confidence bounds):
       a =        2473  (548.7, 4398)
       b =     -0.9889  (-1.541, -0.4369)
       c =         388  (280.1, 495.9)
       d =    -0.01715  (-0.03318, -0.001115)
```

Trend line wide fender panels:

```
General model Exp2:
     val(x) = a*exp(b*x) + c*exp(d*x)
     Coefficients (with 95% confidence bounds):
       a =        1383  (918.3, 1848)
       b =     -0.0787  (-0.1615, 0.004077)
       c =      0.3194  (-37.43, 38.07)
       d =      0.1617  (-3.091, 3.415)
```

## Container vessel 4

Trend line high fender panels:

```
General model Exp2:
     val(x) = a*exp(b*x) + c*exp(d*x)
     Coefficients (with 95% confidence bounds):
       a =       462.2  (-397, 1321)
       b =     -0.1622  (-0.6804, 0.3561)
       c =       244.9  (-769.8, 1260)
       d =   -0.008825  (-0.1358, 0.1181)
```

Trend line wide fender panels:

```
General model Exp2:
     val(x) = a*exp(b*x) + c*exp(d*x)
     Coefficients (with 95% confidence bounds):
       a =       830.5  (-8339, 1e+04)
       b =    -0.09012  (-1.158, 0.9783)
       c =       155.2  (-9570, 9880)
```

```
       d =   -0.003459  (-1.486, 1.479)
```

## Bulk carrier 1

Trend line high fender panels:

```
General model Exp1:
     val(x) = a*exp(b*x)
     Coefficients (with 95% confidence bounds):
       a =       273.4  (162.9, 383.8)
       b =   -0.006627  (-0.03477, 0.02152)
```

Trend line wide fender panels:

```
General model Exp2:
     val(x) = a*exp(b*x) + c*exp(d*x)
     Coefficients (with 95% confidence bounds):
       a =        2230  (1709, 2751)
       b =     -0.6355  (-0.8141, -0.4569)
       c =         414  (297.4, 530.5)
       d =    -0.03331  (-0.05117, -0.01545)
```

## Bulk carrier 2

Trend line high fender panels:

```
General model Exp2:
     val(x) = a*exp(b*x) + c*exp(d*x)
     Coefficients (with 95% confidence bounds):
       a =        2100  (849.3, 3350)
       b =     -0.2946  (-0.6291, 0.03983)
       c =       189.6  (-334.1, 713.2)
       d =     0.03519  (-0.05115, 0.1215)
```

Trend line wide fender panels:

```
General model Exp2:
     val(x) = a*exp(b*x) + c*exp(d*x)
     Coefficients (with 95% confidence bounds):
       a =       918.8  (-65.51, 1903)
       b =    -0.01114  (-0.3094, 0.2872)
       c =       0.187  (-292.2, 292.6)
       d =      0.1587  (-40.46, 40.78)
```

## Bulk carrier 3

Trend line high fender panels:

```
General model Exp2:
     val(x) = a*exp(b*x) + c*exp(d*x)
     Coefficients (with 95% confidence bounds):
       a =        1162  (13.81, 2310)
       b =     -0.4521  (-1.235, 0.331)
       c =       376.8  (-153.8, 907.3)
       d =     -0.0168  (-0.07945, 0.04586)
```

Trend line wide fender panels:

```
General model Exp2:
     val(x) = a*exp(b*x) + c*exp(d*x)
     Coefficients (with 95% confidence bounds):
       a =        1145  (287.7, 2002)
       b =     -0.2436  (-0.7152, 0.228)
       c =       250.5  (-739.1, 1240)
       d =   -0.004877  (-0.1411, 0.1313)
```

# C

# Trend lines allowable total fender force

The following part presents the obtained total fender reaction force trend lines for different vessels for wide and high panels in the body of this research. The trend lines are divided into two categories: panels with a height/width ratio above or equal to one and panels with a height/width ratio below one. The visual representation of these trend lines in comparison to the outcomes of the numerical simulations, the PIANC criterion and prior studies are presented in Chapter 6.

## Tanker 1

Trend line high fender panels:

```
General model Exp2:
     val(x) = a*exp(b*x) + c*exp(d*x)
     Coefficients (with 95% confidence bounds):
       a =   1.296e+05  (-5.515e+14, 5.515e+14)
       b =    -0.03741  (-5970, 5970)
       c =  -1.296e+05  (-5.515e+14, 5.515e+14)
       d =    -0.03741  (-5970, 5970)
```

Trend line wide fender panels:

```
General model Exp2:
     val(x) = a*exp(b*x) + c*exp(d*x)
     Coefficients (with 95% confidence bounds):
       a =       2.291  (1.624, 2.958)
       b =    0.007294  (-0.006303, 0.02089)
       c =      -2.281  (-3.494, -1.068)
       d =      -1.151  (-3.137, 0.8345)
```

## Container vessel 1

Trend line all fender panels:

```
General model Exp2:
     val(x) = a*exp(b*x) + c*exp(d*x)
     Coefficients (with 95% confidence bounds):
       a =   2.075e+04  (-3.819e+12, 3.819e+12)
       b =   -0.001271  (-3761, 3761)
       c =  -2.075e+04  (-3.819e+12, 3.819e+12)
       d =   -0.001312  (-3762, 3762)
```

## Container vessel 2

Trend line high fender panels:

```
General model Exp1:
     val(x) = a*exp(b*x)
     Coefficients (with 95% confidence bounds):
       a =       1.404  (0.4536, 2.355)
       b =     0.02998  (0.00304, 0.05692)
```

Trend line wide fender panels:

```
General model Exp2:
     val(x) = a*exp(b*x) + c*exp(d*x)
     Coefficients (with 95% confidence bounds):
       a =       2.405  (1.556, 3.255)
       b =     0.01235  (-0.00437, 0.02906)
       c =      -2.405  (-4.268, -0.5417)
       d =      -15.31  (-4.831e+09, 4.831e+09)
```

## Container vessel 3

Trend line high fender panels:

```
General model Exp2:
     val(x) = a*exp(b*x) + c*exp(d*x)
     Coefficients (with 95% confidence bounds):
       a =  -6.291e+04  (-6.377e+15, 6.377e+15)
       b =     0.05093  (-5.561e+04, 5.561e+04)
       c =   6.292e+04  (-6.377e+15, 6.377e+15)
       d =     0.05093  (-5.561e+04, 5.561e+04)
```

Trend line wide fender panels:

```
General model Exp2:
     val(x) = a*exp(b*x) + c*exp(d*x)
     Coefficients (with 95% confidence bounds):
       a =  -6.291e+04  (-6.377e+15, 6.377e+15)
       b =     0.05093  (-5.561e+04, 5.561e+04)
       c =   6.292e+04  (-6.377e+15, 6.377e+15)
       d =     0.05093  (-5.561e+04, 5.561e+04)
```

## Container vessel 4

Trend line high fender panels:

```
General model Exp2:
     val(x) = a*exp(b*x) + c*exp(d*x)
     Coefficients (with 95% confidence bounds):
       a =       4.541  (-2.812, 11.89)
       b =     0.00922  (-0.03265, 0.05109)
       c =      -4.312  (-11.35, 2.729)
       d =    -0.09518  (-0.2968, 0.1064)
```

Trend line wide fender panels:

```
General model Exp2:
     val(x) = a*exp(b*x) + c*exp(d*x)
     Coefficients (with 95% confidence bounds):
       a =       5.397  (-1.218, 12.01)
       b =    0.003279  (-0.03603, 0.04258)
       c =      -5.566  (-11.1, -0.02912)
       d =     -0.1988  (-0.6952, 0.2976)
```

## Bulk carrier 1

Trend line high fender panels:

```
General model Exp1:
     val(x) = a*exp(b*x)
     Coefficients (with 95% confidence bounds):
       a =       1.346  (0.01901, 2.673)
       b =     0.04569  (0.0121, 0.07927)
```

Trend line wide fender panels:

```
General model Exp2:
     val(x) = a*exp(b*x) + c*exp(d*x)
     Coefficients (with 95% confidence bounds):
       a =       2.661  (0.8132, 4.509)
       b =     0.01908  (-0.01081, 0.04898)
       c =      -2.661  (-6.886, 1.564)
       d =      -16.82  (-9.562e+10, 9.562e+10)
```

## Bulk carrier 2

Trend line high fender panels:

```
General model Exp2:
     val(x) = a*exp(b*x) + c*exp(d*x)
     Coefficients (with 95% confidence bounds):
       a =       2.265  (1.57, 2.961)
       b =     0.06564  (0.05632, 0.07495)
       c =      -2.267  (-4.517, -0.01734)
       d =      -2.104  (-17.86, 13.65)
```

Trend line wide fender panels:

```
General model Exp1:
     val(x) = a*exp(b*x)
     Coefficients (with 95% confidence bounds):
       a =       3.251  (1.002, 5.5)
       b =      0.0575  (0.03559, 0.07942)
```

## Bulk carrier 3

Trend line high fender panels:

```
General model Exp2:
     val(x) = a*exp(b*x) + c*exp(d*x)
     Coefficients (with 95% confidence bounds):
       a =       3.495  (0.9342, 6.057)
       b =     0.02122  (-0.0007693, 0.0432)
       c =       -3.14  (-5.585, -0.6952)
       d =     -0.1527  (-0.3874, 0.08206)
```

Trend line wide fender panels:

```
General model Exp2:
     val(x) = a*exp(b*x) + c*exp(d*x)
     Coefficients (with 95% confidence bounds):
       a =        2.66  (1.852, 3.467)
       b =     0.02882  (0.0184, 0.03924)
       c =      -2.665  (-3.979, -1.35)
       d =     -0.5441  (-1.157, 0.06899)
```

# D

# Comparison analytical result Vredeveldt and Rhijnsburger (2019)

In table D.1, an full comparison is presented of the allowable analytical reaction force for cylindrical fender impact on a single stiffener to the LS-DYNA simulations with a similar panel area [32]. The stated area of the results of Vredeveldt and Rhijnsburger is the contact area for maximum compression of the cylindrical fender. Moreover, there appear to be large discrepancies between the results of the small vessels. It suggests that the influence of the web frames, the panels do engage with web frames, contribute significantly to the allowable reaction force.

Table D.1: Comparison of hull capacities according to analytical single stiffener impact study [32] and LS-DYNA simulations.

| Vessel (Appendix A) | Fender type* [32] | Full compression cylindrical fender contact area [$m^2$][32] | Analytical single stiffener allowable reaction force [kN][32] | LS-DYNA fender panel contact area [m] | Numerical simulations allowable reaction force [kN] |
|---|---|---|---|---|---|
| Tanker coaster (T1) | ⌀1000-600-1500 | 1.40 | 171 | 1.5 | 2035 |
| Tanker coaster (T1) | ⌀1400-800-2200 | 2.76 | 210 | 3.0 | 2155 |
| Container feeder (C1) | ⌀1000-600-1500 | 1.40 | 304 | 1.5 | 2248 |
| Container feeder (C1) | ⌀1400-800-2200 | 2.76 | 301 | 3.0 | 3095 |
| Container coaster (C2) | ⌀1000-600-1500 | 1.40 | 304 | 1.5 | 1725 |
| Container coaster (C2) | ⌀1400-800-2200 | 2.76 | 301 | 3.0 | 2239 |
| Container Panamax (C3) | ⌀1000-600-1500 | 1.40 | 434** | 1.5 | 1762 |
| Container Panamax (C3) | ⌀1400-800-2200 | 2.76 | 732 | 3.0 | 3160 |
| Container ULCV (C4) | ⌀1000-600-1500 | 1.40 | 434** | 1.5 | 886 |
| Container ULCV (C4) | ⌀1400-800-2200 | 2.76 | 835 | 3.0 | 968 |
| Bulker Handysize (B1) | ⌀1000-600-1500 | 1.40 | 434** | 1.5 | 1185 |
| Bulker Handysize (B1) | ⌀1400-800-2200 | 2.76 | 1062** | 3.0 | 2037 |
| Bulker Capesize/VLBC (B2) | ⌀1000-600-1500 | 1.40 | 434** | 1.5 | 999 |
| Bulker Capesize/VLBC (B2) | ⌀1400-800-2200 | 2.76 | 1062** | 3.0 | 1093 |
| Bulker Panamax (B3) | ⌀1000-600-1500 | 1.40 | 434** | 1.5 | 1469 |
| Bulker Panamax (B3) | ⌀1400-800-2200 | 2.76 | 1062** | 3.0 | 1648 |

**Fender dimensions (⌀1000-600-1500) is outer diameter - inner diameter - width.*

***Fender reaches the allowable compression before yielding occurs in the ship structure.*

# Bibliography


[1] J. C. Adamchak. *Design Equations for Tripping of Stiffeners Under Inplane and Lateral Loads*. Oct. 1979. URL: https://apps.dtic.mil/sti/citations/ADA074752.

[2] J. Amdahl. “Impact from ice floes and icebergs on ships and offshore structures in Polar Regions”. In: *IOP Conference Series: Materials Science and Engineering*. Vol. 700. 1. IOP Publishing Ltd, Nov. 2019. DOI: 10.1088/1757-899X/700/1/012039.

[3] D. Barber. “The bulk carrier side shell and its vulnerabilities”. In: *The Naval Architect* 20.January (Jan. 2020), pp. 2–4.

[4] E. J. Broos, M. P. M. Rhijnsburger, A. W. Vredeveldt, and W. Hoebee. “The safe use of cylindrical fenders on LNG, Oil and Container Terminals”. In: *PIANC-World Congress Panama City*. Panama, 2018. URL: https://conference-service.com/pianc-panama/documents/agenda/data/full_papers/full_paper_20.pdf.

[5] H. L. Budweg, Y. S. Shin, and Y. S. Shin. “Experimental studies on the tripping behavior of narrow t-stiffened flat plates subjected to hydrostatic pressure and underwater shock”. In: *NASA-Marshall Space Flight Center, The 58th Shock and Vibration Symposium, Volume 1* (1987).

[6] D. A. Danielson. “Analytical tripping loads for stiffened plates”. In: *International Journal of Solids and Structures* 32.8-9 (Apr. 1995), pp. 1319–1328. ISSN: 0020-7683. DOI: 10.1016/0020-7683(94)00196-4.

[7] D. Danielson. *Tripping of Stiffened Plates Using a Refined Beam Theory.* Tech. rep. NAVAL POSTGRADUATE SCHOOL MONTEREY CA, 1988.

[8] W. Galor. “THE MODELLING OF BUCKLING FENDERS TO PROTECT THE SHIP BERTHING PROCESS”. In: *Journal of KONES Powertrain and Transport* 14.3 (2007).

[9] M. J. Gudmunsen and J. Morris. *Strength of Side Shell Structure to Resist Quayside Fender Loads Report No. CSD 89 /24 [confidential]*. Tech. rep. Lloyd’s Register of Shipping Class Computational Services Group, 1989.

[10] I. Heemskerk. *Determining the mechanisms causing the hydraulic damping during ship berthing: Comprehending the water cushion effect (MSc thesis)*. 2020. URL: https://repository.tudelft.nl/islandora/object/uuid%3A4f92840c-1627-4f3d-8487-9e122cc561ba.

[11] O. F. Hughes and M. Ma. “Elastic tripping analysis of asymmetrical stiffeners”. In: *Computers & Structures* 60.3 (Aug. 1996), pp. 369–389. ISSN: 0045-7949. DOI: 10.1016/0045-7949(95)00389-4.

[12] T. IJzerman. *Allowable Hull Loading due to Fender Contact (MSc Thesis)*. Delft University of Technology Repository, Sept. 2021. URL: http://resolver.tudelft.nl/uuid:75d401f9-adce-4384-8a84-15f0d6a92fe5.

[13] T. von Kármán, E. E. Sechler, and L. Donnell. “The Strength of Thin Plates in Compression.” In: *Transactions of the American Society of Mechanical Engineers* (1932). URL: https://www.ce.jhu.edu/cfs/cfslibrary/von%20karman%20eff%20width%20paper.pdf.

[14] L. Li, Z. Hu, and Z. Jiang. “Plastic and elastic responses of a jacket platform subjected to ship impacts”. In: *Mathematical Problems in Engineering* 2013 (2013). ISSN: 1024123X. DOI: 10.1155/2013/790586.

[15] Lloyd’s Register. *Rules and Regulations for the Classification of Ships*. URL: https://www.lr.org/en/rules-and-regulations-for-the-classification-of-ships/.

[16] R. Luo and B. Edlund. “Ultimate strength of girders with trapezoidally corrugated webs under patch loading”. In: *Thin-Walled Structures* 24.2 (Jan. 1996), pp. 135–156. ISSN: 0263-8231. DOI: 10.1016/0263-8231(95)00029-1.

[17] H. Ma, Q. Xiong, and D. Wang. “Experimental and numerical study on the ultimate strength of stiffened plates subjected to combined biaxial compression and lateral loads”. In: *Ocean Engineering* 228 (May 2021). ISSN: 00298018. DOI: 10.1016/j.oceaneng.2021.108928.

[18] MarCom Working Group 211 and PIANC The World Association for Waterborne Transport Infrastructure. “[Unpublished] Guidelines on Design, Manufacturing and Testing of Fender Systems 2023”.

[19] MarCom Working Group 33. *Guidelines for the Design of Fender Systems*. Tech. rep. PIANC The World Association for Waterborne Transport Infrastructure, Nov. 2002. URL: https://www.pianc.org/publications/marcom/guidelines-for-the-design-of-fender-systems.

[20] Norwegian Technology Standards Institution. *N-004 DESIGN OF STEEL STRUCTURES*. Tech. rep. Oslo: Norwegian Technology Standards Institution, 2021. URL: https://www.standard.no/pagefiles/1145/n-004.pdf.

[21] A. Price, B. W. Quinton, and B. Veitch. “Shared-Energy Prediction Model for Ship-Ice Interactions”. In: *SNAME Maritime Convention 2021, SMC 2021* (Oct. 2021). DOI: 10.5957/SMC-2021-033.

[22] B. W. T. Quinton. “Progressive Damage to a Ship’s Structure due to Ice Loading”. PhD thesis. Newfoundland: Memorial University of Newfoundland, Jan. 2008.

[23] *Recommendation 47 - Shipbuidling and Repair Quality Standard*. Tech. rep. International Association of Classification Societies.

[24] A. Roubos, L. Groenewegen, and D. J. Peters. “Berthing velocity of large seagoing vessels in the port of Rotterdam”. In: *Marine Structures* 51 (Jan. 2017), pp. 202–219. ISSN: 09518339. DOI: 10.1016/j.marstruc.2016.10.011.

[25] F. Shahabian and T. M. Roberts. “Buckling of slender web plates subjected to combinations of in-plane loading”. In: *Journal of Constructional Steel Research* 51.2 (1999), pp. 99–121. ISSN: 0143974X. DOI: 10.1016/S0143-974X(99)00020-6. URL: www.elsevier.com/locate/jcsr.

[26] I. A. Sheikh, A. E. Elwi, and G. Y. Grondin. “Stiffened steel plates under combined compression and bending”. In: *Journal of Constructional Steel Research* 59.7 (2003), pp. 911–930. ISSN: 0143974X. DOI: 10.1016/S0143-974X(02)00079-2.

[27] ShibataFenderTeam. *SFT Product Catalogue*. Tech. rep. URL: https://www.shibata-fender.team/en/downloads.html.

[28] S. J. Sisworo, O. Mursid, and Samuel. “The Strength Evaluation of 5600 DWT Double Hull Oil Tanker Subjected to Fender Load”. In: *IOP Conference Series: Earth and Environmental Science* 972.1 (Jan. 2022), p. 012027. ISSN: 1755-1307. DOI: 10.1088/1755-1315/972/1/012027. URL: https://iopscience.iop.org/article/10.1088/1755-1315/972/1/012027.

[29] C. S. Smith. “Compressive Strength of Welded Steel Ship Grillages”. In: *undefined*. NAVAL CONSTRUCTION RESEARCH ESTABLISHMENT DUNFERMLINE, 1975. URL: https://apps.dtic.mil/sti/citations/ADA023670.

[30] W. J. Son and I. S. Cho. “Analysis of Trends in Mega-Sized Container Ships Using the K-Means Clustering Algorithm”. In: *Applied Sciences 2022, Vol. 12, Page 2115* 12.4 (Feb. 2022), p. 2115. ISSN: 2076-3417. DOI: 10.3390/APP12042115. URL: https://www.mdpi.com/2076-3417/12/4/2115/htm%20https://www.mdpi.com/2076-3417/12/4/2115.

[31] Trelleborg Marine and Infrastructure. *DESIGN MANUAL Fender Application Design Manual*. Tech. rep.

[32] A. Vredeveldt and M. Rhijnsburger. *Ship side-cylindrical fender contact characteristics, a systematic investigation*. Tech. rep. TNO, 2019. URL: www.tno.nl.

[33] B. Wang, H.-C. Yu, and R. Basu. “SHIP AND ICE COLLISION MODELING AND STRENGTH EVALUATION OF LNG SHIP STRUCTURE”. In: *ASME 27th International Conference on Offshore Mechanics and Arctic Engineering*. Estoril, Portugal, 2008.

[34] G. Wang, K. Tamura, D. Jiang, and Q. J. Zhou. “DESIGN AGAINST CONTACT DAMAGE FOR OFFSHORE SUPPLY VESSELS”. In: *International Marine Design Conference*. Ed. by A. Arbor. Michigan: University of Michigan, May 2006.